Wide Binary Companions To Tycho-Gaia Stars

Conor Talbot
Supervisor: Prof. Boris Gäensicke

January 30, 2018

Masters Thesis

Submitted to the University of Warwick
for the degree of

MSc by Research

Astronomy & Astrophysics Group
Department of Physics

Contents

List of Figures

List of Tables

Declaration

This thesis is the sole work of Conor Talbot, all other works and contributions are acknowledged.

This work has not been submitted to any other university or for the purpose of any other degree or qualification.

The La Palma spectra in Figures 23 and 24 was the work of Boris Gäensicke collected from March 31st to April 3rd 2017.

The main sequence star spectra for 2 of our final candidates in Figures 33 and 35 was the work of David Boyd.

Acknowledgements

I would firstly like to thank my parents who are always there to help reassure and motivate me, even when the goal seems impossible.

I would also like to thank John Dolan who was always there to help me with technical issues, to provide support, but most of all be a very good friend throughout the whole year.

Next I have to thank Dr. Nicola Gentile-Fussilo and Dr. Roberto Raddi, who helped me make progress with Python and computing in general. Whenever I needed guidance they could adapt to the problem at hand. Even though it was not their research they always found a solution.

Another valuable person was Dr. Danny Steeghs, my Feedback Supervisor. Thank you for the useful guidance you gave me throughout the year to help improve this thesis.

A significant contribution to this work was from David Boyd. He obtained two main sequence star spectra for this research, for which I am beyond grateful. Thank you so much, I really appreciate your generosity.

I cannot forget Professor Don Pollacco who believed in me and gave me the opportunity to make this thesis the best it could be. Thank you for the direction you have given me to help me improve my scientific writing drastically, it is a valuable skill that I will use throughout my life.

Last, but certainly not least, is Professor Boris Gäensicke. Not only were you extremely patient with me and always helped me if I had a problem, but you inspired me with your attitude to research and work in general. Even if you were not having the best day there was a smile on your face, and your work ethic is second to none. Your ability to meet with your many students throughout the day and be totally invested in the moment and their work amazes me. I hope going forward I can use both the academic and life skills you have taught me in everything I do, their value is something I greatly appreciate.

Abstract

We present a catalogue of 112 white dwarf-main sequence binary candidates within the SDSS footprint, including ≈65 binary candidates containing cool white dwarfs. Our catalogue includes 8 previously found systems from Tremblay et al. (2017) with 1 previously found system from Farihi et al. (2005a). White dwarfs themselves can be used as cosmic laboratories with extreme conditions and for various tests of stellar evolution theories. White dwarf-MS binaries can be used to help refine the white dwarf mass-radius relation, white dwarf initial-to-final mass relation, luminosity function, to test for dark matter, and the history of star formation in the Galaxy. The TGAS catalogue from the recent *Gaia* data release 1 provides parallaxes to the 2 million brightest stars. Using the TGAS catalogue and cross-matching it by coordinates, proper-motions and magnitudes with the PPMXL catalogue creates a clean TGAS subset. Taking the clean TGAS subset and identifying common proper-motion pairs, we search for candidate wide white dwarf-MS binaries. Using primarily photometry for the candidate binaries to determine their basic properties, the binaries that most likely contain white dwarfs are selected, including confirmed white dwarfs with available spectra. These systems should be confirmed by others and used for future follow-up studies.

1 Introduction

White Dwarfs

White dwarfs (WDs) are extremely important in astronomical research as they represent the end states of ≈95% of all stars in the Galaxy, including the Sun. WDs are the result of a star near the end of its life on the main sequence (MS) expanding into a red giant and blowing off its outer shell to leave behind the cooling remnant (Catalán et al., 2008a; Koester, 2013).

The first known WDs, classical WDs, are 40 Eridani B, Van Maanen 2 and Sirius B. On a Hertzsprung-Russell (HR) diagram they lie in the lower left corner, with hot surface temperatures but extremely low luminosities compared to MS stars with similar temperatures. Their location on the HR diagram implies that their radii are ≈100 times smaller than those of MS stars. Fortuitously, Sirius B, the closest WD to Earth, is in fact part of a binary with the MS star Sirius A, the brightest star in the night sky. Using the orbital parameters of this binary system, the mass of Sirius B has been calculated to be $1M_{\odot}$, with a mean density of $\approx 10^6$g cm^{-1}. This information helped astronomers of the early 1900's begin to understand WDs (Koester, 2013, p. 562-563).

The average masses and radii for WDs are now known to be $\approx 0.5 M_{\odot}$ and $\approx 0.0125 R_{\odot}$, respectively (Koester, 2013, p. 561). The upper limit of the mass is $\approx 1.4 M_{\odot}$ for WDs containing elements heavier than Hydrogen in their interiors (Chandrasekhar, 1931). The enormous surface gravities ($\approx 1 \times 10^{8} \mathrm{cms}^{-2}$) of WDs explain why they are chemically stratified (Koester, 2013, p. 564).

There are 2 main spectral types of WDs, DA and DB. The D stands for degenerate as the interiors of WDs are electron degenerate. This is the mechanism that provides the pressure of these stars that balances their enormous gravity, as explained by the Pauli principle for fermions (Fowler, 1926; Pauli, 1925). DAs contain broad Hydrogen (H) Balmer Lines and are the most common spectral type, making up $\approx 80\%$ of WDs. The second main type are DB WDs, which contain broad Helium (He) Lines. Other spectral types include DZs, which are WDs with metal lines and no H or He lines (Koester, 2013, p. 563-565).

WDs provide experimental conditions impossible to recreate on Earth. They are therefore used as cosmic laboratories for astronomy, quantum mechanics and cosmology. One reason is that their interiors supply conditions for the macroscopic manifestation of the Pauli exclusion principle. Their extremely high magnetic fields up to 10^{9} G in their atmospheres, very high pressures and very high densities are also useful in many fields (Koester, 2013, p. 561).

The evolution of WDs can be described as a cooling process as WDs are no longer burning in their interiors (Mestel, 1952). Therefore, accurate ages can be obtained from WDs as they are natural clocks (Rebassa-Mansergas et al., 2016a). The ages of WDs are obtained from their measured surface gravities and temperatures very accurately through evolutionary cooling tracks (Fontaine et al., 2001; Renedo et al., 2010). Furthermore, the time spent on the MS for WD progenitors can be calculated using the MS masses of WD progenitors. These masses are obtained by using the initial-final mass relation (Catalán et al., 2008b; Ferrario et al., 2005) with evolutionary sequences. Finally, the total ages of WDs are given by the sum of the MS lifetimes of WD precursors and the cooling ages of the resulting WDs observed today (Rebassa-Mansergas et al., 2016a).

To conclude, WDs provide properties and statistical information on the relation between a WD's MS progenitor mass at birth and a WD's mass as its final remnant, information on the age of stellar systems, the history of star formation within the Galaxy, and the chemical composition of planetary material from WDs that have accreted debris from destroyed asteroids or planets (Koester, 2013, p. 561-562).

Wide WD-MS binaries

A wide WD-MS binary is a WD and MS star in a common proper-motion pair. The binary starts as a MS star binary where their separation (or semi-major axis a) is wide enough ($a > 100 - 10^3$au) that they do not undergo any mass transfer Catalán et al. (2008a). Therefore, the stars evolve as if they are single stars and eventually the more massive star of the binary evolves into a WD (Rebassa-Mansergas et al., 2016b)(Koester, 2013, p. 608).

A wide WD-MS binary can provide the amount of post MS mass loss a WD progenitor experiences, which is obtained with the metallicity of the WD MS progenitor (Zhao et al., 2012). This progenitor metallicity is acquired from the entire binary's metallicity, which is inferred by the MS star in the binary. Furthermore, the age of a WD-MS binary can be determined from the WD's age, as the WD and MS star companion are the same age (Rebassa-Mansergas et al., 2016a). Therefore, wide WD-MS binaries provide important insight into stellar evolution as they can be viewed as the smallest and simplest forms of stellar clusters (Koester, 2013; Kouwenhoven et al., 2010).

We will use the most common method of identifying individual wide binaries in our research, which is through their common proper-motions on the sky (Chanamé and Gould, 2004; Lépine and Bongiorno, 2007; Makarov et al., 2008; Wasserman and Weinberg, 1991). Tremblay et al. (2017) utilise 6 directly observed WDs and 46 WD members of wide binaries from the TGAS Data Release 1 in order to refine the mass-radius relation. The mass-radius relation is useful for type Ia supernovae which are used as standard candles to measure the expansion of the Universe (Perlmutter et al., 1999; Riess et al., 1998) and help determine the distances of remote galaxies. The mass-radius relation is used to accurately obtain a WD's mass through spectroscopy, photometry or gravitational red-shift measurements (e.g.(Bergeron et al., 2001, 1992; Falcon et al., 2012; Koester, 1987; Koester et al., 1979; Shipman, 1979)).

We will employ the 46 WD-MS binaries from Tremblay et al. (2017) as test cases for our method, i.e. the fraction of their binaries that are re-identified will help determine how successful and reliable our method is.

Currently, there are few wide WD-MS binaries known. In their research, Holberg et al. (2013) refer to binaries or multiple star systems composed of a WD and at least one star of spectral type K or earlier as a Sirius-like-system (SLS). Their

wide WD-MS binary catalogue of 98 SLSs is one of the largest to date, our research will therefore provide a significant increase in the number of known systems.

Approximately 30% of all nearby WDs are in a binary or multiple star system, with the simplest to detect and most abundant type containing an M star companion. This is because the luminosity of a WD at optical wavelengths is either easily detectable, or more intense than the companion, regardless if the system is resolved or not. Holberg et al. (2013) claim that ≈8% of all known WDs within 20pc are members of SLSs. In contrast, they state that the frequency of SLSs is 1-2% beyond 20pc (Holberg et al., 2013).

Since A, F, G, K stars outshine WDs at optical wavelengths, Holberg et al. (2013) state that most unidentified SLSs are probably insufficiently separated. They conclude that many more SLSs will be unearthed through various new observational techniques in the future, with the most promising being the *Gaia* survey.

Initial Final Mass-Radius Relation and the Luminosity Function

Common proper-motion pairs containing a WD are useful to refine the initial-final mass relation (IFMR) as they usually cover a wide range of masses, ages and metallicities (e.g. (Day-Jones et al., 2011; Farihi et al., 2005b; Zhao et al., 2011)). The IFMR is used to calculate the luminosity function, which is the number of WDs within a given luminosity interval for a stellar system, such as a cluster or the Galactic disc (Koester, 2013, p. 584). The IFMR is also used to understand the Galaxy's mass budget. This is the amount of mass from MS stars that is fed back into the interstellar medium for use in star formation, rather than being stored forever within cold WDs (Koester, 2013, p. 586). Unfortunately, it is still poorly constrained. Most research makes use of WDs in open clusters. However, open clusters are normally relatively young, so contain more WDs that had more massive progenitors ($>2M_{\odot}$). Open clusters cannot cover typical WDs which require lower mass progenitors, as these stars are still on the MS. Therefore, common proper-motion pairs are more representative of the Galactic WD field population (Catalán et al., 2008a). Using common proper-motion pairs of DA WDs with F, G, K stars, Catalán et al. (2008a) cover the low-mass domain where little exploration has been performed.

Just like the studies of WDs in open clusters, Catalán et al. (2008a) find a large scatter in the distribution of the semi-empirical data, higher than the expected uncertainties in the derived values. This leads to the possibility that the IFMR might not be a single-valued function. New surveys including *Gaia* will uncover many

new WDs in binary systems and help develop a better understanding of the IFMR.

Wide Binary Frequency

Another study into wide binaries is the Sloan Low-mass Wide Pairs of Kinematically Equivalent Stars (SLoWPoKES) catalogue from Dhital et al. (2010). The catalogue is the largest for stellar neighbours brighter than $r = 20$ with a sample of 577,459 stars. They deduce that their sample encompasses 2 populations of wide binaries: a "young" population of weakly bound systems that will last to only a few Gyr, and an "old" population of tightly bound systems. This is because their sample displays a bimodal distribution in the semi-major axes.

Dhital et al. (2010) find that their sample amounts to a lower limit for the wide binary frequency of 1.1% for the mid-K to mid-M spectral types. As wide binaries age their Galactic scale height increases, this is because close encounters with other stars provides them with some perpendicular momentum to the Galactic disc. Wide binaries at larger distances above the Galactic disc break up with time which results in fewer binaries. Dhital et al. (2010) conclude that there is probably a time evolution of the wide binary frequency because it decreases as a function of Galactic height. This is therefore evidence of the dynamical destruction of old systems.

WD-MS binaries containing cool WDs

Stellar evolution

Open clusters only exist up to ≈1Gyr before being dissolved by Galactic tides and stellar encounters (Jiang and Tremaine, 2010; Vande Putte et al., 2010). However, wide WD-MS binaries with old cool WDs can be older than open clusters. Therefore, these binaries provide important insight into stellar evolution (Koester, 2013).

The age-metallicity relation

WD-MS binaries that contain cool WDs can also be used to study the age-metallicity relation (AMR). The AMR is a critical constraint which helps understanding how the Galactic disc formed and evolved chemically in time. For individual stars, obtaining their precise ages proves difficult which subsequently means there is so far no agreement in the observational properties of the AMR for the solar neighbourhood (Rebassa-Mansergas et al., 2016a). A frequently used technique for constraining the AMR is using open clusters which show for metallicities the same scatter in field stars (Carraro et al., 1998; Friel, 1995; Pancino

et al., 2010). Therefore, the results add validity to the lack of correlation between the metallicity and age. However, there are a few factors to take into consideration with these conclusions. For one, open clusters only exist up to ≈1Gyr (Vande Putte et al., 2010) which limits the study of intermediate to old ages. In addition, the results may also be inconclusive as there is only a small number of open clusters that have been homogeneously analysed, which hinders the research about the existence of an AMR (Casamiquela et al., 2016).

Rebassa-Mansergas et al. (2016a) use 23 WD-MS binaries as observational inputs to constrain the properties of the AMR robustly. Through obtaining the WD ages, MS star metallicities and the AMR for their sample, they provide clear observational evidence for young and intermediate ages (0-7 Gyrs) for the lack of correlation between age and metallicity [Fe/H].

The existence of a physical mechanism causing the observed scatter of [Fe/H] in the observed AMR is supplied in the observational results. They suggest the mechanism could be self-enrichment of gas in star forming regions (Pilyugin and Edmunds, 1996) or episodic gas infall onto the disc (Köppen and Hensler, 2005). The most widely accepted hypothesis is invoking radial migration effects where metal-rich stars form in the inner disc and subsequently migrate to the metal-poorer outer disc (Minchev et al., 2011; Roškar et al., 2008; Sellwood and Binney, 2002). They state any of these scenarios are just as likely as a larger sample is needed to come to a more resolved conclusion.

The WD-MS binaries Rebassa-Mansergas et al. (2016a) use contain no cool WDs. Even though they use physically wide WD-MS binaries with ≈100AU separation, they are within only a few 100pc so are still unresolved. WD-MS binaries containing cool WDs can not only be ≥1Gyr old, but also spatially resolved so spectroscopy for each constituent can be independently obtained, simplifying the analysis. These type of candidate systems can help with understanding how the Galactic disc formed and evolved chemically in time, and help refine the AMR further.

The rotation-age relationship

The age of stars is a fundamental aspect to astronomy, yet is difficult to measure (Epstein and Pinsonneault, 2014). Stars lose angular momentum and mass as they become older, therefore their surface rotation slows down (Skumanich, 1972). Open clusters have been critical in the understanding of angular momentum in low mass stars (Stauffer et al., 1989) as they provide a large variety of rotation rates for

stars which are all the same age (Prialnik, 2000). There are some known difficulties in calculating age through measuring the rotation of a star, such as the rotation distribution (Epstein and Pinsonneault, 2014). When low-mass proto-stars form they have a bi-modal distribution in rotation rates, consisting of 2 separate groups. The first being rapid rotators with a rotation rate of 2.2 days with a 1 day dispersion. And the second being slow rotators with a rotation rate of 8.5 days with a 2.5 day dispersion. This means it is hard to predict what their rotation rates will be (e.g. Attridge and Herbst (1992)). Even though by the time the young stars arrive on the MS they have similar rotation rates (Stauffer et al., 1989), there still is a rotation distribution present. The width of the rotation distribution does narrow with time, faster for solar objects and slower for lower mass stars (Epstein and Pinsonneault, 2014). However, it is this distribution in rotation rates that makes it hard to predict what the rotation rate will be for a star at a particular age.

WD-MS binaries that contain cool WDs can be viewed as a collection of many small clusters, containing not only different types of stars with different masses, but also many systems with a distribution of ages (Zhao et al., 2011). Finding these type of candidate systems can provide a better distribution for the rotation-age relationship than an open cluster which contains stars all with the same age (Prialnik, 2000).

To conclude, wide binaries are also used to constrain the properties of the Milky Way, place limits on massive compact halo objects (MACHOs) including other unseen material (Bahcall et al., 1985; Quinn et al., 2009), the history of the Galaxy (Hartkopf et al., 2007) and to test for dark matter (Hernandez and Lee, 2008).

However, the large separations of wide binaries means it is difficult to confidently determine whether the 2 constituents of a candidate system are just a chance superposition or actually bound (Kouwenhoven et al., 2010).

Our motivation is to identify as many new and previously discovered (Tremblay et al., 2017) WD-MS binaries as possible. These systems can help improve our understanding of topics such as the WD mass-radius relation, WD IFMR and the luminosity function in the future.

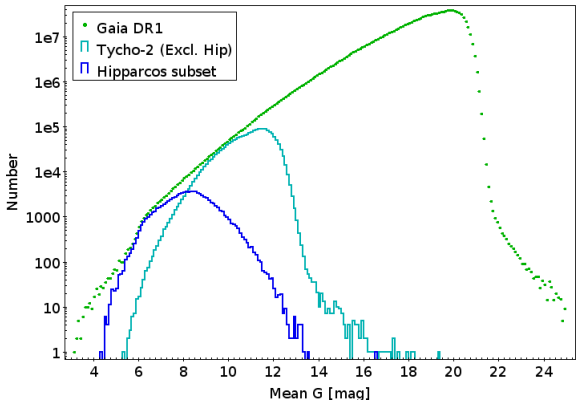

Figure 1: Gaia Data Release 1 G-band magnitude distribution (European Space Agency, 2016).

2 Methodology

2.1 Introduction

2.1.1 *Gaia* and the TGAS Catalogue

The *Gaia* satellite (European Space Agency, 2016) launched at the end of 2013 with the aim to determine highly accurate positions, parallaxes, and proper-motions for more than 1 billion sources brighter than magnitude 20.7 in the white-light photometric G band (as seen in Figure 1). *Gaia* set out with the nominal 5 year mission lifetime to deliver a parallax accuracy of 24 micro-arc-seconds for a 15th magnitude solar-type star.

In our research we made use of the *Tycho-Gaia* (TGAS) catalogue which was the result of the data collected from the first 14 months of the *Gaia* mission in conjunction with the Tycho astrometry (Gaia Collaboration et al., 2016).

TGAS contained the positions, parallaxes and mean proper-motions for 2,057,050 stars in common between the *Gaia* Data Release 1, HIPPARCOS and Tycho-2 catalogues, where 90% of all TGAS sources had a magnitude brighter than G=12.05.

The Tycho stars within TGAS had typical positional uncertainties of ≈0.3 milli-arc-seconds and proper-motion uncertainties of ≈1 milli-arc-seconds yr^{-1}. As well as a parallax uncertainty of 0.3 arc-seconds, the HIPPARCOS subset had more accurate proper-motions with an uncertainty of ≈0.06 milli-arc-seconds yr^{-1}. However, the HIPPARCOS parallaxes should have had a systematic component of ≈0.3 milli-arc-seconds added (Gaia Collaboration et al., 2016).

2.1.2 The PPMXL Catalogue

The PPMXL catalogue (Roeser et al., 2010) was a combination of the astrometry from 2 different surveys with new mean positions and proper-motions determined on the International Celestial Reference System. The first survey was USNO-B1.0, which was the largest catalogue in the optical regime with more than 1 billion objects (Monet et al., 2003). However, USNO-B1.0 contained relative not absolute proper-motions (see (Monet et al., 2003)). The second survey was the Two Micron All Sky Survey (Skrutskie et al., 2006) (2MASS). It operated from 1997 to 2001 and was an all sky survey in the J, H and K_S bands, but it did not contain any proper-motions. PPMXL was comprised of 900 million objects of which 410 million had 2MASS photometry, and was the largest collection of International Celestial Reference System proper-motions. It aimed to be complete over the entire sky from $V \approx 20$ up to the brightest stars.

The mean errors for the positions at epoch J2000 were $\simeq 80 - 120$ milli-arc-seconds for objects with 2MASS astrometry, otherwise $\simeq 150 - 300$ milli-arc-seconds. The typical individual mean errors of the proper-motions were $\simeq 4 - 10$ milli-arc-seconds yr^{-1} depending on observational history.

2.1.3 Synopsis of the methodology

(A quick summary of the full methodology explained in Sect. 2.2 on P. 21).

The main objective was to find already confirmed (Tremblay et al., 2017) and new WD-MS binaries using the TGAS (Gaia Collaboration et al., 2016) and PPMXL (Roeser et al., 2010) catalogues. The first goal was to create a clean TGAS subset from TGAS, this contained the MS stars of the WD-MS binary candidates. In TGAS, a star's G-band magnitude should not have been fainter than 12.5 as it was based on the TYCHO bright star catalogue. WDs are much fainter than MS stars at the same $T_{\rm eff}$, which is why no new WD companions should have been found in TGAS. Multiple cuts were performed to ensure the clean TGAS subset would consist of TGAS stars that were not artefacts.

Two of the parameters we used for selection in TGAS were the magnitudes and parallaxes. As seen in Figure 2 there were many entries with wrong or statistically insignificant values, i.e. G-magnitudes fainter than 12.5 mag and TGAS stars with parallax significances less than 3.

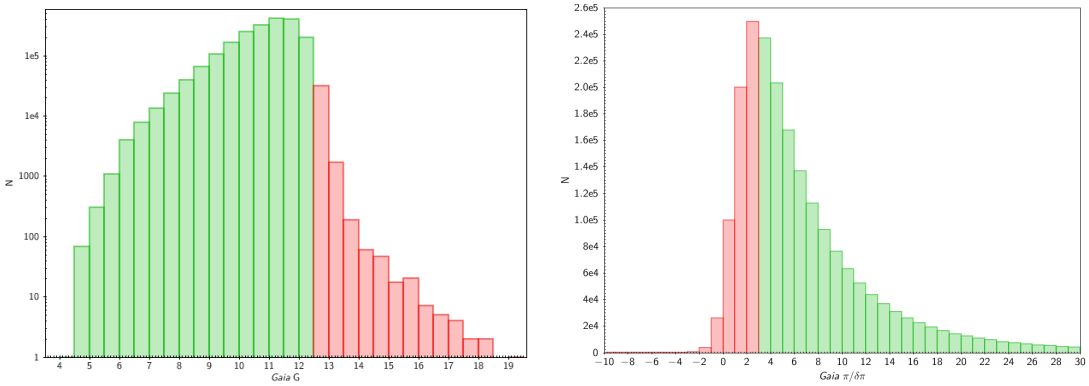

(a) (b)

Figure 2: (a): TGAS G-band magnitudes fainter than 12.5 in red. (b): Statistically insignificant TGAS parallaxes, in green are objects with a parallax of $\geq 3\sigma$.

The TGAS stars were then cross-matched with PPMXL which contained 900 million objects all with proper-motions. A search radius of 5 arc-seconds (c.f. section. 2.2.1 P. 21) was used to check if they were also within PPMXL. Only TGAS stars that coincided closely to a PPMXL star with a similar proper-motion and magnitude were kept. However, a large amount of TGAS and PPMXL stars had proper-motions with low significances which were discarded (as seen in Figure 3).

Once the clean TGAS subset was created, binary candidates were identified through the method of common proper-motion pairs. The remaining TGAS stars were cross-matched with PPMXL using a 2 arc-minute radius (c.f. section. 2.2.2 P. 25) to look for objects with similar proper-motions, some of which were WDs.

Within PPMXL the same issue as with the TGAS catalogue recurred: a large fraction of objects had statistically insignificant proper-motions (as seen in Figure 4). A stricter cut was used for the common proper-motion companions due to a large amount of stars being within the 2 arc-minute radius for each TGAS star. Throughout the methodology deciding which cuts to impose was the most difficult aspect. Being too lenient would have lead to having too many candidates to visually inspect later, however, being too strict would have cut potential WD-MS binaries in the process.

The common proper-motion candidates were narrowed down to potential WD companions by first using colour and magnitude cuts on the 2 arc-minute PPMXL companions. Candidates that visually looked the most like WDs were identified

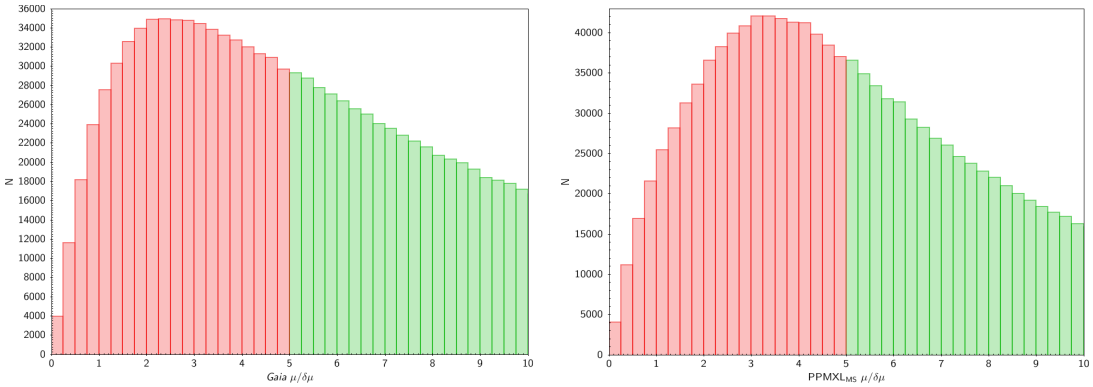

(a) (b)

Figure 3: Shown in (a): Proper-motion significance in the TGAS catalogue and shown in (b): Proper-motion significance of PPMXL measurements corresponding to TGAS stars of at least 3σ proper-motion significance. In green are stars with proper-motions $\geq 5\sigma$ significance and in red are stars with proper-motions $< 5\sigma$ significance.

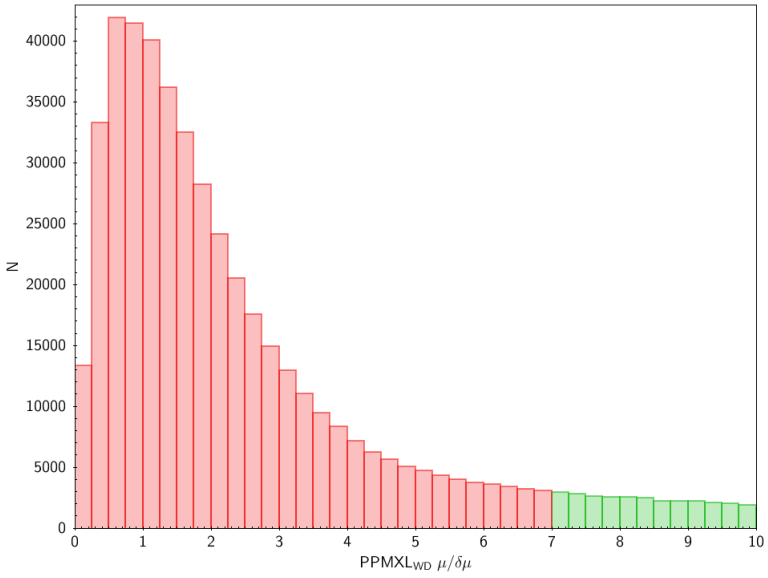

Figure 4: Proper-motion significances of common proper-motion companion PPMXL stars to the clean TGAS subset. Shown in green are stars with a proper-motion significance $\geq 7\sigma$.

through visually inspecting images from the Sloan Digital Sky Survey (SDSS) (Alam et al., 2015). Various photometric diagrams were created and evaluated to derive the candidate's properties and identify the best potential candidates. Finally, the WD companion's atmospheric parameters were computed using DA and DB WD models. These fits were used to discard any unlikely binaries and increase the validity of the final candidates. Spectra was obtained with allocated telescope time to confirm some of the WD-MS binary candidates.

2.2 Method

2.2.1 Creating the clean TGAS subset

The first goal was to create the clean TGAS subset that contained genuine stars from within both TGAS and PPMXL and no artefacts. This clean TGAS subset would be used to search for common proper-motion companions.

The complete TGAS catalogue contained 2,057,050 objects which required filtering to identify genuine stars. To begin, all of the TGAS stars that had a parallax of less than 3σ significance ($\pi/\delta\pi \geq 3$) were omitted to check that the stars in the TGAS catalogue were actually stars and not artefacts. All stars that had statistically insignificant proper-motions were discarded using the standard error propagation:

$$\mu = \sqrt{(\mu^{\mathrm{T}}_{\mathrm{pmra}})^2 + (\mu^{\mathrm{T}}_{\mathrm{pmdec}})^2}$$

(Where $\mu^{\mathrm{T}}_{\mathrm{pmra}}$ and $\mu^{\mathrm{T}}_{\mathrm{pmdec}}$ were the TGAS proper-motions in right ascension and declination.)

and

$$\delta\mu = \frac{1}{\mu}\sqrt{(\mu^{\mathrm{T}}_{\mathrm{pmra}}\delta\mu^{\mathrm{T}}_{\mathrm{pmra}})^2 + (\mu^{\mathrm{T}}_{\mathrm{pmdec}}\delta\mu^{\mathrm{T}}_{\mathrm{pmdec}})^2}$$

(Where $\delta\mu^{\mathrm{T}}_{\mathrm{pmra}}$ and $\delta\mu^{\mathrm{T}}_{\mathrm{pmdec}}$ were the errors for the TGAS proper-motions in right ascension and declination.)

The value of $\mu/\delta\mu$, which was analogous to a signal-to-noise ratio, was calculated for the proper-motions of the TGAS stars. A cutoff of $\mu/\delta\mu \geq 5$ was used to keep stars that had proper-motions of at least 5σ significance.

A cross-match of 5 arc-seconds was used to check that the TGAS stars were also in the PPMXL catalogue. We refered to the objects from this cross-match

with PPMXL for potential MS TGAS stars as PPMXL_{MS}.

A 5 arc-second radius was used to search for the same star because PPMXL relied on old photographic plates taken around 1950 to 1990, which meant the proper-motions had large uncertainties. Also, the TGAS positions were in the 2015 epoch, so the accumulated error in the PPMXL positions could have been fairly large when translating both catalogues' coordinates to the J2000 epoch. Even after translating both catalogues to the J2000 epoch, a radius of 5 arc-seconds could have been needed to pick up a high proper-motion star due to PPMXL's large errors.

Many PPMXL_{MS} stars also suffered from statistically insignificant proper-motions, so a 5σ cut-off was imposed with the same error propagation equations used previously.

Comparing the apparent magnitudes in both catalogues provided an additional method to check if the TGAS stars were the same as the objects in PPMXL_{MS}. Average magnitudes were calculated using the $B1$, $B2$, $R1$ and $R2$ magnitudes from PPMXL_{MS}, $\frac{B1+B2+R1+R2}{4}$, or whatever subsets of B, R were available. These averages were compared to the G-band magnitudes from TGAS. This was justified because the TGAS G-band was a broad band which spanned both the B and R bands. It was required that the average PPMXL_{MS} magnitudes and TGAS G-bands were within 2 magnitudes of each other.

Next, the ranges of a star's proper-motion in right ascension and declination plus-or-minus 3 of its respective errors were calculated. We refered to them as 3σ proper-motion ranges.

In order to conclude the same star existed in both catalogues, the 3σ proper-motion ranges had to overlap in both right ascension and declination for TGAS and PPMXL_{MS}.

The Tremblay et al. (2017) WD-MS binaries were used as a test cases for the methodology. Testing 1σ proper-motion ranges caused a large number (31=76%) of the Tremblay et al. (2017) binaries to be cut, which was too strict. Whereas 3σ proper-motion ranges cut 7 binaries ($\approx 15\%$), which was a large improvement. This indicated that PPMXL and TGAS had underestimated their uncertainties.

To ensure this cut did not lead to retaining any artefacts, the 3σ proper-motion ranges were tested on a random sample of 1000 stars. When all 1000 POSS-2 im-

ages (Caltech) from online were visually inspected, it was clear that the objects in $\mathrm{PPMXL_{MS}}$ were in fact the TGAS stars and not image artefacts.

Therefore, taking into account a) the 1000 star test, b) all the stars had at least 5σ proper-motions in both catalogues, c) the magnitudes of the stars were similar in both catalogues, and d) the 3σ proper-motion ranges overlapped, we were confident that the TGAS entries in the clean TGAS subset corresponded to genuine stars. The clean TGAS subset was finally created and contained 886,494 stars.

The entire procedure producing the clean TGAS subset was illustrated in the flow chart in Figure 5.

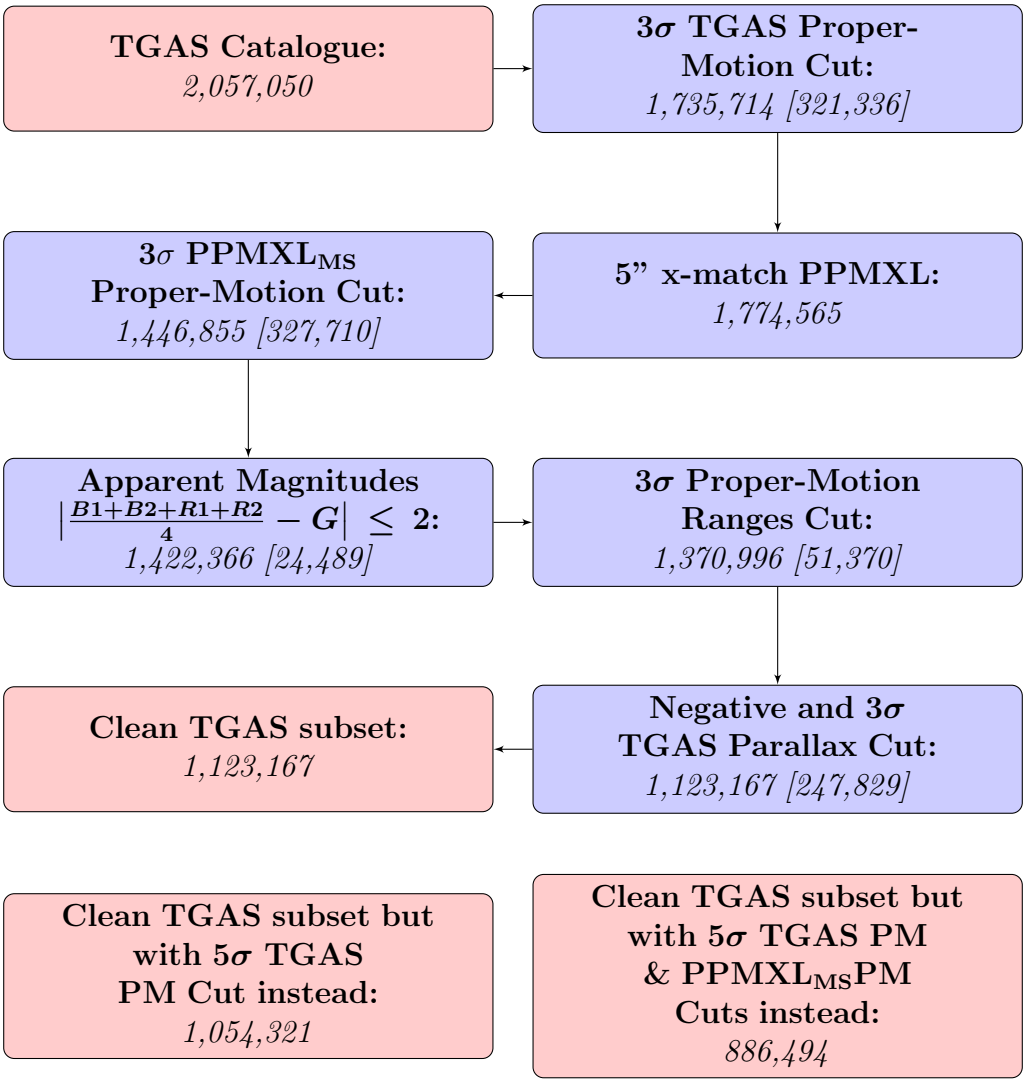

Figure 5: A flow chart documenting the stages of the cuts imposed in creating the clean TGAS subset. It also shows the number of TGAS stars left at every stage with the amount lost in square brackets. (PM=proper-motion). The clean TGAS subset required 5σ proper-motions for both TGAS and $\mathrm{PPMXL_{MS}}$.

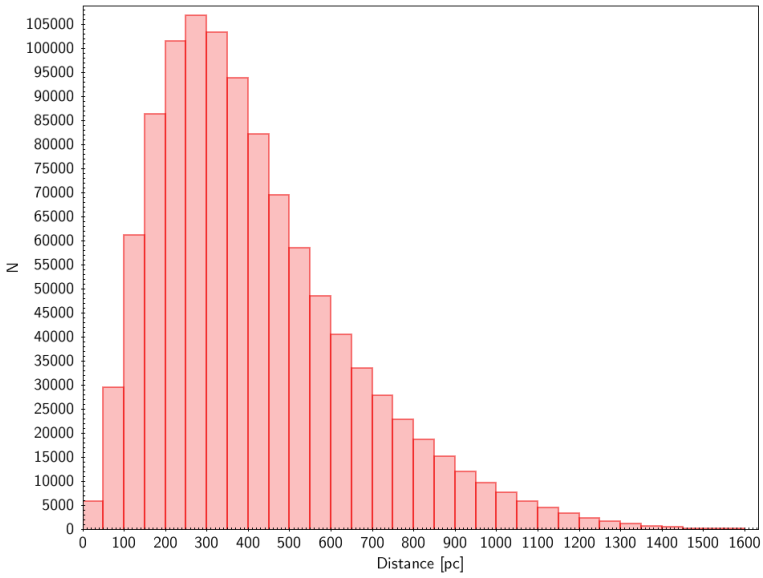

Figure 6: Distances of objects in the clean TGAS subset.

2.2.2 Finding common proper-motion companions to the clean TGAS subset

A 2 arc-minute radius cross-match with PPMXL was used to find common proper-motion companions to the TGAS stars in the clean TGAS subset. We referred to the objects in this cross-match with PPMXL for the companion as PPMXL_{WD}.

The reasoning for this search radius was that the median distance of all the objects in the clean TGAS subset was approximately 336pc (as seen in Figure 6). Companions in wide binaries were expected to be at a separation in the semi-major axis (a) range of approximately $10^3\text{AU} < a < 20{,}626.5\text{AU}$ (0.1pc) (Kouwenhoven et al., 2010). With a search radius of 2 arc-minutes, this equated to a projected separation of approximately 40,000AU. This cutoff was sufficient for detecting wide binaries at the median distance and for wide binaries for the vast amount of closer TGAS stars.

Next, all instances were discarded from the catalogue where a TGAS star had found itself in the 2 arc-minute cross match in PPMXL_{WD}.

The same error propagation equations as before were then used to impose a 7σ cut-off on the PPMXL_{WD} proper-motions (c.f. P. 26).

In order to conclude the TGAS star and the PPMXL_{WD} object were in a com-

mon proper-motion pair, we calculated 2σ proper-motion ranges. These were the ranges of a star's proper-motion in right ascension and declination plus-or-minus 2 of its respective errors. The 2σ proper-motion ranges had to overlap in both right ascension and declination for TGAS and PPMXL_{WD}.

We believed that the PPMXL proper-motion errors were incorrect when working with them. Not only were the errors much greater than the TGAS errors, but the errors for the proper-motions in right ascension and declination were frequently identical for the same star. This occurred even when the proper-motions in right ascension and declination were vastly different from each other. We also believed that the TGAS proper-motion errors were incorrect. A cut-off of 3σ should have meant in 1000 stars only 3 of them were artefacts or contaminants. Throughout the research these statistical cut-offs did not agree with the PPMXL and TGAS proper-motion errors, but gave a larger number of contaminants than expected.

Therefore, different values of σ had to be experimented with for the PPMXL_{WD} proper-motions and for the proper-motion ranges of TGAS and PPMXL_{WD}. A 7σ proper-motion significance cut for PPMXL_{WD} and 2σ proper-motion ranges for TGAS and PPMXL_{WD} were eventually used. This was to obtain candidates that were most likely common proper-motion pairs without generating too many to visually inspect later.

The justifications for these cuts were discussed further in the Appendix under Section 6.2 on P. 80.

WD Companions

The previous stage was finding common proper-motion companions, however, these companions could have been any type of star. The next stage was to begin constraining the companions to potential WDs. Observed absolute magnitudes were calculated for the companions from the PPMXL_{WD} apparent magnitudes (B_{avg} and R_{avg}) and TGAS parallax values (π). The TGAS π were used assuming the TGAS stars and companions were at the same distance ($1/\pi \approx d$).

Observed absolute magnitudes were calculated as:

$$\text{M}_{\text{B}}^{\text{o}} = \text{B}_{\text{avg}} - (5\log_{10}(\frac{1}{\pi}) - 5)$$

$$\text{M}_{\text{R}}^{\text{o}} = \text{R}_{\text{avg}} - (5\log_{10}(\frac{1}{\pi}) - 5)$$

A table of theoretical absolute magnitudes for DA WDs from Holberg and Bergeron (2006)[1] was then used to obtain WD parameters for the companions. These parameters included effective temperature ($T_{\rm eff}$), surface gravity ($\log(g)$), mass, M_B, M_R and age.

The $\mathrm{M_B^o}$ & $\mathrm{M_R^o}$ values for each companion were compared to each model from the Holberg and Bergeron (2006) table using their theoretical absolute magnitude values ($\mathrm{M_B^t}$ & $\mathrm{M_R^t}$). Finding the model with the smallest geometric separation (d) in the M_B , M_R plane to the observed values gave the best model for that companion.

$$\mathrm{d} = \sqrt{(\mathrm{M_B^o} - \mathrm{M_B^t})^2 + (\mathrm{M_R^o} - \mathrm{M_R^t})^2}$$

A cut of $-0.5 \leq d \leq 0.5$ was then performed, i.e. the companion's observed absolute magnitude was required to be within plus-or-minus 0.5 of the best-fitting theoretical absolute magnitude (as seen in Figure 7). This cut left 22,083 candidates with possible WD companions.

Main sequence star parameters and spectral type

A combination of ATLAS and PHOENIX model tables were utilised to obtain estimates for the masses, radii, $T_{\rm eff}$'s, $\log(g)$'s, fluxes and various photometric bands of the TGAS stars (Bayo et al., 2008; Husser et al., 2013; Munari et al., 2005). Additionally, the Pickles magnitude table was used to acquire estimates for the TGAS stars' spectral types (Pickles, 1998).

To do this, a position on an M_G , $J-K$ colour-magnitude diagram was calculated for each TGAS star using the J and K bands from $\mathrm{PPMXL_{MS}}$ and G band from TGAS. Where M_G was:

$$\mathrm{M_G} = \mathrm{G} - (5\log 10(\frac{1}{\pi}) - 5)$$

A geometric separation was used again but within M_G , $J-K$ space to acquire the best models. These models contained the best parameters and spectral types for the TGAS stars.

[1]Available at *http://www.astro.umontreal.ca/∼bergeron/CoolingModels* (02/08/2017)
Color and Model Calculations: Holberg & Bergeron (2006, AJ, 132, 1221), Kowalski & Saumon (2006, ApJ, 651, L137), Tremblay et al. (2011, ApJ, 730, 128), and Bergeron et al. (2011, ApJ, 737, 28).

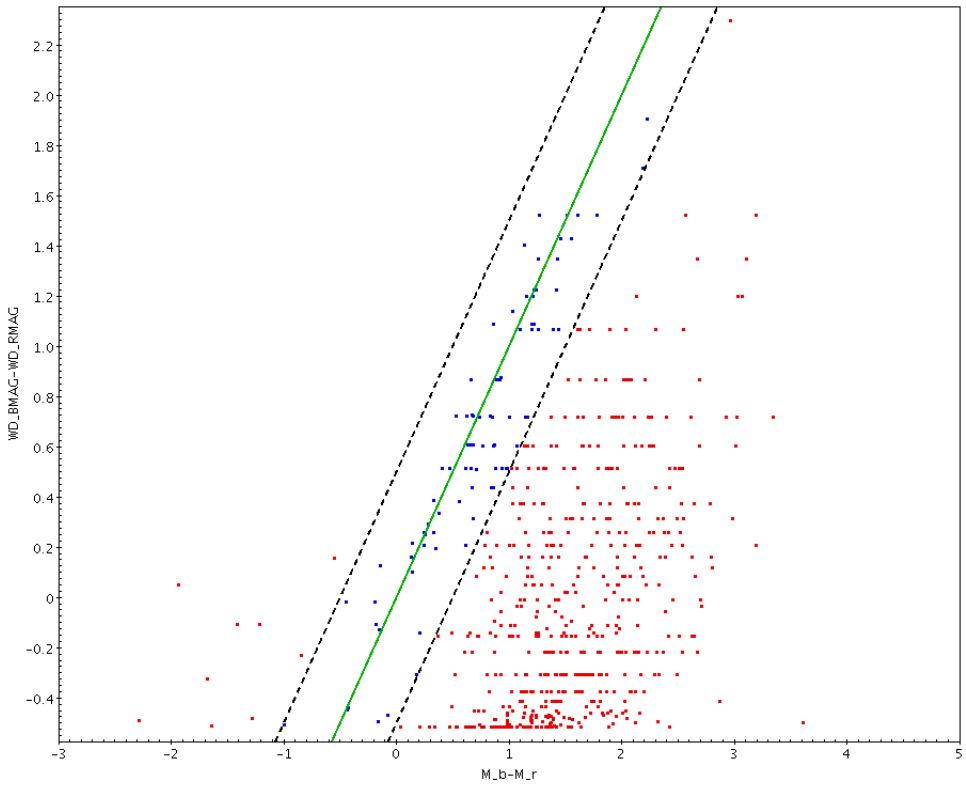

Figure 7: The cut of $-0.5 \leq d \leq 0.5$. The green line represents d=0, which means the common proper-motion companion's observed absolute magnitude matches exactly with its best WD model's theoretical absolute magnitude. The dashed lines are the cut-offs of plus-or-minus half a magnitude where the blue dots are the WD candidate companions we keep, and the red dots are the companions we discard.

Visual inspection of common proper-motion binary candidates

POSS-2 Images

Diagnostic plots were created using POSS-2 files from online (Caltech) to filter out any obvious artefacts from the 22,083 candidates that remained. Various parameter information and proper-motion arrows for the TGAS and $\mathrm{PPMXL_{WD}}$ objects were also included. A candidate could fall into 1 of 3 defined categories:

Candidate systems that appeared to be a possible wide WD-MS binary were assigned to the 'Possible WD common proper-motion candidate' category. Faint WDs could have been hard to see in the images because POSS-2 images were taken on photographic plates. Therefore, a candidate could have fallen into this category even if a companion was only marginally seen on the image.

Candidate systems that clearly did not contain a stellar companion (a Galaxy or a diffraction spike from the TGAS star) were assigned to the 'Bad common proper-motion candidate' category.

Finally, candidate systems where the $\mathrm{PPMXL_{WD}}$ companion was stellar, but so bright that it clearly could not have been a WD companion, were assigned to the 'Non WD common proper-motion candidate' category. These systems were kept as they could be useful for other research in the future. Examples for all 3 groups were displayed in Figure 8.

Once this procedure was complete, 7,945 Possible WD common proper-motion candidates remained. These candidates would later be searched for in the SDSS survey.

The entire procedure of finding the common proper-motion companions to the clean TGAS subset was illustrated in the flow chart in Figure 9.

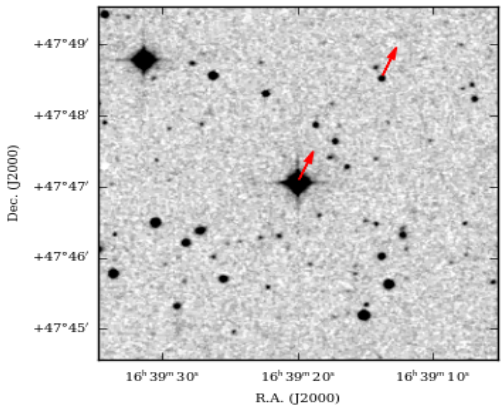

(a) 'Possible WD common proper-motion candidate'

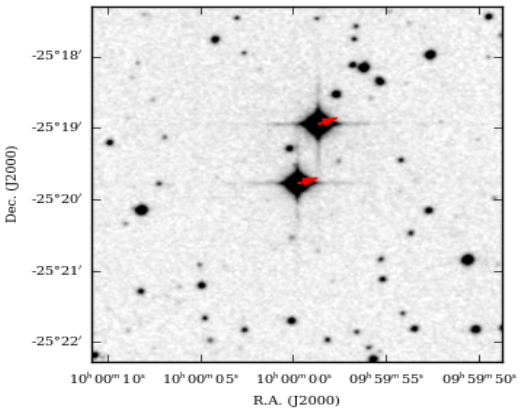

(b) 'Non WD common proper-motion candidate'

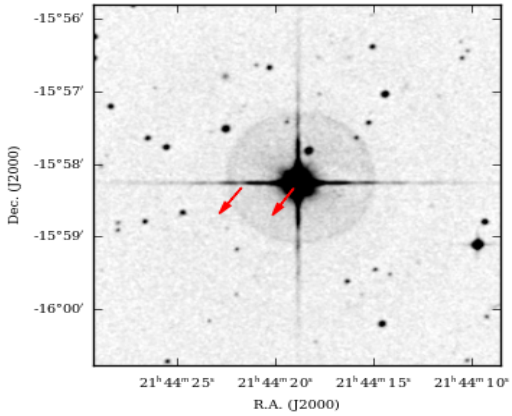

(c) 'Bad common proper-motion candidate' - Diffraction Spike

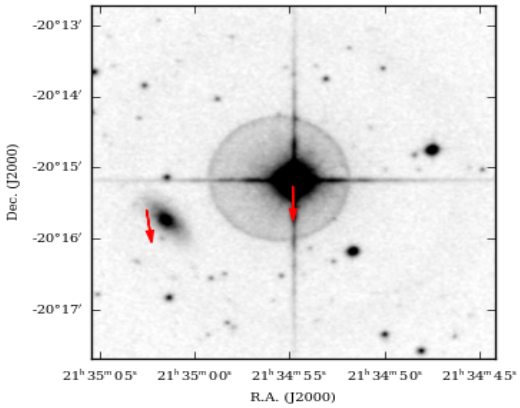

(d) 'Bad common proper-motion candidate' - Galaxy

Figure 8: 4 examples illustrating the different classifications for the visual inspection of the common proper-motion candidates.

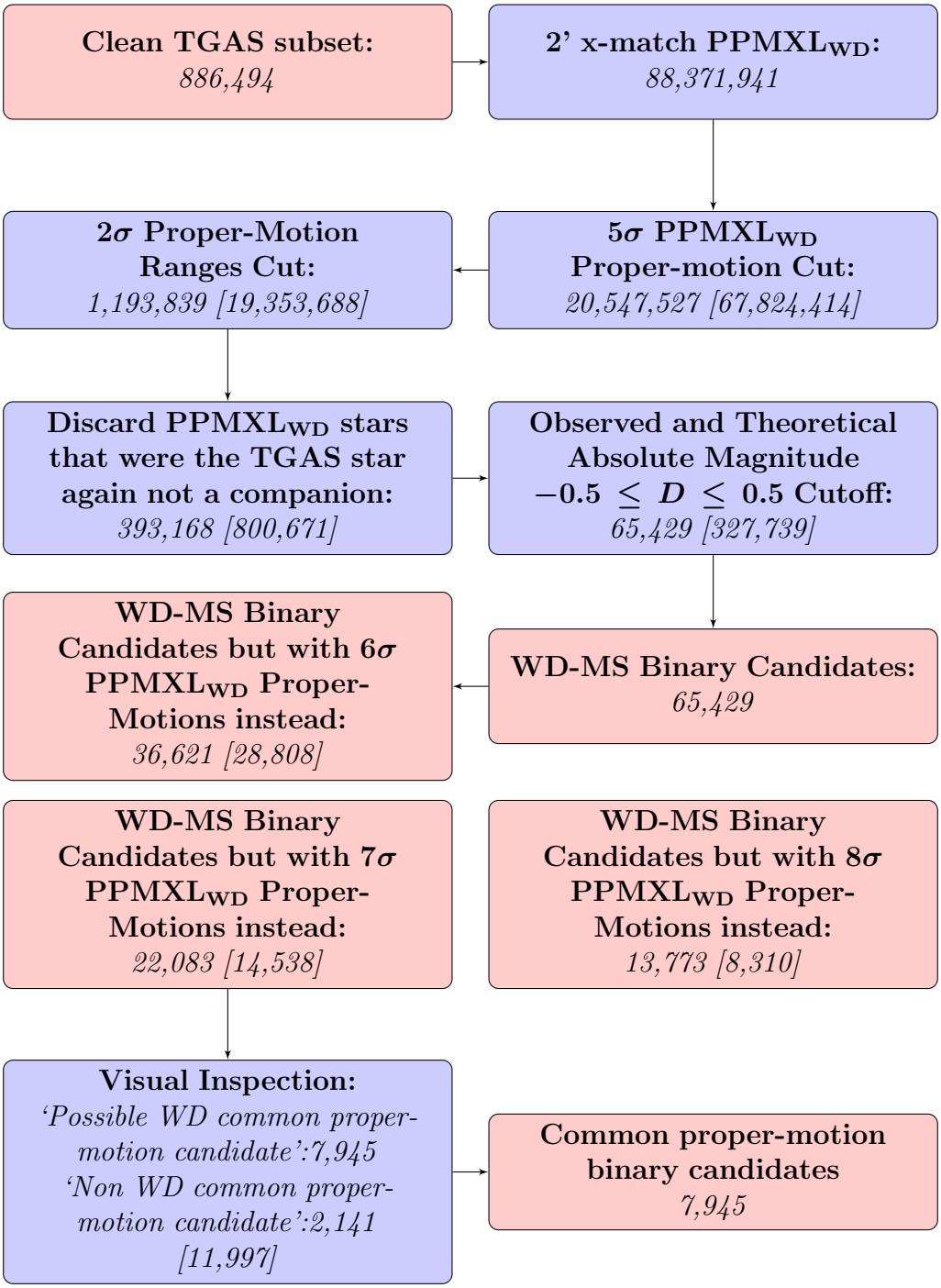

Figure 9: A flow chart documenting the stages of the cuts imposed finding common proper-motion companions to the clean TGAS subset. It also shows the number of candidate systems left at every stage with the amount lost in square brackets. (PM=proper-motion). Our common proper-motion binary candidates contained stars with $\mu/\delta\mu \geq 7$ PPMXL$_{\rm WD}$ proper-motions.

2.2.3 Finding the WD-MS binary candidates

There were 7,945 common proper-motion companion candidates containing possible WDs remaining. However, they needed to be filtered down to systems with a confirmed or high-confidence WD companion. The systems that remained would form the final WD-MS binary candidates catalogue.

SDSS

It was difficult to define which candidates were robust WD-MS binary candidates with the available information so far. u, g, r, i, z band photometry was required to help select the best binary candidates and filter down the large number of candidates left (7,945) to systems with WD companions. Therefore, SDSS (Alam et al., 2015) was used to cross-match with the candidates. However, SDSS only covered $\approx 1/3$ of the sky which was a large limitation on the amount of final candidates that could be detected. Using the SDSS sky-server online (Skyserver), the postage-stamp images were visually inspected for systems containing a blue or grey dot, as these were likely the candidates that were truly WDs. Some of the candidates also had spectra in SDSS which was used to confirm whether the candidate was a WD or not. In the end, 271 WD candidates in SDSS were found.

Useful colour diagrams to classify the companion

Colour-colour diagrams: Colour-colour diagrams in the $u - g$, $g - r$ plane were created using the u, g, r, i, z bands from SDSS (as seen in Figure 10). The position of a candidate on a colour-colour diagram suggested the nature of the object. A colour within the blue ellipse suggested the candidate was a WD, a colour within the red ellipse suggested the candidate was an M Dwarf-WD binary and the orange line was the MS, where a candidate could have been a cool metal-polluted WD.

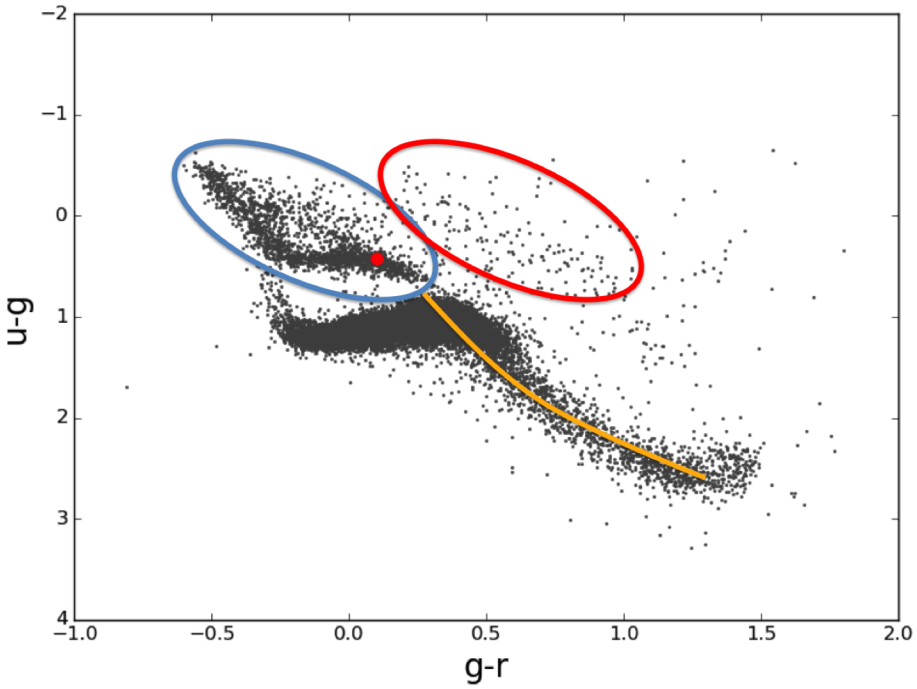

Figure 10: $u-g$ vs. $g-r$ colour-colour diagram. The red dot is candidate ID:14112. A colour within the blue ellipse suggests the candidate is a WD, a colour within the red ellipse suggests the candidate is an M Dwarf-WD binary, and the orange line is the MS, where a candidate could be a cool metal-polluted WD.

Reduced proper-motion - colour diagrams: Another useful plot which used the SDSS bands was suggested by Gentile Fusillo et al. (2015), known as a reduced proper-motion - colour diagram. These diagrams were in the plane of H_g , $g - r$, where H_g was the reduced proper-motion:

$$H_g = g + 5 \log \mu + 5$$

$$\mu = \sqrt{(\mu_{ra})^2 + (\mu_{dec})^2}$$

(Where μ = proper-motion.)

H_g was essentially analogous to an absolute magnitude for the g-band photometry for a given transverse velocity (Gentile Fusillo et al., 2015).

The position of a candidate on a reduced proper-motion - colour diagram again suggested the nature of the object. In Figure 11, a colour within the blue ellipse suggested the candidate could have been a WD, a colour within the red ellipse suggested the candidate could have been a MS star, and a colour within the orange ellipse suggested the candidate could have been a cool metal-polluted WD (Gentile Fusillo et al., 2015).

Therefore, using both a colour-colour diagram and a reduced proper-motion - colour diagram together strongly helped assess the likelihood that a candidate was actually a WD.

Visual inspection and classification of our common proper-motion pair candidates

We needed to further reduce the 271 common proper-motion pair candidates to the most likely binaries containing a WD. 'Master Plots' were created in order to screen all 271 binary candidates (examples in Sect. 6.1). The Master Plots contained:

· An SDSS image of the MS star
· An SDSS image of the WD companion
· A POSS-2 red image of the WD-MS binary candidate with arrows that indicated the individual proper-motions
· A POSS-2 red image of the WD-MS binary candidate that illustrated the proper-motions of all objects within a 2 arc-minute radius
· A colour-colour diagram of the WD
· A reduced proper-motion - colour diagram of the WD
· The SDSS spectrum of the WD (if they were available)

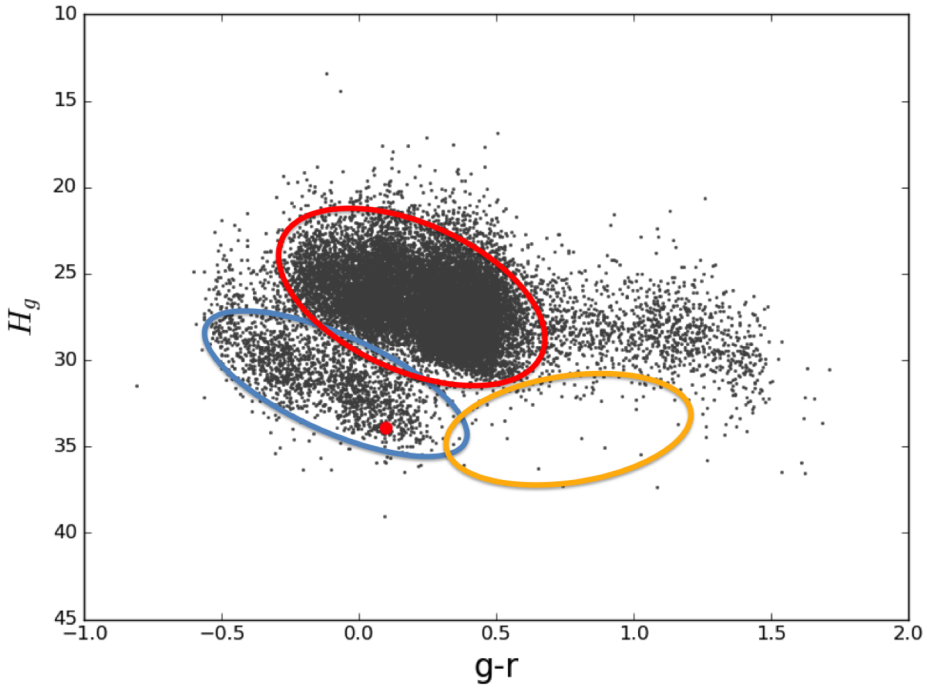

Figure 11: H_g vs. $g - r$ reduced proper-motion - colour diagram. The red dot is candidate ID:14112. The blue ellipse suggests the candidate is a WD, the red ellipse suggests the candidate is a MS star and the orange ellipse suggests the candidate could be a cool metal-polluted WD.

The Master plots were used to categorise each candidate into 1 of 6 categories:

· WD candidates with SDSS spectra
· Good Candidates: Colour-colour and reduced proper-motion - colour diagrams suggested a WD companion, a good candidate for spectroscopy
· Confirmed WDs (SIMBAD)
· Possible WDs/Undetermined
· Colour-colour and reduced proper-motion colour diagrams suggested a MS Star companion
· Bad candidates e.g. Diffraction Spike/Inconclusive/Crowded Field

The number of candidates in each category were listed in Table 1 and illustrated in Figure 12:

Classication Group	**Amount**
WD candidates with SDSS spectra	29
Good Candidates	164
Confirmed WDs	7
Possible WDs/Undetermined	13
MS Star Companion	38
Bad Candidates	20

Table 1: The common proper-motion pair candidates classifications.

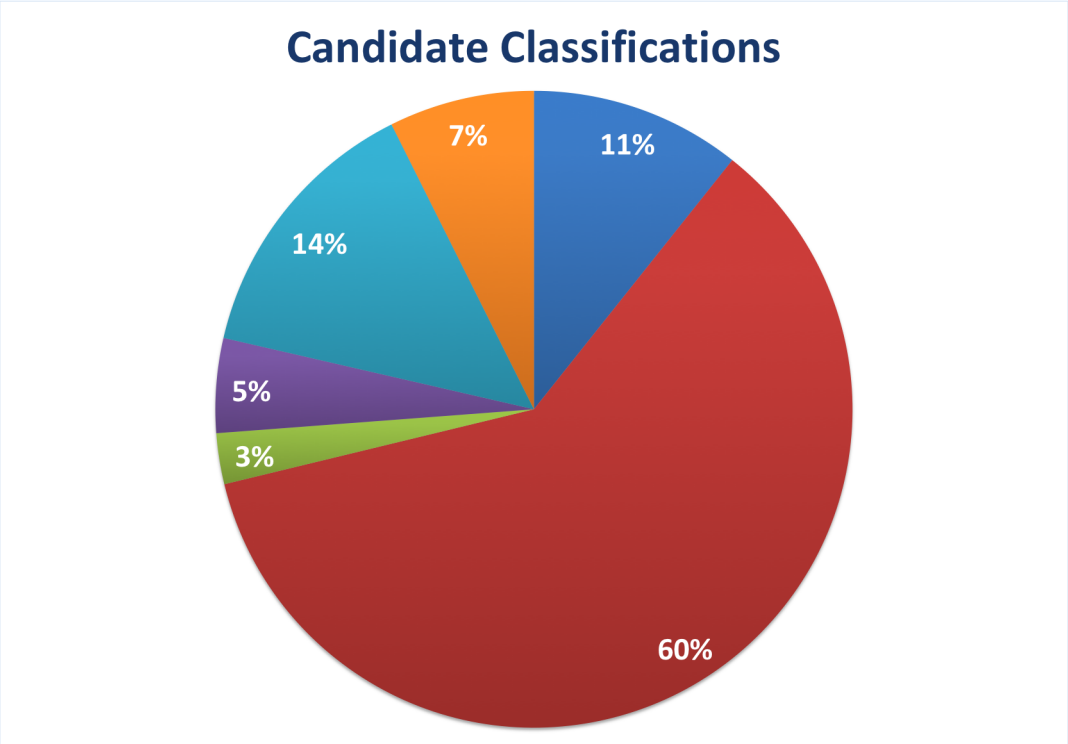

Figure 12: Complete common proper-motion binary candidates classification pie chart. SDSS WDs = Blue, Good Candidates = Red, Confirmed WDs = Green, Possible WDs/Undetermined = Purple, MS Star Companion = Light Blue, Bad Candidates = Orange

Estimates of WD parameters

The 200 candidates kept were from the WD candidates with SDSS spectra, Good candidates and Confirmed WDs categories. The next goal was to obtain more precise estimates for the WD parameters T_{eff}, $\log(g)$, mass and age. The u, g, r, i, z bands from SDSS were used with the DA and DB model tables of Holberg and Bergeron (2006)[2] to obtain these parameters.

The Holberg and Bergeron (2006) DA model table provided the mentioned WD parameters as a function of T_{eff} and $\log(g)$ spanning the range from 1500K-140000K (60 values) and 7.5-9.5 (6 values), respectively. The slight difference with the Holberg and Bergeron (2006) DB model table was that T_{eff} and $\log(g)$ ranged

[2]Available at *http://www.astro.umontreal.ca/∼bergeron/CoolingModels* (02/08/2017) Color and Model Calculations: Holberg & Bergeron (2006, AJ, 132, 1221), Kowalski & Saumon (2006, ApJ, 651, L137), Tremblay et al. (2011, ApJ, 730, 128), and Bergeron et al. (2011, ApJ, 737, 28).

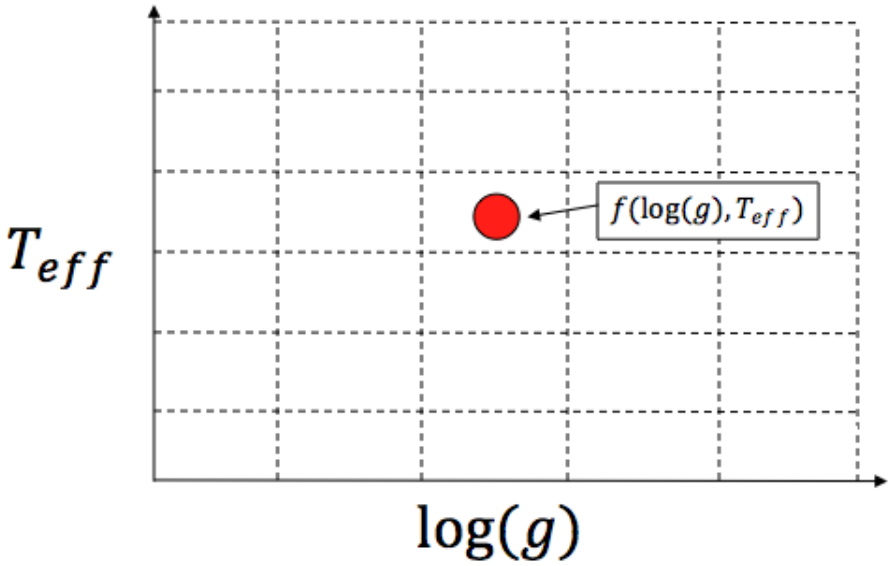

Figure 13: A visualisation of the theoretical 2D-interpolation grid for the Holberg and Bergeron (2006) WD models. The red dot represents a WD candidate's potential T_{eff} and $\log(g)$ values. However, the WD models originally are not precise enough for these values. Therefore interpolation is performed so that values of T_{eff} and $\log(g)$ from a more precise model can be obtained.

from 3500K-40000K (48 values) and 7.5-9.0 (5 values), respectively. In both tables the $\log(g)$ values only increased in steps of 0.5, however, models that increased in smaller values of $\log(g)$ would yield more precise estimates.

Therefore, 2D-interpolation was used to obtain the necessary WD parameters but in $\log(g)$ steps of 0.05 instead (a visualisation of this interpolation grid was displayed in Figure 13). This meant there were then 50 and 40 $\log(g)$ grid points for the DA and DB tables respectively, instead of 6 and 5. Once the new parameter values for the WD model tables were computed, the best model for each WD companion candidate could be identified.

The WD companion's colour within the $u-g$, $g-r$ plane was then calculated. Only the T_{eff} model for each $\log(g)$ with the smallest geometric separation was kept. This was because the colour primarily depended on T_{eff}, and only mildly on $\log(g)$.

With the best T_{eff} model for each $\log(g)$, the WD model distance from Earth

was computed:

$$d_{\mathrm{Earth}} = 10^{(\frac{\mathrm{g}-\mathrm{M_g}}{5}+1)}$$

Where g was the apparent magnitude from SDSS and $\mathrm{M_g}$ was the absolute magnitude from the best Holberg and Bergeron (2006) T_{eff} model for that particular $\log(g)$.

The d_{Earth} for each candidate was then compared to the TGAS distance value for the MS companion, as the MS star and WD companion should have had the same distance.

The only WD parameters kept were from the $\log(g)$ and T_{eff} model with the closest d_{Earth} to the TGAS distance $(1/\pi)$.

$$|1/\pi - d_{\mathrm{Earth}}|$$

Some of the companion stars also had SDSS spectra. Therefore, the computed Holberg and Bergeron (2006) parameters for these companions could be compared to the published parameters by Kleinman et al. (2013) as test cases. This would help add validity to the method.

6 DA and 5 non-DA WD-MS binary candidates with SDSS spectroscopy were used, respectively. The computed values of $\log(g)$, T_{eff} and distance were compared to the fits from Kleinman et al. (2013) for those specific WDs. The Kleinman fits were computed using only SDSS spectroscopy. However, the computed WD distances from the best fitting Holberg and Bergeron (2006) models had the TGAS distances for the MS stars to compare to. Therefore, comparing the computed and Kleinman distances for each WD with the TGAS distances would reveal which model was more accurate.

The results in Table 2 and Figures 14 and 15 suggested the method was reliable. The computed parameters had similar T_{eff}'s to Kleinman but closer WD model distances to the TGAS distances. Based on these test cases being so successful, this interpolation method was used for all of the candidates.

Binary ID	Kleinman T_{eff} [K]	Kleinman $\log(g)$	Kleinman Distance [pc]	Comp. T_{eff} [K]	Comp. $\log(g)$	Comp. Distance [pc]	TGAS Binary Distance [pc]
14895	16284	7.99	356	15000	8.3	260	257
15288	9735	7.63	358	10500	8.05	328	330
21483	17284	7.9	281	15500	8.25	196	193
22554	10269	8.28	117	9000	7.95	136	138
33115	6653	7.83	86	7000	7.8	105	104
34258	8612	8.4	52	8500	8.25	58	59
14303	15584	8.03	376	13000	8.7	180	182
19385	13288	8.47	226	12000	8.0	280	276
24555	15436	8.42	211	15000	7.95	292	293
42087	11146	8.71	162	10000	8.35	188	190
44810	10147	9.44	94	10000	8.6	135	134

Table 2: A comparison of the Kleinman and the computed (Comp) WD parameters. The computed parameters were from fitting the u, g, r, i, z photometry with the Holberg and Bergeron (2006) WD models and the TGAS distances for the MS star. The top 6 systems are the SDSS DA WDs in Figure 20 and the bottom 5 are the SDSS non-DA WDs in Figure 21.

Plots of $\log(g)$ vs. distance (examples in Figures 14 and 15) were created for all 200 remaining candidates and visually inspected. All the candidates where the WD model distance did not agree closely with the TGAS distance and its errors were discarded, leaving 161 candidates.

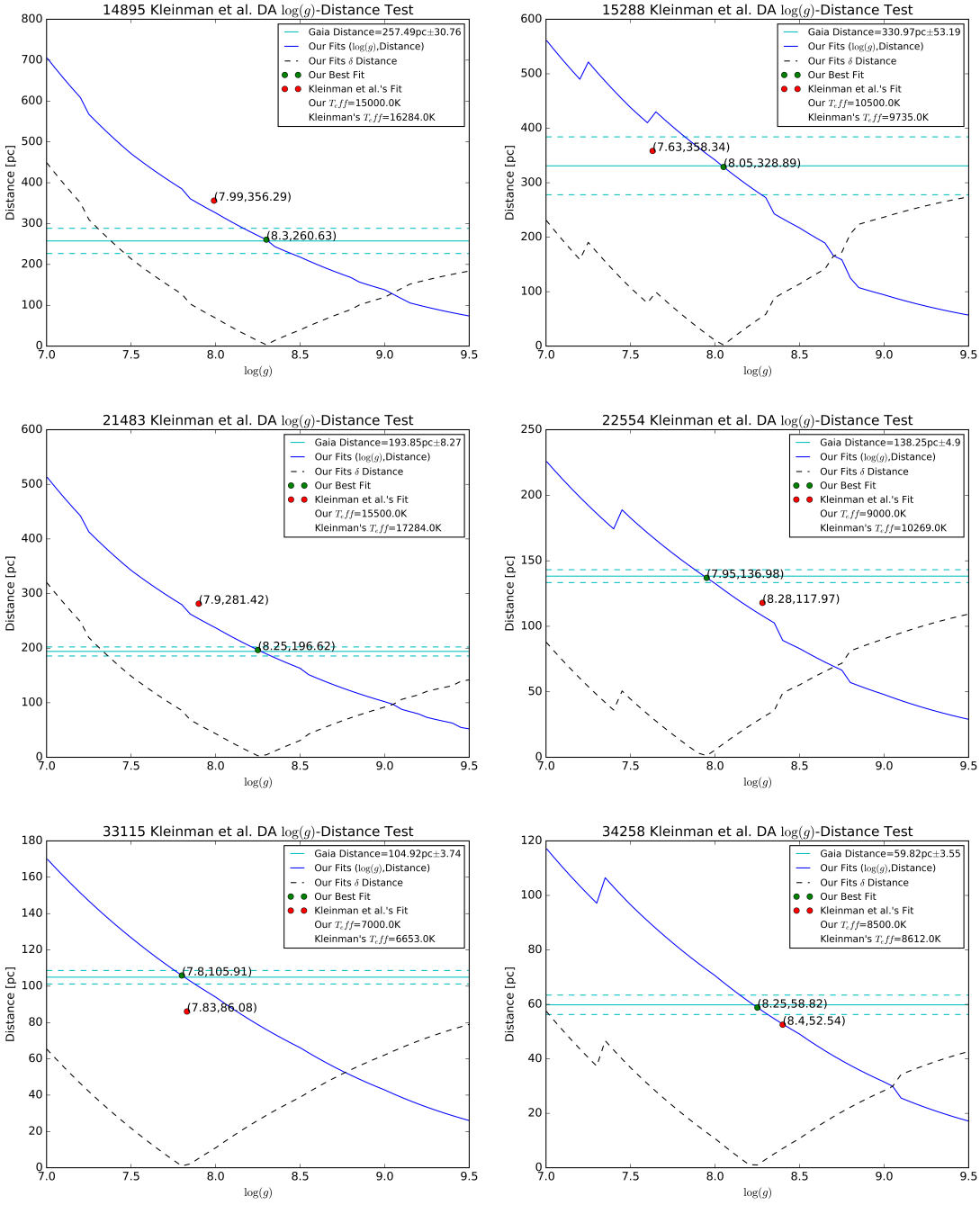

Figure 14: The computed Holberg and Bergeron (2006) DA WD fits compared with the Kleinman et al. (2013) fits to the SDSS u, g, r, i, z photometry for the 6 SDSS DA candidates. *Gaia* distance is the same as TGAS distance.

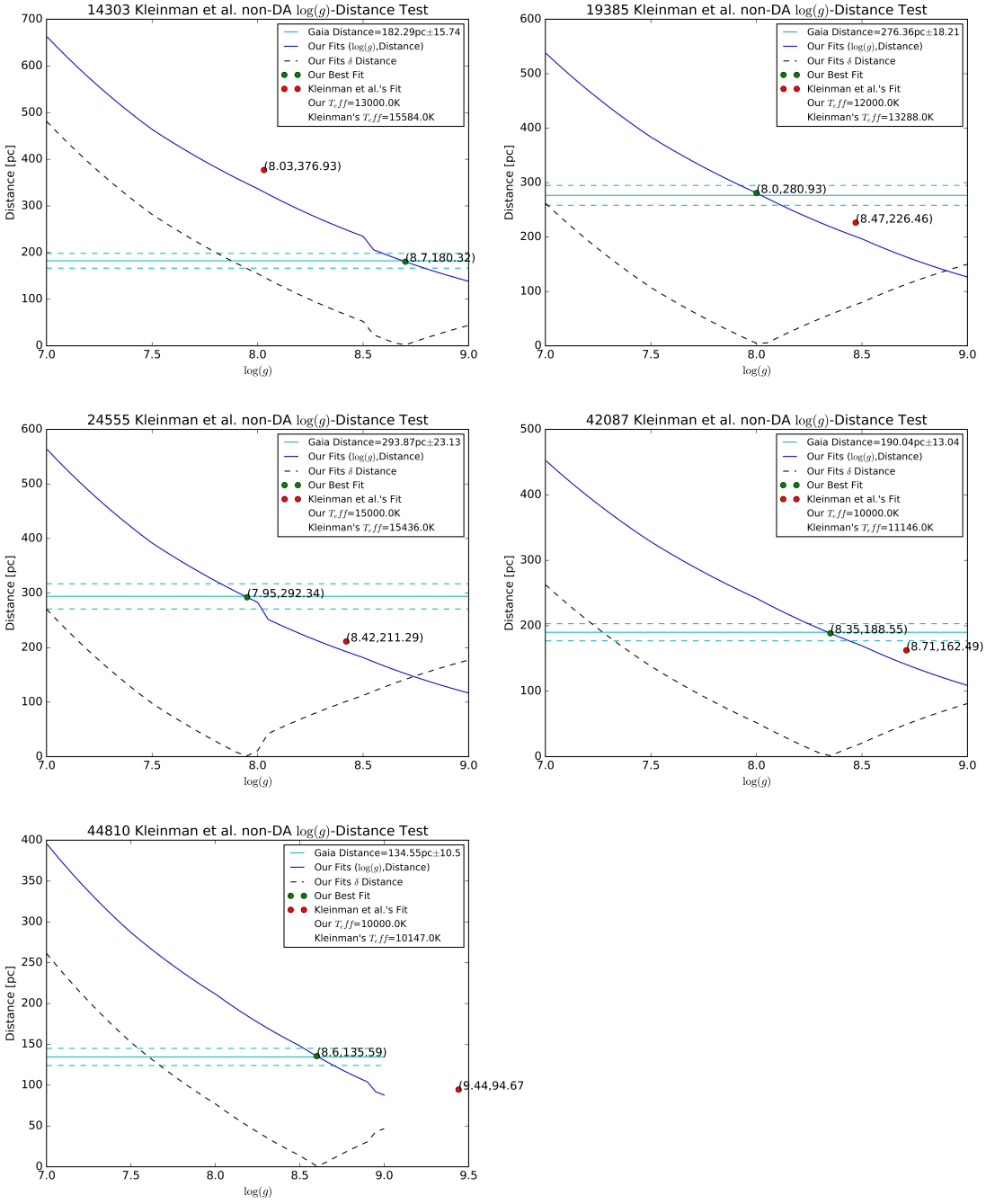

Figure 15: The computed Holberg and Bergeron (2006) DB WD fits compared with the Kleinman et al. (2013) fits to the SDSS u, g, r, i, z photometry for the 5 SDSS non-DA candidates. *Gaia* distance is the same as TGAS distance.

WD MS progenitor mass and MS lifetime

The WD MS progenitor evolved quicker than the MS companion in a WD-MS binary as it had a larger mass. Therefore, an effective cut to remove bad candidates was to discard all candidates where the TGAS MS star masses were larger than the WD MS progenitor masses. WD MS progenitor masses could be calculated by using the WD mass values from the Holberg and Bergeron (2006) model fits and applying an initial-final mass relation (IFMR).

The IMFR equations used were from Cummings et al. (2016). M_{Prog} was the WD MS progenitor mass and M_{WD} was the WD mass in solar masses:

For $M_{Prog} < 4M_{\odot}$:

$$M_{WD} = (0.154 \pm 0.013)M_{Prog} + 0.261 \pm 0.048M_{\odot}$$

For $M_{Prog} \geq 4M_{\odot}$:

$$M_{WD} = (0.097 \pm 0.005)M_{Prog} + 0.514 \pm 0.029M_{\odot}$$

M_{Prog} was the value which needed to be calculated, so a boundary for M_{WD} was necessary to know which equation to use for a particular WD candidate. By solving the equations above for M_{WD} using the M_{Prog} boundary of $4M_{\odot}$ for each equation, the M_{WD} values were $0.877M_{\odot}$ and $0.902M_{\odot}$, respectively. Using the average of these as the M_{WD} boundary, $0.8895M_{\odot}$, (ignoring the uncertainties), the IFMR equations were then:

For $M_{WD} < 0.8895M_{\odot}$:

$$M_{Prog} = \frac{M_{WD} - 0.261}{0.154}$$

For $M_{WD} \geq 0.8895M_{\odot}$:

$$M_{Prog} = \frac{M_{WD} - 0.514}{0.097}$$

The MS lifetimes of the WD MS progenitors were found by taking the M_{Prog} approximations for all of the candidates and using a polynomial fit (Massey and Meyer, 2001):

$$\tau_{Prog} = 10^{10.044571-(3.544350x))+(0.357527x^2)+(0.669038x^3)-(0.205983x^4)}$$

(Where $x = \log_{10}(M_{Prog})$.)

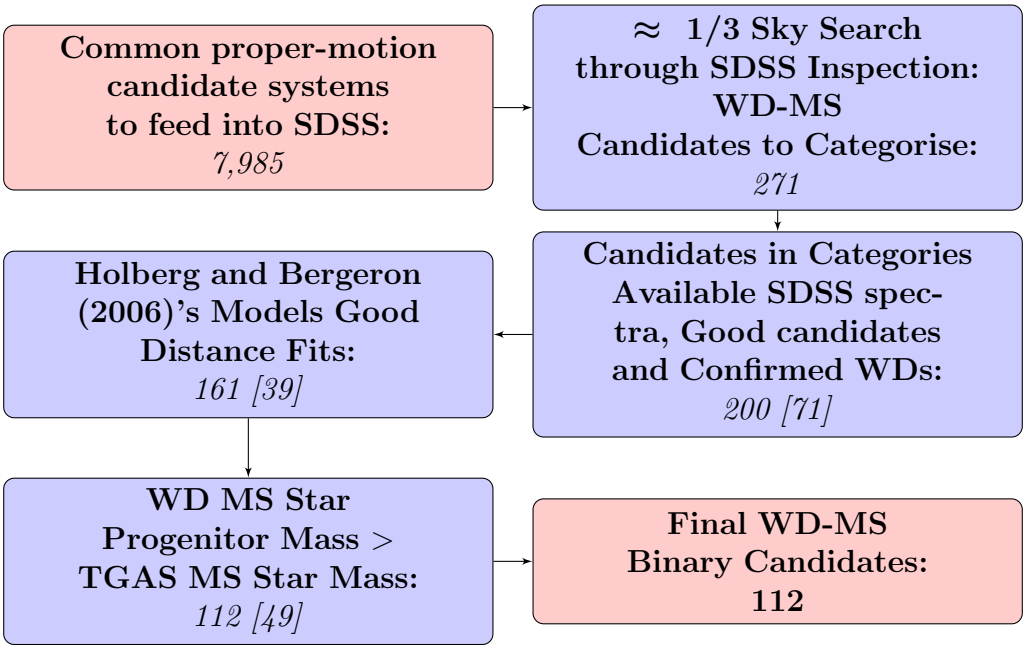

Figure 16: A flow chart documenting the stages of the cuts imposed in finding the WD-MS binary candidates. It also shows the number of candidate systems left at every stage with the amount lost in square brackets.

The WD MS progenitor masses from the IFMR were compared to the MS masses estimated earlier from the ATLAS and PHOENIX tables for the TGAS stars. All candidates with TGAS MS masses larger than the calculated WD MS progenitor masses were discarded. 112 WD-MS binary candidates remained.

The entire procedure of finding the WD-MS binary candidates was illustrated in the flow chart in Figure 16.

We discussed some candidates that were found with interesting characteristics in Section 3.4 on P. 61.

2.3 TGAS error propagation proper-motion correlation term

When the cuts in the methodology were originally made, we failed to realise there was a correlation term in the TGAS catalogue. This term described the relation between the proper-motions in right ascension and declination. When supplied with this value, the error propagation equation changed to:

$$\delta\mu = \frac{1}{\mu}\sqrt{(\mu^{\mathrm{T}}_{\mathrm{pmra}}\delta\mu^{\mathrm{T}}_{\mathrm{pmra}})^2 + (\mu^{\mathrm{T}}_{\mathrm{pmdec}}\delta\mu^{\mathrm{T}}_{\mathrm{pmdec}})^2 + (2\mu^{\mathrm{T}}_{\mathrm{pmra}}\mu^{\mathrm{T}}_{\mathrm{pmdec}}\delta\mu^{\mathrm{T}}_{\mathrm{pmra}}\delta\mu^{\mathrm{T}}_{\mathrm{pmdec}} \times \rho)}$$

(Where $\mu^{\mathrm{T}}_{\mathrm{pmra}}$ and $\mu^{\mathrm{T}}_{\mathrm{pmdec}}$ were the TGAS proper-motions in right ascension and declination, the $\delta\mu^{\mathrm{T}}_{\mathrm{pmra}}$ and $\delta\mu^{\mathrm{T}}_{\mathrm{pmdec}}$ were the errors for the TGAS proper-motions in right ascension and declination, and where ρ was the correlation term of the TGAS proper-motions in right ascension and declination.)

The correlation term could range between -1 and 1, so could have either increased the value of $\delta\mu$ or decreased it. This could have caused the value of $\mu/\delta\mu$ to drastically change. The correlation term was only supplied in the TGAS catalogue, not the PPMXL catalogue, so only the TGAS proper-motion significances would have changed in the method. A new 5σ cut for the TGAS proper-motions was calculated, taking the correlation term into account.

This revealed that 29,844 TGAS objects had been originally cross-matched with PPMXL that were no longer $\geq 5\sigma$. It also revealed that 37,873 TGAS objects had not been cross-matched that had changed to $\geq 5\sigma$. This meant after all of the cuts to create the clean TGAS subset were made, there were 9,500 candidates which should have been included that were not originally.

However, none of the stars that were accidentally cut out of the clean TGAS subset remained after the SDSS visual inspection stage. There were only 3 stars remaining if a 5σ cut on the $\mathrm{PPMXL_{WD}}$ proper-motions was chosen instead of the 7σ cut used. These 3 candidates could have been discarded with the Holberg and Bergeron (2006) WD model fits or when the WD MS progenitor mass cut was performed.

All of the final WD-MS binary candidates still contained TGAS stars with $\geq 5\sigma$ proper-motions when taking the correlation term into account. We concluded that ignoring the correlation term did not change the results.

3 Results

3.1 Validation of the methodology using Tremblay et al. (2017) binaries as a test sample

The aim of the research was to find both new WD-MS binaries, and to confirm previously found Tremblay et al. (2017) binaries. Having a test case of binaries was very important, as it was a way to confirm the validity of the methodology and to identify what steps of the methodology were more successful than others.

There were 46 test binaries at the beginning and 36 were retained within the clean TGAS subset. This means the cuts made in creating the clean TGAS subset were good compromises between efficiency and completeness. However, using the 3σ proper-motion ranges to conclude if the same star existed in both TGAS and PPMXL_{MS} was where the most test binaries were cut. Nevertheless, we felt this cut was justified. If a smaller value of σ was used for the proper-motion ranges, there would have been too many candidates to visually inspect later. We concluded that creating the clean TGAS subset was successful.

Then common proper-motion binary candidates to the clean TGAS subset were identified. The 2σ proper-motion ranges with TGAS and PPMXL_{WD} was where a large number (12) of test binaries were first lost. This was because the 2σ proper-motion ranges were rather strict. Through concluding that the proper-motion uncertainties in TGAS and PPMXL were underestimated, we believed this cut was justified. The 2σ proper-motion ranges were the best balance of having candidates that were most likely common proper-motion pairs without generating too many spurious binary candidates to visually inspect later. The SDSS visual inspection stage was where another large number (11) of test binaries were lost. This was to be expected as SDSS only covered $\approx 1/3$ of the sky. However, this cut was necessary to obtain the u, g, r, i, z band photometry to classify the WD companions.

Finding the WD-MS binary candidates was largely successful, as only 2 test binaries were cut in total. They were cut when candidates were discarded if their computed WD MS progenitor masses were smaller than their TGAS MS companion masses.

Upon reflection, 8 test binaries out of 46 was not a large number. However, restricting ourselves to the SDSS footprint was the biggest limitation of the methodology. The most difficult aspect was the balance of retaining as many WD-MS binary candidates as possible, but not having too many candidates to visually in-

spect later.

It is important to note that the binary T14/HIP 80182 (as seen in Table 3) was also found by Farihi et al. (2005a).

The entire methodology when tested on the Tremblay et al. (2017) test binaries (as seen in Table 3) was illustrated in the flow charts in Figures 17, 18 and 19.

T-ID	**Hip / Tycho 2 IDs**	**T-ID**	**Hip / Tycho 2 IDs**
T1	2600	T24	113244
T2	3550	T25	113786
T3	21088	T26	117308
T4	21482	T27	1011-534-1
T5	34082	T28	1221-1534-1
T6	38594	T29	1438-418-2
T7	52621	T30	1456-876-1
T8	54530	T31	1502-1772-1
T9	59519	T32	1817-1583-1
T10	68145	T33	2023-1076-1
T11	73224	T34	2219-1647-1
T12	76902	T35	2835-349-1
T13	77358	T36	3220-1119-1
T14	80182	T37	4040-1662-1
T15	80522	T38	4153-706-1
T16	83899	T39	4421-2830-1
T17	86938	T40	4598-133-1
T18	92306	T41	4700-510-1
T19	103393	T42	527-72-1
T20	106335	T43	5815-1030-1
T21	108405	T44	5831-189-1
T22	110218	T45	6533-994-1
T23	113231	T46	8712-1589-1

Table 3: A table of known WD-MS binaries from Tremblay et al. (2017). The T-ID numbers are used to easily identify where each test binary was lost during our subsequent cuts illustrated in the flow charts in Figures 17, 18 and 19.

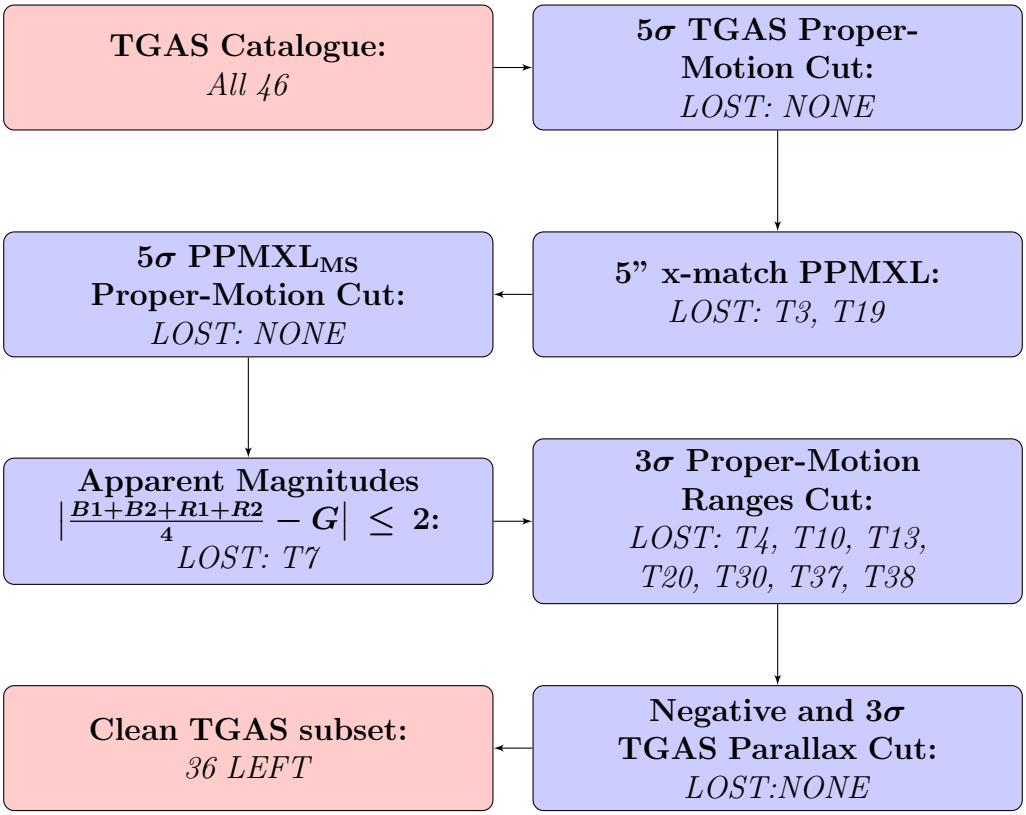

Figure 17: Flow chart documenting the stages of the cuts imposed in creating the clean TGAS subset for the Tremblay et al. (2017) test binaries. ID numbers from Table 3.

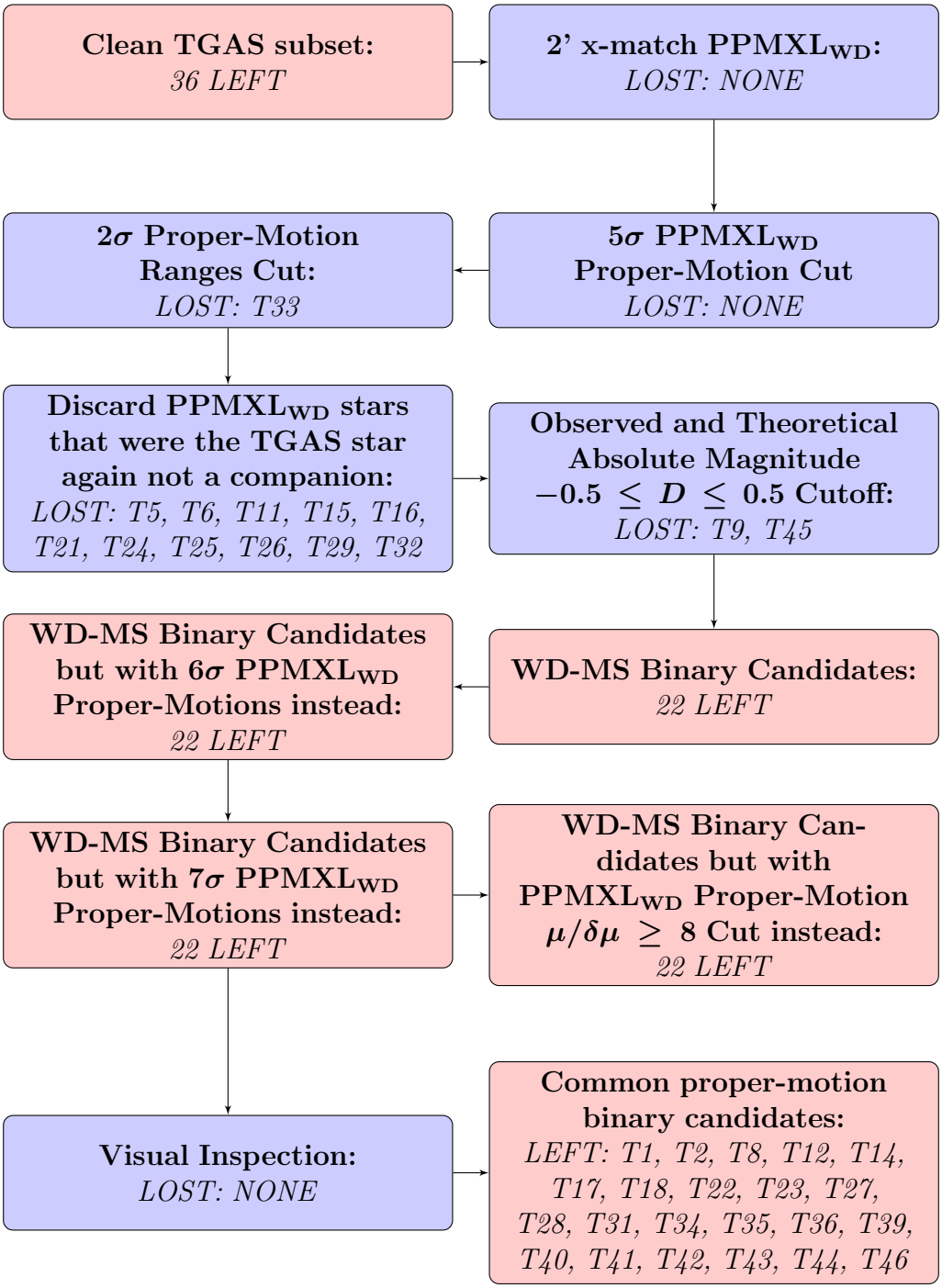

Figure 18: Flow chart documenting the stages of the cuts imposed in finding common proper-motion companions to the clean TGAS subset for the Tremblay et al. (2017) test binaries. ID numbers from Table 3.

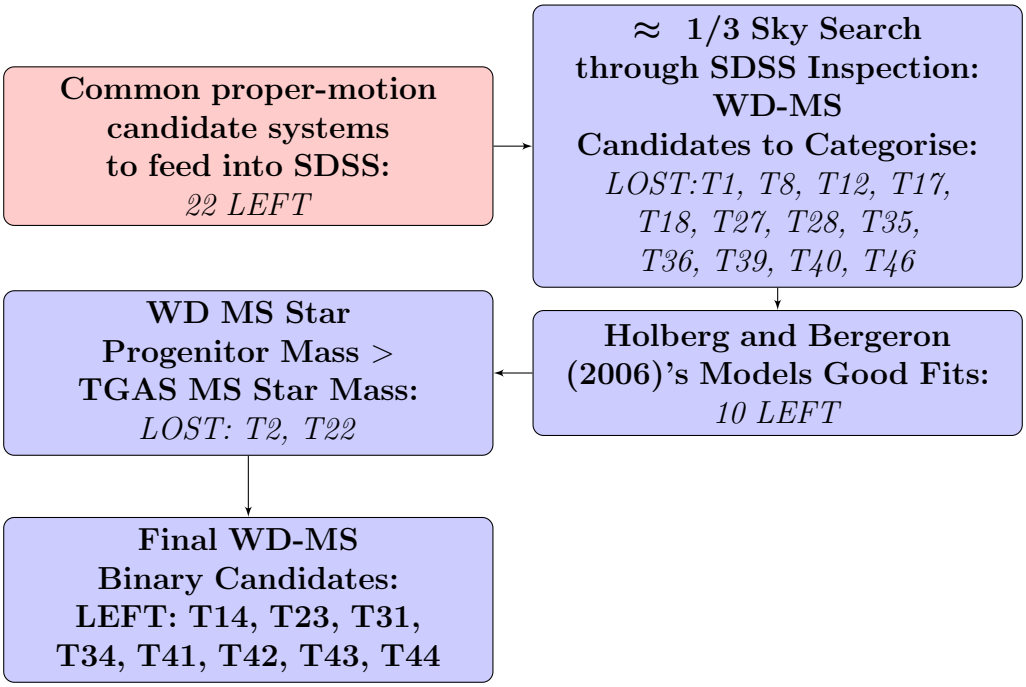

Figure 19: Flow chart documenting the stages of the cuts imposed in finding the WD-MS binary candidates for the Tremblay et al. (2017) test binaries. ID numbers from Table 3.

3.2 Common proper-motion binary candidates with SDSS spectra

There were 271 binary candidates to classify during the methodology. This was before the DA and DB model tables were used to discard any WD candidates with different model distances to the TGAS MS distances (P. 37). As shown in Table 1 on P. 36, 1 of the classification groups contained 29 WD candidates with SDSS spectra.

The SDSS WD spectra of these 29 candidates were normalised and arranged in order of $u - g$, from hot candidates to cooler candidates (Figures 20 and 21 on Pages 51 & 52). The candidates were then individually classified (Table 4 P. 53) and then sorted into 5 groups (Table 5 and Figure 22 on P. 54). These groups were DA, DB, Other, Non-WD and Undetermined.

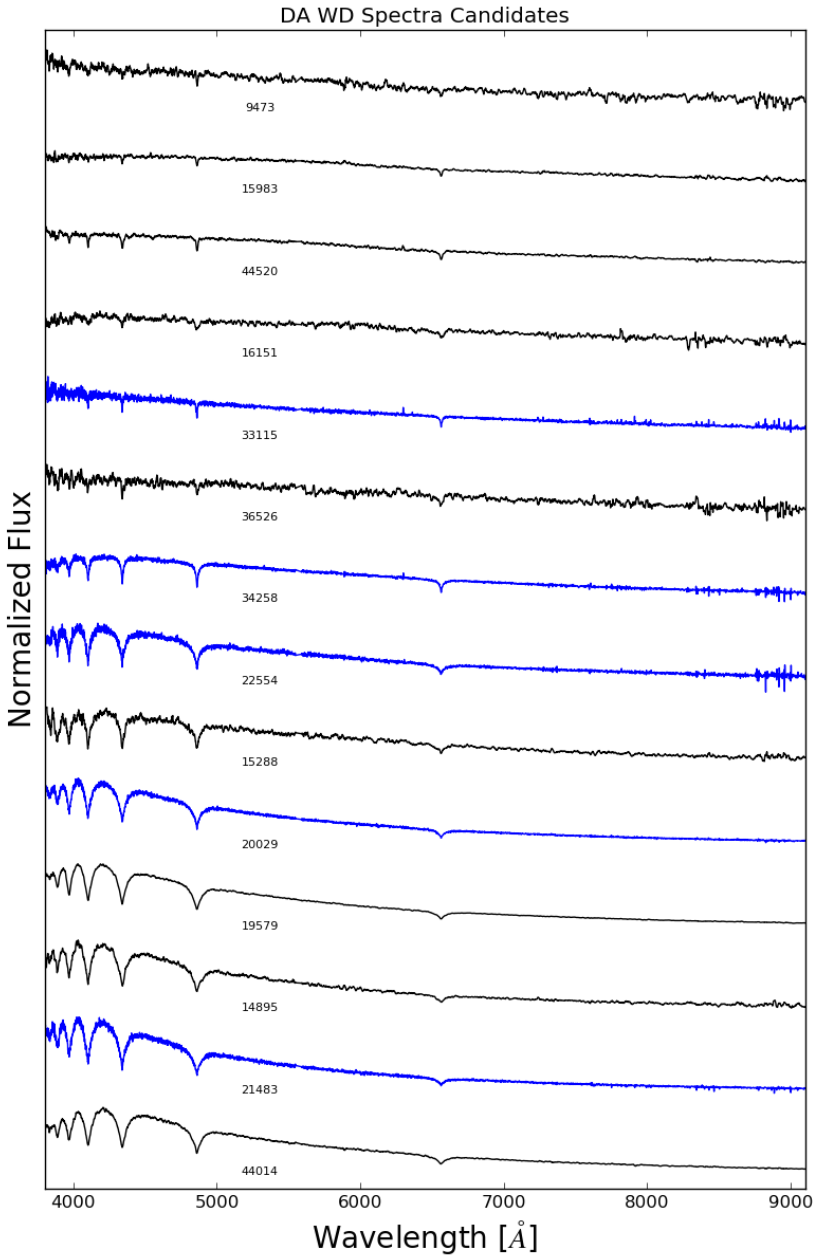

Figure 20: Normalised spectra of our WD candidates confirmed as DA WDs from their SDSS spectroscopy. Ordered by $u - g$ descending from hot candidates to cool candidates. The IDs refer to the binary IDs in our Final WD-MS binary candidates tables (Tables 8, 9 and 10). A Savitzky-Golay filter with a polynomial order of 1 and a window size of 9 is used to smooth the spectra for candidates with a signal-to-noise ratio (S/N) < 10 shown in black. Spectra with a S/N >10 are plotted in blue.

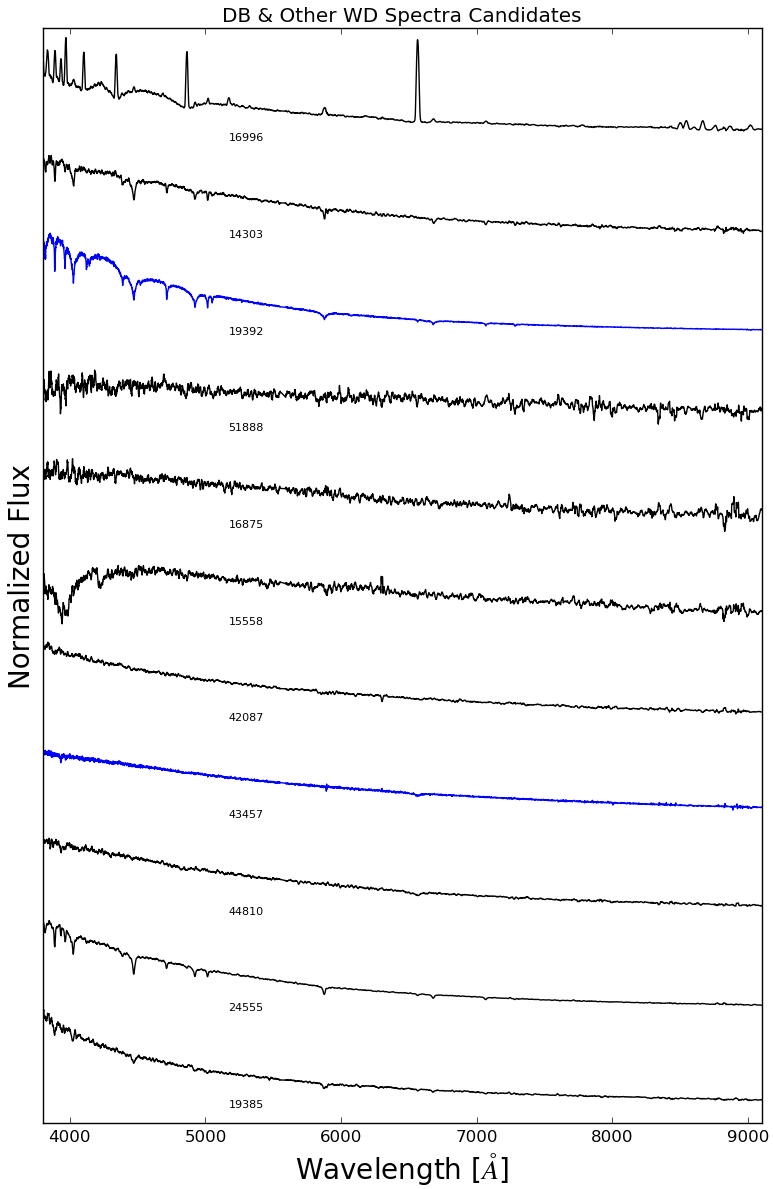

Figure 21: Normalised spectra of our WD candidates confirmed as DB and Other WDs from their SDSS spectroscopy. Ordered by $u - g$ descending from hot candidates to cool candidates. The IDs refer to the binary IDs in our Final WD-MS binary candidates tables (Tables 8, 9 and 10). The top candidate is a CV candidate, the next 2 are spectra of our DB SDSS candidates, the rest are spectra of our Other WD SDSS candidates. A Savitzky-Golay filter with a polynomial order of 1 and a window size of 9 is used to smooth the spectra for candidates with a signal-to-noise ratio (S/N) < 10 shown in black. Spectra with a S/N >10 are plotted in blue.

IDs	Classification based on normalised Spectra	Group
9473	Cool DA	DA
14895	DA	DA
15288	DA	DA
15983	Cool DA	DA
16151	Cool DA	DA
19579	DA	DA
20029	DA	DA
21483	DA	DA
22554	DA (2 WDs)	DA
33115	DA	DA
34258	DA	DA
36526	Cool DA	DA
44014	DA	DA
44520	DA	DA
14303	DB	DB
19392	DB	DB
15558	DZ	Other
16996	CV	Other
19385	Hot DBA	Other
24555	DBZ	Other
42087	DB/DC	Other
43457	Peculiar, DZA	Other
44810	DBA	Other
14060	QSO	Non
17789	QSO	Non
22479	A-Star	Non
34462	No Spectra Data	Non
16875	Cool DC:	Undetermined
51888	Cool DZA:	Undetermined

Table 4: The individual classifications of the WD candidates with SDSS spectra, based on the normalised spectra in Figures 27 and 28. (':' Means undetermined).

Classification Group	Amount
DA	14
DB	2
Other	7
Non-WD	4
Undetermined	2

Table 5: WD candidates with SDSS spectra classifications

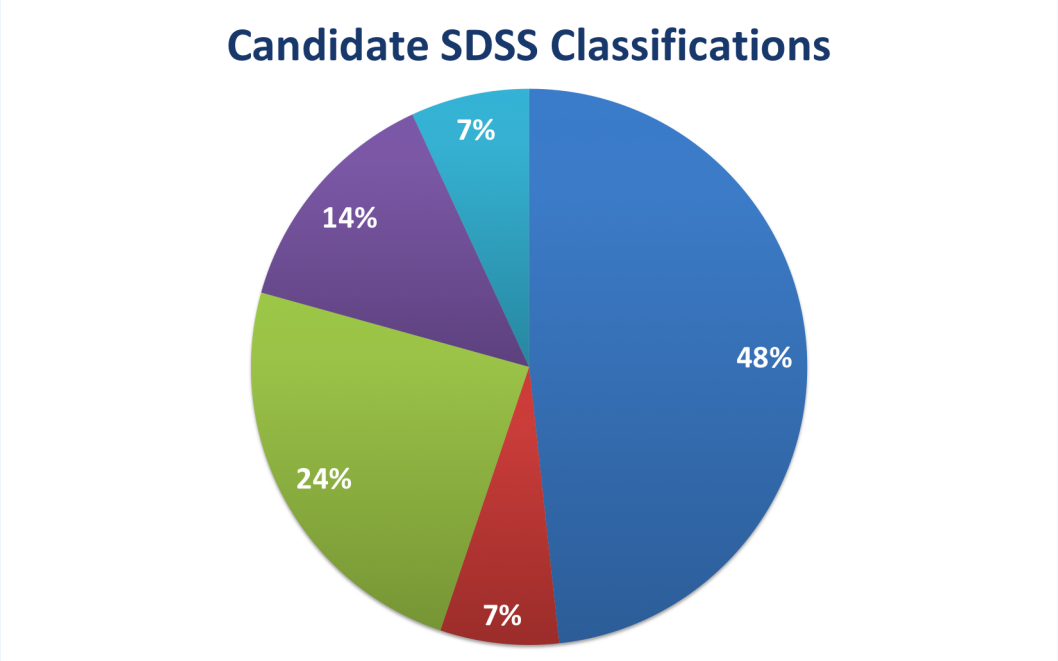

Figure 22: SDSS candidates classification pie chart: (DA WD=Blue, DB WD=Red, Other WD=Green, Non-WD=Purple, Undetermined WD=Light Blue.)

Only 4 of the 29 candidates with SDSS spectra were not WDs. 1 of the 4 non-WD candidates (binary ID:34662) did not have any SDSS spectra data, so the nature of this object could not be identified. The success rate of ≈86% being WDs could be applied onto the final WD-MS binary catalogue, excluding the candidates with SDSS spectra (as shown in Table 6 on P. 55). This suggested that out of the 84 binary candidates that remained ≈72 contained WD companions.

3.3 Final WD-MS binary candidates

The final WD-MS binary candidates left from performing the full methodology was summarised in this subsection. We used 3 classification groups as well as sub groups:

Classification Group	Amount
SDSS DA	10
SDSS Non-DA	11
SDSS Total:	**21**
Good DA	32
Good DB	1
Good DA or DB	51
Good Total:	**84**
Confirmed Total:	**7**
CATALOGUE TOTAL:	**112**

Table 6: Final WD-MS binary candidates classifications

3.3.1 Definitions of final WD-MS binary candidate classification groups

SDSS DA: DA WD candidates with SDSS spectra. WD parameters were from the Holberg and Bergeron (2006) DA WD models.

SDDS Non-DA: Non-DA WD candidates with SDSS spectra. WD parameters were from the Holberg and Bergeron (2006) DB WD models.

Good DA: Good Candidates (P. 36) that had good DA model fits only (P. 40). Also a DA model WD MS progenitor mass > model TGAS MS companion mass (P. 43). WD parameters were from the Holberg and Bergeron (2006) DA WD models.

Good DB: Good Candidates (P. 36) that had good DB model fits only (P. 40). Also a DB model WD MS progenitor mass > model TGAS MS companion mass (P. 43). WD parameters were from the Holberg and Bergeron (2006) DB WD models.

Good DA or DB: Good Candidates (P. 36) that had good DA and DB model fits (P. 40). Also both DA and DB model WD MS progenitor masses > model

TGAS MS companion mass (P. 43). WD parameters were from the Holberg and Bergeron (2006) DA and DB WD models.

Confirmed: Confirmed WDs (on SIMBAD). (Note, Candidates ID:27134 & ID:34821 DB models provided implausible masses and ages, so these must have been strictly DA WDs). WD parameters were from the Holberg and Bergeron (2006) DA and DB WD models.

3.3.2 Final WD-MS binary candidate catalogues

The final WD-MS binary candidates were split into 3 separate catalogues. The catalogues contain ID numbers which we assigned, they represent the entire binary and not just the TGAS or PPMXL star.

Catalogue 1 (as seen in Table 8):
For some of the candidates, their photometry could only be fitted with either the DA or DB Holberg and Bergeron (2006) WD models. Therefore, only 1 set of WD parameters was listed for these candidates. Catalogue 1 contained the 10 'SDSS DA', 11 'SDSS Non-DA', 32 'Good DA' and 1 'Good DB' candidates (as seen in Table 6 in Section 3.3.1).

The other 2 catalogues contained the exact same candidates as each other. However, one contained the DA Holberg and Bergeron (2006) WD parameters and the other contained the DB WD parameters. This was because the photometry for those candidates did not allow us to determine the WD spectral type, as they fitted both the DA and DB Holberg and Bergeron (2006) WD models.

Catalogue 2-DA (as seen in Table 9):
The first of these 2 catalogues, Catalogue 2-DA, contained the 51 'Good DA or DB' and 7 'Confirmed WDs' candidates (as seen in Table 6 in Section 3.3.1). The WD parameters included were the DA Holberg and Bergeron (2006) models.

Catalogue 2-DB (as seen in Table 10):
The second of these 2 catalogues, Catalogue 2-DB, contained the same 51 'Good DA or DB' candidates, but only 5 of the 7 'Confirmed WDs' candidates (as seen in Table 6 in Section 3.3.1). The 2 omitted Confirmed WDs candidates were IDs 27134 and 34821, as they provided implausible WD MS progenitor masses and WD ages with the DB models. Therefore these candidates must have strictly been DA WDs. The WD parameters included were the DB Holberg and Bergeron (2006) models.

Within the final catalogues, some of the values in the MS spectral type column were numbers not letters. This is where the Pickles spectral type model tables estimated a non-MS star for the TGAS star in the binary candidate. We still kept these candidates as the spectral types were only estimates.

Catalogue 1

Classification Group	**Amount**
SDSS DA	10
SDSS Non-DA	11
Good DA	32
Good DB	1

Catalogue 2-DA:
(DA Holberg and Bergeron (2006) WD Models)

Classification Group	**Amount**
Good DA or DB	51
Confirmed WDs	7

Catalogue 2-DB:
(DB Holberg and Bergeron (2006) WD Models)

Classification Group	**Amount**
Good DA or DB	51
Confirmed WDs	5

Table 7: Contents of the final WD-MS binary candidate catalogues

Table 8: **Catalogue 1**: 'SDSS DA', 'SDSS Non-DA', 'Good DA' and 'Good DB' Candidates.

Binary ID	MS RA	MS DEC	WD RA	WD DEC	HIP/Tycho ID	Binary Distance [pc]	Min. Binary Sep. [au]	MS Mass [$M_\odot$]	WD Mass [$M_\odot$]	WD $T_{\rm eff}$ [K]	WD $\log(g)$	WD Age [yrs]	MS SpT	MS G-mag	WD Prog. Mass [$M_\odot$]	WD τ MS [yrs]
9473	01:59:50.6	+15:48:52.2	01:59:50.1	+15:49:55.0	1207-662-1	198	12498	1.31	0.54	6500	7.9	1.67E9	F.8	10.52	1.81	1.46E9
14895	09:35:25.6	+31:12:35.0	09:35:20.6	+31:13:58.5	2494-92-1	257	27210	1.27	0.8	15000	8.3	3.45E8	G.0	11.21	3.51	2.04E8
15288	10:06:26.9	+34:04:22.6	10:06:25.6	+34:04:04.2	2506-833-1	331	8090	1.01	0.63	10500	8.05	5.98E8	F.8	11.55	2.42	5.89E8
16151	10:54:50.5	+60:45:23.7	10:54:53.3	+60:43:36.3	4145-189-1	177	19375	0.9	0.62	6500	8.05	2.09E9	G.2	10.66	2.35	6.47E8
20029	14:56:50.4	+23:55:12.2	14:56:50.0	+23:54:59.5	2017-546-1	223	3059	0.88	0.42	15000	7.6	1.19E8	G.8	12.08	1.05	9.35E9
21483	15:32:47.4	+37:55:18.8	15:32:52.6	+37:53:58.0	3052-1941-1	194	19701	1.25	0.77	15500	8.25	2.92E8	F.5	9.75	3.31	2.39E8
33115	01:28:24.3	-08:23:37.4	01:28:25.0	-08:22:52.6	5274-489-1	105	4806	1.31	0.49	7000	7.8	1.26E9	F.8	9.1	1.5	2.71E9
34258	22:45:25.4	-10:02:36.5	22:45:29.5	-10:02:44.4	5815-1030-1	60	3628	0.72	0.76	8500	8.25	1.65E9	K.2	9.92	3.22	2.58E8
36526	23:55:34.9	+26:57:08.1	23:55:35.8	+26:57:43.1	2255-1593-1	404	14864	1.05	0.52	8000	7.85	9.41E8	14	10.62	1.69	1.85E9
44014	11:51:32.7	+06:23:58.5	11:51:32.1	+06:23:49.1	279-639-1	217	2725	1.08	0.74	17000	8.2	2.04E8	G.2	11.38	3.12	2.81E8
14303	08:30:55.5	+19:33:19.8	08:30:59.4	+19:32:14.5	1387-851-1	182	15585	1.19	1.02	13000	8.7	9.84E8	G.0	10.61	5.2	7.6E7
15558	10:41:58.7	+41:11:14.6	10:41:56.4	+41:10:13.1	3009-1252-1	229	15317	1.25	0.57	7000	8.0	1.55E9	F.5	10.09	2.03	1.01E9
16875	07:49:35.4	+38:15:26.2	07:49:40.5	+38:16:00.6	2959-1526-1	237	16583	1.12	0.57	7000	8.0	1.55E9	G.2	11.43	2.03	1.01E9
16996	07:45:29.0	+45:36:42.3	07:45:31.9	+45:38:30.0	3407-1377-1	313	35001	1.21	0.54	12000	7.9	3.5E8	F.5	10.81	1.79	1.53E9
19385	15:50:31.1	+20:20:24.5	15:50:26.7	+20:19:52.1	1502-375-1	276	19325	1.23	0.58	12000	8.0	3.83E8	24.8	7.26	2.1	9.15E8
19392	15:59:19.2	+19:04:20.1	15:59:21.1	+19:04:08.5	1499-1002-1	144	4150	0.81	0.57	18000	7.95	1.01E8	K.0	11.42	2.02	1.03E9
24555	13:33:02.6	+63:50:34.0	13:33:06.9	+63:49:36.6	4167-380-1	294	18875	1.57	0.57	15000	7.95	1.9E8	F.0	9.9	1.98	1.09E9
42087	14:48:13.7	-00:14:20.3	14:48:13.9	-00:13:24.2	4986-518-1	190	10686	1.05	0.81	10000	8.35	1.21E9	G.2	11.14	3.54	1.99E8
43457	10:24:51.1	-00:24:06.7	10:24:48.9	-00:23:12.3	4905-269-1	74	4746	1.47	0.77	10000	8.3	1.13E9	F.6	7.89	3.33	2.35E8
44810	11:21:26.5	+14:17:33.9	11:21:25.8	+14:17:14.0	861-401-1	135	3023	0.91	0.96	10000	8.6	1.63E9	G.5	10.77	4.6	1.02E8
51888	16:11:19.2	+14:05:40.4	16:11:14.7	+14:06:35.4	957-727-1	132	11245	0.91	0.52	5000	7.9	4.95E9	G.5	10.76	1.67	1.92E9
9973	02:23:23.7	+30:09:53.0	02:23:24.0	+30:08:40.6	2310-1089-1	86	6209	0.83	0.55	9500	7.9	6.33E8	F.5	8.12	1.88	1.3E9
11069	04:33:16.0	+55:27:43.7	04:33:17.5	+55:27:15.4	3736-577-1	72	2232	1.25	0.47	8000	7.75	8.52E8	F.5	7.57	1.36	3.76E9
11128	01:50:45.7	+25:40:44.4	01:50:47.2	+25:41:04.3	1759-1841-1	174	4965	1.43	0.53	10000	7.85	5.29E8	F.6	9.96	1.73	1.71E9
12018	00:33:35.8	+35:07:58.9	00:33:33.2	+35:07:21.6	2270-724-1	111	5452	0.88	0.4	5000	7.65	3.22E9	G.8	10.54	0.92	1.51E10
14472	07:42:05.7	+16:52:26.8	07:42:11.9	+16:53:18.8	1361-1562-1	189	19533	1.23	0.46	6000	7.75	1.73E9	G.0	10.59	1.31	4.29E9
14697	09:08:02.7	+27:33:32.5	09:07:58.2	+27:33:18.9	1957-283-1	84	5194	1.21	0.7	11000	8.15	6.4E8	F.5	7.98	2.84	3.67E8
14767	08:52:56.6	+21:59:00.8	08:53:01.7	+21:59:27.8	1399-180-1	236	17909	0.99	0.57	9500	7.95	6.61E8	G.5	11.73	2.04	1.01E9
15239	10:13:07.8	+35:25:03.6	10:13:09.5	+35:25:07.1	50050	207	4348	1.37	0.74	13500	8.2	3.99E8	F.8	10.48	3.08	2.92E8
15443	11:24:44.4	+33:23:09.7	11:24:43.1	+33:23:25.0	2523-2507-1	214	4839	0.88	0.47	8500	7.75	7.29E8	G.8	11.98	1.37	3.67E9
15604	11:44:33.9	+49:00:17.1	11:44:23.7	+49:00:50.9	3454-721-1	328	34556	1.27	0.46	6000	7.75	1.73E9	G.0	11.7	1.31	4.29E9
15613	11:29:19.9	+49:14:29.1	11:29:16.3	+49:15:57.8	3453-2114-1	226	21539	1.77	0.57	9000	7.95	7.6E8	13.8	9.01	2.03	1.02E9
15625	10:25:03.0	+41:58:16.6	10:24:59.4	+41:58:19.4	3004-782-1	195	7791	1.47	0.76	10500	8.25	8.68E8	F.6	10.05	3.25	2.52E8
16156	10:59:29.1	+60:35:41.1	10:59:23.1	+60:36:23.0	4145-377-1	429	26173	1.13	0.63	10500	8.05	5.98E8	F.6	11.8	2.42	5.89E8
17926	10:08:16.4	+56:46:48.3	10:08:18.5	+56:47:18.5	3818-384-1	163	5625	1.17	0.64	14500	8.05	2.46E8	G.0	10.42	2.48	5.49E8
19765	14:29:13.4	+17:31:56.3	14:29:14.4	+17:32:19.0	70843	160	4311	1.19	0.58	11000	7.95	4.5E8	G.0	10.32	2.06	9.63E8
21867	16:35:06.0	+50:53:13.1	16:35:05.4	+50:53:59.4	3505-2099-1	74	3471	0.91	0.55	10500	7.9	4.87E8	G.5	9.54	1.9	1.25E9
21883	16:39:20.3	+47:47:06.4	16:39:14.3	+47:48:35.8	3502-104-1	132	14249	0.78	0.53	9500	7.85	6.05E8	K.0	11.41	1.72	1.74E9
23124	13:54:24.5	+51:19:21.8	13:54:32.7	+51:18:51.3	3470-405-1	207	17143	1.27	0.65	6000	8.1	2.84E9	F.8	10.59	2.55	5.06E8
23743	12:17:44.4	+62:07:08.0	12:17:55.2	+62:05:56.7	4155-51-1	370	38525	1.27	0.55	10000	7.9	5.53E8	G.0	11.96	1.88	1.29E9
33845	00:17:12.2	-01:18:59.6	00:17:10.1	-01:20:51.9	4664-877-1	310	36056	1.08	0.58	20000	7.9	6.15E7	G.2	12.07	2.06	9.71E8
34553	22:45:00.4	-00:43:54.8	22:44:55.3	-00:42:30.3	5234-990-1	98	11066	1.09	0.5	4750	7.85	5.51E9	13.8	7.43	1.56	2.38E9
34735	22:27:11.6	-00:18:43.8	22:27:15.5	-00:18:17.6	5226-28-1	88	5611	1.37	0.48	4750	7.8	5.10E9	F.8	8.66	1.4	3.47E9
35351	23:24:30.3	+10:08:56.9	23:24:32.8	+10:08:53.0	1165-1185-1	155	5869	1.01	0.65	20000	8.05	8.17E7	F.8	9.98	2.56	4.99E8
41285	12:47:27.0	-17:14:59.6	12:47:25.1	-17:14:22.5	6104-178-1	206	9422	1.25	0.58	10000	7.95	5.78E8	F.5	9.85	2.04	9.94E8
41884	11:56:41.2	-02:46:44.2	11:56:40.3	-02:48:15.2	4935-756-1	46	4220	0.75	1.37	6000	9.5	3.04E9	K.0	9.15	8.77	2.62E7
42329	13:05:32.7	+00:13:05.6	13:05:33.4	+00:13:18.7	298-336-1	346	5702	1.31	0.53	10000	7.85	5.29E8	F.8	11.72	1.73	1.71E9
42690	13:13:26.6	+12:12:24.8	13:13:31.9	+12:11:16.3	887-831-1	99	10248	0.72	0.48	5500	7.8	2.51E9	K.2	11.1	1.45	3.08E9
43661	10:33:56.2	+02:58:00.0	10:33:58.8	+02:57:44.6	51712	156	6428	1.41	0.66	8500	8.1	1.21E9	14.2	8.91	2.59	4.8E8
44050	12:13:53.5	+06:55:11.7	12:13:51.9	+06:54:47.8	287-592-1	151	5182	1.05	0.63	10500	8.05	5.98E8	F.8	9.79	2.42	5.89E8
45101	12:00:12.6	+26:37:06.6	12:00:20.5	+26:37:31.7	1988-1319-1	157	17065	1.09	0.45	5000	7.75	3.92E9	F.6	9.67	1.25	5.12E9
51768	16:06:29.2	+09:19:02.4	16:06:26.2	+09:19:30.2	945-949-1	80	4247	0.91	1.25	8000	9.15	3.03E9	G.8	9.77	7.56	3.45E7
53367	17:22:53.2	+28:48:31.5	17:22:51.9	+28:48:47.1	2086-1185-1	59	1325	0.83	0.53	5000	7.9	4.98E9	G.8	9.37	1.74	1.66E9
21003	16:40:12.8	+34:23:29.2	16:40:09.9	+34:24:43.7	2585-2617-1	366	30290	1.09	0.47	7000	7.8	1.28E9	F.6	11.53	1.39	3.56E9

The first block are the 'SDSS DA' WDs, the second block are the 'SDSS Non-DA' WDs, the third block are the 'Good DA' WDs and the last candidate is the 'Good DB' WD. Non-letter spectral types are for candidates where their Pickles estimate predicted a non-MS TGAS star.

Table 9: **Catalogue 2-DA**: 'Good DA or DB' and 'Confirmed WDs' candidates: DA Holberg and Bergeron (2006) WD Models.

Binary ID	MS RA	MS DEC	WD RA	WD DEC	HIP/Tycho ID	Binary Distance [pc]	Min. Binary Sep. [au]	MS Mass [$M_\odot$]	WD Mass [$M_\odot$]	WD $T_{\rm eff}$ [K]	WD $\log(g)$	WD Age [yrs]	MS SpT	MS G-mag	WD Prog. Mass [$M_\odot$]	WD τ MS [yrs]
9642	02:34:28.8	+23:30:03.7	02:34:26.1	+23:31:18.3	11976	124	10290	0.89	0.78	5500	8.3	5.51E9	13.8	7.84	3.37	2.27E8
12372	01:09:31.6	+45:57:30.0	01:09:40.8	+45:58:38.1	3264-405-1	157	18436	0.94	0.75	5250	8.25	6.21E9	G.5	11.05	3.15	2.74E8
13943	10:06:39.8	+20:08:13.1	10:06:37.4	+20:09:38.5	1418-63-1	179	16410	0.87	0.51	6000	7.85	1.94E9	14.5	9.59	1.64	2.04E9
14112	09:53:16.9	+24:45:36.2	09:53:16.0	+24:45:16.0	1961-23-1	180	4277	1.09	0.75	7500	8.25	2.27E9	F.6	10.02	3.2	2.61E8
14118	09:43:46.8	+24:03:54.6	09:43:51.5	+24:05:13.3	1960-1029-1	270	27438	1.3	0.66	7500	8.1	1.67E9	14.5	10.21	2.58	4.89E8
14398	08:34:07.7	+16:56:43.6	08:34:05.6	+16:57:03.9	1392-804-1	196	7224	0.9	1.21	10500	9.05	2.21E9	14.5	9.71	7.22	3.78E7
15357	11:37:24.6	+40:19:52.5	11:37:26.0	+40:19:44.4	3013-1689-1	94	1627	0.66	0.76	8000	8.25	1.93E9	K.2	11.18	3.21	2.59E8
15419	11:02:19.6	+33:49:19.4	11:02:18.3	+33:51:05.6	2521-2011-1	77	8270	0.72	0.75	5500	8.25	5.12E9	K.2	10.4	3.16	2.71E8
15615	11:26:56.0	+49:50:45.9	11:27:04.2	+49:50:01.3	3453-1591-1	119	10834	0.78	0.51	6000	7.85	1.94E9	K.0	11.13	1.64	2.04E9
16373	07:43:19.7	+32:02:25.4	07:43:17.9	+32:01:06.0	2458-68-1	86	7125	0.58	0.97	5500	8.6	6.87E9	K.4	11.67	4.68	9.78E7
16394	08:01:08.1	+29:43:10.1	08:01:09.1	+29:43:33.9	1938-507-1	134	3580	0.99	0.59	6000	8.0	2.24E9	G.5	10.49	2.12	8.81E8
16519	07:34:21.6	+31:13:53.3	07:34:28.1	+31:13:07.4	2453-1175-1	157	14837	1.41	1.0	12000	8.65	1.1E9	14.2	8.8	5.06	8.11E7
16895	07:49:29.1	+37:37:00.4	07:49:20.4	+37:37:35.6	2959-1475-1	130	14275	0.84	1.08	6000	8.8	5.16E9	G.8	11.01	5.86	5.83E7
17148	06:27:51.9	+35:00:12.0	06:27:48.8	+35:00:02.5	2430-652-1	53	2044	1.01	0.59	6500	8.0	1.83E9	G.2	8.41	2.14	8.64E8
19057	14:34:19.1	+05:52:00.8	14:34:16.6	+05:51:13.6	331-608-1	159	9503	0.94	1.05	6500	8.75	4.42E9	G.0	10.24	5.57	6.51E7
20366	14:38:55.1	+26:39:15.2	14:39:01.0	+26:40:03.3	2018-121-1	140	12886	0.68	1.26	6500	9.2	3.69E9	K.2	11.98	7.72	3.31E7
20682	16:39:02.8	+30:05:17.7	16:38:59.3	+30:03:48.6	2582-2246-1	197	19712	0.88	0.51	5250	7.85	3.6E9	G.8	11.84	1.59	2.23E9
20811	16:41:05.5	+33:37:49.1	16:41:13.4	+33:37:51.4	2585-993-1	179	17821	1.12	1.03	6500	8.7	4.42E9	G.2	10.77	5.28	7.34E7
21882	16:39:20.3	+47:47:06.4	16:39:15.9	+47:45:50.7	3502-104-1	132	11559	0.78	0.97	6000	8.6	5.22E9	K.0	11.41	4.69	9.69E7
25211	21:30:01.2	+08:41:07.9	21:30:03.8	+08:39:22.2	1119-528-1	173	19386	1.13	1.0	6000	8.65	5.2E9	F.6	9.83	4.99	8.4E7
25547	22:01:23.9	+14:59:16.2	22:01:19.7	+14:58:22.4	1147-1365-1	246	19992	0.8	0.73	9500	8.2	1.1E9	F.6	10.58	3.03	3.06E8
25691	21:58:41.4	+22:34:20.0	21:58:47.7	+22:35:02.9	2203-1857-1	97	9481	1.3	1.11	5500	8.85	6.36E9	14.5	8.08	6.14	5.27E7
27552	22:28:36.8	+35:33:47.9	22:28:45.7	+35:32:57.0	2742-83-1	266	31956	1.23	0.95	11500	8.55	1.01E9	G.0	11.37	4.49	1.08E8
32330	00:16:22.2	-19:23:58.6	00:16:20.8	-19:23:31.3	5842-923-1	77	2655	1.27	1.0	11000	8.65	1.35E9	G.0	8.58	5.05	8.15E7
33129	01:05:43.2	-07:16:16.3	01:05:44.5	-07:15:59.4	4683-183-1	119	3096	0.78	0.82	7000	8.35	3.11E9	K.0	11.06	3.62	1.88E8
33444	02:14:02.5	+01:56:58.3	02:14:02.2	+01:57:56.7	38-508-1	318	18566	1.05	0.88	7500	8.45	3.06E9	F.8	11.35	4.04	1.4E8
33482	02:22:00.9	+04:44:48.3	02:21:57.9	+04:45:17.9	42-1187-1	39	2062	0.94	0.59	7000	8.0	1.52E9	G.5	8.01	2.15	8.48E8
34100	01:15:31.5	+12:23:36.0	01:15:35.6	+12:22:15.3	616-345-1	89	8941	0.61	1.11	7500	8.85	3.55E9	K.3	11.52	6.16	5.22E7
34462	22:31:13.3	-02:31:07.5	22:31:09.7	-02:30:04.4	5236-62-1	159	13208	1.09	0.72	6500	8.2	2.87E9	F.6	9.74	2.98	3.21E8
34527	23:38:23.0	+00:21:52.8	23:38:18.2	+00:21:51.8	585-841-1	146	10531	0.84	0.91	6000	8.5	5.24E9	G.8	11.28	4.11	1.34E8
34558	22:34:01.8	+00:32:34.2	22:33:58.9	+00:32:39.1	567-371-1	209	9187	1.01	0.75	6000	8.25	3.74E9	G.5	11.48	3.18	2.67E8
35219	00:15:21.4	+04:47:55.9	00:15:19.8	+04:48:50.6	5-747-1	133	7895	0.88	1.01	13000	8.65	9.22E8	G.8	10.92	5.07	8.06E7
35261	00:05:27.4	+06:55:56.5	00:05:32.1	+06:55:23.9	7-988-1	165	12521	0.78	1.33	15000	9.4	1.25E9	K.0	11.79	8.44	2.81E7
36813	23:35:10.9	+33:49:23.7	23:35:11.8	+33:47:26.3	2774-1673-1	143	16810	0.99	0.97	5500	8.6	6.87E9	F.8	9.8	4.68	9.78E7
38569	07:35:56.6	+14:07:23.4	07:36:00.9	+14:08:44.1	777-826-1	224	23004	1.05	0.72	6000	8.2	3.44E9	G.2	11.51	2.97	3.24E8
42234	13:48:28.6	+03:23:49.4	13:48:21.6	+03:24:06.0	311-1198-1	283	30079	1.15	0.65	6000	8.1	2.84E9	G.2	11.72	2.55	5.06E8
42260	13:58:17.4	+04:48:52.2	13:58:20.9	+04:50:23.0	312-254-1	122	12846	1.27	0.65	6500	8.1	2.35E9	G.0	9.56	2.56	4.99E8
42332	12:57:28.3	+01:30:47.4	12:57:32.3	+01:31:51.4	291-793-1	255	22395	1.25	0.91	6000	8.5	5.24E9	F.5	10.34	4.11	1.34E8
42487	12:41:23.4	+08:15:28.7	12:41:19.0	+08:15:12.2	875-668-1	256	17100	1.62	0.65	6500	8.1	2.35E9	F.0	9.54	2.56	4.99E8
42775	13:44:55.3	+15:39:28.6	13:44:52.1	+15:41:17.8	1460-765-1	115	13578	0.91	0.91	5250	8.5	8.02E9	G.5	10.47	4.08	1.37E8
44190	11:26:11.1	+07:24:13.6	11:26:16.4	+07:25:09.0	270-421-1	126	12162	1.47	1.25	9000	9.15	2.6E9	F.6	9.2	7.56	3.45E7
44328	11:54:20.3	+13:46:06.9	11:54:28.0	+13:46:39.8	870-836-1	132	15422	0.72	0.65	5500	8.1	3.95E9	K.2	11.6	2.52	5.2E8
44424	12:52:34.1	+13:32:34.4	12:52:31.9	+13:32:41.0	888-843-1	68	2217	1.01	0.49	6000	7.8	1.84E9	K.2	10.28	1.47	2.89E9
44475	12:42:40.1	+18:46:24.1	12:42:41.2	+18:46:39.7	1448-21-1	81	1714	1.19	0.66	7500	8.1	1.67E9	G.0	8.87	2.58	4.89E8
44476	13:06:59.2	+14:53:36.1	13:06:58.3	+14:53:07.0	890-669-1	161	5144	0.75	0.75	7500	8.25	2.27E9	K.2	11.98	3.2	2.61E8
44770	11:09:38.5	+15:40:52.4	11:09:44.4	+15:40:57.7	1430-1443-1	124	10640	0.81	1.2	6500	9.0	4.4E9	K.0	11.05	7.02	3.99E7
49875	20:14:15.6	+00:43:51.7	20:14:09.9	+00:43:58.6	495-1108-1	125	10772	1.34	1.08	4250	8.8	8.16E9	14.2	8.44	5.84	5.88E7
50927	16:27:36.2	-00:40:57.2	16:27:43.3	-00:41:35.5	5035-543-1	140	15755	0.94	0.75	6000	8.25	3.74E9	G.5	10.83	3.18	2.67E8
51256	15:37:43.6	-02:06:16.0	15:37:35.8	-02:05:59.5	5021-299-1	100	11800	1.01	0.85	5500	8.4	6.29E9	G.2	9.76	3.8	1.65E8
51850	16:02:11.0	+11:53:51.9	16:02:05.8	+11:53:12.1	952-279-1	89	7642	0.66	0.71	5000	8.2	6.90E9	K.3	11.16	2.93	3.36E8
52654	17:44:40.5	+18:14:54.8	17:44:33.7	+18:15:07.6	1556-669-1	68	6679	0.78	0.88	5250	8.45	7.66E9	K.0	9.94	4.0	1.44E8
19370	15:56:13.7	+21:23:27.8	15:56:18.8	+21:23:55.1	1502-1772-1	103	7771	0.99	0.57	25000	7.85	2.05E7	G.5	10.0	1.99	1.08E9
27134	22:31:53.2	+23:51:50.6	22:31:45.5	+23:51:23.5	2219-1647-1	111	12217	1.3	0.55	17000	7.85	1.1E8	14.5	8.3	1.86	1.35E9
32983	23:53:28.7	-08:04:19.4	23:53:27.8	-08:04:39.0	5831-189-1	100	2365	0.78	0.78	20000	8.25	1.33E8	K.0	10.8	3.36	2.3E8
33321	02:53:31.3	-00:34:08.0	02:53:32.3	-00:33:44.8	4700-510-1	48	1306	0.83	0.47	7500	7.75	1.0E9	G.8	8.87	1.35	3.90E9
34238	22:55:50.0	-07:49:21.4	22:55:49.5	-07:50:02.4	113231	36	1492	0.98	0.54	6500	7.9	1.67E9	G.5	7.8	1.81	1.46E9
34821	21:11:46.7	+01:21:27.5	21:11:46.4	+01:20:54.5	527-72-1	61	2040	0.64	0.61	15500	8.0	1.78E8	K.3	10.52	2.29	6.95E8
51869	16:22:07.1	+12:12:52.4	16:22:03.9	+12:13:33.6	967-190-1	56	3528	1.23	1.19	140000	9.35	0.01589	G.0	8.01	6.96	4.06E7

The first block are the 'Good DA or DB' WDs and the second block are the 'Confirmed WDs'. All of their WD parameters are for the Holberg and Bergeron (2006) DA WD models. Non-letter spectral types are for candidates where their Pickles estimate predicted a non-MS TGAS star.

Table 10: **Catalogue 2-DB**: 'Good DA or DB' and 'Confirmed WDs' candidates: DB Holberg and Bergeron (2006) WD Models.

Binary ID	MS RA	MS DEC	WD RA	WD DEC	HIP/Tycho ID	Binary Distance [pc]	Min. Binary Sep. [au]	MS Mass [$M_\odot$]	WD Mass [$M_\odot$]	WD $T_{\rm eff}$ [K]	WD $\log(g)$	WD Age [yrs]	MS SpT	MS G-mag	WD Prog. Mass [$M_\odot$]	WD τ MS [yrs]
9642	02:34:28.8	+23:30:03.7	02:34:26.1	+23:31:18.3	11976	124	10290	0.89	0.67	5250	8.15	5.39E9	13.8	7.84	2.64	4.53E8
12372	01:09:31.6	+45:57:30.0	01:09:40.8	+45:58:38.1	3264-405-1	157	18436	0.94	0.6	5000	8.05	5.76E9	G.5	11.05	2.21	7.79E8
13943	10:06:39.8	+20:08:13.1	10:06:37.4	+20:09:38.5	1418-63-1	179	16410	0.87	0.47	6000	7.8	2.07E9	14.5	9.59	1.37	3.72E9
14112	09:53:16.9	+24:45:36.2	09:53:16.0	+24:45:16.0	1961-23-1	180	4277	1.09	0.74	7500	8.25	2.25E9	F.6	10.02	3.1	2.87E8
14118	09:43:46.8	+24:03:54.6	09:43:51.5	+24:05:13.3	1960-1029-1	270	27438	1.3	0.74	8000	8.25	1.93E9	14.5	10.21	3.1	2.85E8
14398	08:34:07.7	+16:56:43.6	08:34:05.6	+16:57:03.9	1392-804-1	196	7224	0.9	1.05	9000	8.75	2.33E9	14.5	9.71	5.47	6.77E7
15357	11:37:24.6	+40:19:52.5	11:37:26.0	+40:19:44.4	3013-1689-1	94	1627	0.66	0.67	8000	8.15	1.6E9	K.2	11.18	2.68	4.34E8
15419	11:02:19.6	+33:49:19.4	11:02:18.3	+33:51:05.6	2521-2011-1	77	8270	0.72	0.6	5250	8.05	5.0E9	K.2	10.4	2.21	7.73E8
15615	11:26:56.0	+49:50:45.9	11:27:04.2	+49:50:01.3	3453-1591-1	119	10834	0.78	0.5	6000	7.85	2.19E9	K.0	11.13	1.53	2.54E9
16373	07:43:19.7	+32:02:25.4	07:43:17.9	+32:01:06.0	2458-68-1	86	7125	0.58	0.73	5000	8.25	6.35E9	K.4	11.67	3.07	2.95E8
16394	08:01:08.1	+29:43:10.1	08:01:09.1	+29:43:33.9	1938-507-1	134	3580	0.99	0.57	6000	8.0	2.57E9	G.5	10.49	2.02	1.03E9
16519	07:34:21.6	+31:13:53.3	07:34:28.1	+31:13:07.4	2453-1175-1	157	14837	1.41	0.71	9500	8.2	1.12E9	14.2	8.8	2.91	3.44E8
16895	07:49:29.1	+37:37:00.4	07:49:20.4	+37:37:35.6	2959-1475-1	130	14275	0.84	0.93	5500	8.55	6.13E9	G.8	11.01	4.26	1.23E8
17148	06:27:51.9	+35:00:12.0	06:27:48.8	+35:00:02.5	2430-652-1	53	2044	1.01	0.57	6500	8.0	1.87E9	G.2	8.41	2.03	1.02E9
19057	14:34:19.1	+05:52:00.8	14:34:16.6	+05:51:13.6	331-608-1	159	9503	0.94	0.93	6000	8.55	5.18E9	G.0	10.24	4.27	1.22E8
20366	14:38:55.1	+26:39:15.2	14:39:01.0	+26:40:03.3	2018-121-1	140	12886	0.68	1.19	6000	9.0	4.29E9	K.2	11.98	6.93	4.1E7
20682	16:39:02.8	+30:05:17.7	16:38:59.3	+30:03:48.6	2582-2246-1	197	19712	0.88	0.49	5250	7.85	3.99E9	G.8	11.84	1.51	2.68E9
20811	16:41:05.5	+33:37:49.1	16:41:13.4	+33:37:51.4	2585-993-1	179	17821	1.12	0.9	6000	8.5	5.28E9	G.2	10.77	3.98	1.46E8
21882	16:39:20.3	+47:47:06.4	16:39:15.9	+47:45:50.7	3502-104-1	132	11559	0.78	0.96	6000	8.6	5.08E9	K.0	11.41	4.57	1.03E8
25211	21:30:01.2	+08:41:07.9	21:30:03.8	+08:39:22.2	1119-528-1	173	19386	1.13	0.83	5500	8.4	5.82E9	F.6	9.83	3.72	1.75E8
25547	22:01:23.9	+14:59:16.2	22:01:19.7	+14:58:22.4	1147-1365-1	246	19992	0.8	0.43	8000	7.7	8.33E8	F.6	10.58	1.08	8.36E9
25691	21:58:41.4	+22:34:20.0	21:58:47.7	+22:35:02.9	2203-1857-1	97	9481	1.3	1.01	5250	8.7	5.96E9	14.5	8.08	5.15	7.78E7
27552	22:28:36.8	+35:33:47.9	22:28:45.7	+35:32:57.0	2742-83-1	266	31956	1.23	0.58	9000	8.0	8.2E8	G.0	11.37	2.06	9.71E8
32330	00:16:22.2	-19:23:58.6	00:16:20.8	-19:23:31.3	5842-923-1	77	2655	1.27	0.74	9500	8.25	1.22E9	G.0	8.58	3.12	2.82E8
33129	01:05:43.2	-07:16:16.3	01:05:44.5	-07:15:59.4	4683-183-1	119	3096	0.78	0.8	7000	8.35	3.05E9	K.0	11.06	3.52	2.02E8
33444	02:14:02.5	+01:56:58.3	02:14:02.2	+01:57:56.7	38-508-1	318	18566	1.05	0.96	8000	8.6	2.81E9	F.8	11.35	4.59	1.02E8
33482	02:22:00.9	+04:44:48.3	02:21:57.9	+04:45:17.9	42-1187-1	39	2062	0.94	0.71	7500	8.2	2.06E9	G.5	8.01	2.89	3.51E8
34100	01:15:31.5	+12:23:36.0	01:15:35.6	+12:22:15.3	616-345-1	89	8941	0.61	1.1	7500	8.85	3.25E9	K.3	11.52	6.05	5.44E7
34462	22:31:13.3	-02:31:07.5	22:31:09.7	-02:30:04.4	5236-62-1	159	13208	1.09	0.7	6500	8.2	2.87E9	F.6	9.74	2.88	3.54E8
34527	23:38:23.0	+00:21:52.8	23:38:18.2	+00:21:51.8	585-841-1	146	10531	0.84	0.9	6000	8.5	5.28E9	G.8	11.28	3.98	1.46E8
34558	22:34:01.8	+00:32:34.2	22:33:58.9	+00:32:39.1	567-371-1	209	9187	1.01	0.54	5500	7.95	3.73E9	G.5	11.48	1.84	1.38E9
35219	00:15:21.4	+04:47:55.9	00:15:19.8	+04:48:50.6	5-747-1	133	7895	0.88	0.68	10000	8.15	8.76E8	G.8	10.92	2.7	4.25E8
35261	00:05:27.4	+06:55:56.5	00:05:32.1	+06:55:23.9	7-988-1	165	12521	0.78	1.19	11000	9.0	1.95E9	K.0	11.79	6.94	4.08E7
36813	23:35:10.9	+33:49:23.7	23:35:11.8	+33:47:26.3	2774-1673-1	143	16810	0.99	0.77	5000	8.3	6.49E9	F.8	9.8	3.28	2.44E8
38569	07:35:56.6	+14:07:23.4	07:36:00.9	+14:08:44.1	777-826-1	224	23004	1.05	0.7	6000	8.2	3.65E9	G.2	11.51	2.87	3.56E8
42234	13:48:28.6	+03:23:49.4	13:48:21.6	+03:24:06.0	311-1198-1	283	30079	1.15	0.64	6000	8.1	3.11E9	G.2	11.72	2.45	5.71E8
42260	13:58:17.4	+04:48:52.2	13:58:20.9	+04:50:23.0	312-254-1	122	12846	1.27	0.64	6500	8.1	2.37E9	G.0	9.56	2.45	5.67E8
42332	12:57:28.3	+01:30:47.4	12:57:32.3	+01:31:51.4	291-793-1	255	22395	1.25	0.67	5500	8.15	4.65E9	F.5	10.34	2.65	4.51E8
42487	12:41:23.4	+08:15:28.7	12:41:19.0	+08:15:12.2	875-668-1	256	17100	1.62	0.64	6500	8.1	2.37E9	F.0	9.54	2.45	5.67E8
42775	13:44:55.3	+15:39:28.6	13:44:52.1	+15:41:17.8	1460-765-1	115	13578	0.91	0.63	4750	8.1	6.4E9	G.5	10.47	2.42	5.87E8
44190	11:26:11.1	+07:24:13.6	11:26:16.4	+07:25:09.0	270-421-1	126	12162	1.47	1.19	8500	9.0	2.84E9	F.6	9.2	6.94	4.08E7
44328	11:54:20.3	+13:46:06.9	11:54:28.0	+13:46:39.8	870-836-1	132	15422	0.72	0.52	5250	7.9	4.26E9	K.2	11.6	1.67	1.9E9
44424	12:52:34.1	+13:32:34.4	12:52:31.9	+13:32:41.0	888-843-1	68	2217	1.01	0.45	6000	7.75	1.94E9	K.2	10.28	1.2	5.76E9
44475	12:42:40.1	+18:46:24.1	12:42:41.2	+18:46:39.7	1448-21-1	81	1714	1.19	0.64	7500	8.1	1.69E9	G.0	8.87	2.46	5.59E8
44476	13:06:59.2	+14:53:36.1	13:06:58.3	+14:53:07.0	890-669-1	161	5144	0.75	0.74	7500	8.25	2.25E9	K.2	11.98	3.1	2.87E8
44770	11:09:38.5	+15:40:52.4	11:09:44.4	+15:40:57.7	1430-1443-1	124	10640	0.81	1.19	6500	9.0	3.91E9	K.0	11.05	6.93	4.1E7
49875	20:14:15.6	+00:43:51.7	20:14:09.9	+00:43:58.6	495-1108-1	125	10772	1.34	0.57	3750	8.0	8.04E9	14.2	8.44	1.99	1.09E9
50927	16:27:36.2	-00:40:57.2	16:27:43.3	-00:41:35.5	5035-543-1	140	15755	0.94	0.54	5500	7.95	3.73E9	G.5	10.83	1.84	1.38E9
51256	15:37:43.6	-02:06:16.0	15:37:35.8	-02:05:59.5	5021-299-1	100	11800	1.01	0.83	5500	8.4	5.82E9	G.2	9.76	3.72	1.75E8
51850	16:02:11.0	+11:53:51.9	16:02:05.8	+11:53:12.1	952-279-1	89	7642	0.66	0.54	4750	7.95	5.8E9	K.3	11.16	1.83	1.41E9
52654	17:44:40.5	+18:14:54.8	17:44:33.7	+18:15:07.6	1556-669-1	68	6679	0.78	0.57	4750	8.0	6.15E9	K.0	9.94	1.99	1.07E9
19370	15:56:13.7	+21:23:27.8	15:56:18.8	+21:23:55.1	1502-1772-1	103	7771	0.99	0.49	24000	7.75	2.54E7	G.5	10.0	1.51	2.66E9
32983	23:53:28.7	-08:04:19.4	23:53:27.8	-08:04:39.0	5831-189-1	100	2365	0.78	0.44	13000	7.7	2.25E8	K.0	10.8	1.18	6.21E9
33321	02:53:31.3	-00:34:08.0	02:53:32.3	-00:33:44.8	4700-510-1	48	1306	0.83	0.45	7500	7.75	1.03E9	G.8	8.87	1.23	5.30E9
34238	22:55:50.0	-07:49:21.4	22:55:49.5	-07:50:02.4	113231	36	1492	0.98	0.64	7000	8.1	1.98E9	G.5	7.8	2.46	5.63E8
51869	16:22:07.1	+12:12:52.4	16:22:03.9	+12:13:33.6	80182	56	3528	1.23	1.07	40000	8.75	3.93E7	G.0	8.01	5.68	6.23E7

The first block are the 'Good DA or DB' WDs and the second block are the 'Confirmed WDs'. All of their WD parameters are for the Holberg and Bergeron (2006) DB WD models. Non-letter spectral types are for candidates where their Pickles estimate predicted a non-MS TGAS star.

3.4 Notes on individual objects

The specific binaries that appeared to be interesting and stood out within our catalogues were discussed in this subsection. All the figures and information for the systems discussed can be found in the Appendix in Section 6.1. The IDs refer to those assigned in our final WD-MS binary candidate catalogues (as seen in Tables 8, 9 and 10) which contained all the binary parameter information.

ID:42260 - GOOD DA or DB - Figure 31
This system containing the TGAS star TYC 312-254-1 could have been a WD+WD +MS triple system. In Figure 31 there were 2 blue objects, however, only 1 of them was picked up in a 2 arc-minute proper-motion search as the WD binary was unresolved in POSS-2. There was not any information on SIMBAD about there being 2 objects, which implied this was a newly discovered system.

ID:19392 - SDSS Non-DA - Figure 32
This potential binary was composed of the WD KUV 15571+1913, and the TGAS star TYC 1499-1002-1. Spectra obtained for this WD suggested it was a DB WD (Kondo et al., 1984; Wegner and Swanson, 1990), however, it had not been identified as a potential WD-MS binary previously. David Boyd obtained spectra of the TGAS star (as seen in Figure 33) which resembled an early K-star. This was the same as the K.0 spectral type estimate from the Pickles table in the methodology, based on the photometry of the TGAS star.

ID:21483 - SDSS DA - Figure 34
This potential binary was composed of the WD SDSS J153252.62+375357.9, and the TGAS star TYC 3052-1941-1. Spectra obtained for this WD suggested it was a DA WD (Eisenstein et al., 2006), however, it had not been identified as a potential WD-MS binary previously. David Boyd again obtained spectra of the TGAS star (as seen in Figure 35) which resembled a G-star. This differed to the F.5 spectral type estimate from the Pickles table in the methodology, based on the photometry of the TGAS star.

ID:16996 - SDSS Non-DA - Figure 36
There are currently very few cataclysmic variables (CVs) known with accurate distances. We had found the common proper-motion pair candidate containing the TGAS star TYC 3407-1377-1 and the already known CV EQ Lyn, discussed by Mukadam et al. (2013). Although there had been research into this CV, it had not been discussed as a possible common proper-motion companion to TYC 3407-1377-1 previously. Having the accurate parallaxes from TGAS, we estimated a distance for the CV as $d = 313 \pm 25$pc.

IDs:21882 & 21883 - Good DA or DB, Good DA, respectively - Figures 37 and 38
The TGAS star TYC 3502-104-1 appeared twice in the catalogue with 2 possible WD companions. The first, ID:21882, had a slightly different proper-motion to the TGAS star but the PPMXL proper-motion errors were quite large. If this was an actual common proper-motion pair, it had a minimum binary separation of 11,559AU. This WD candidate had a good fit with both the DA and DB Holberg and Bergeron (2006) models. Spectra was obtained for the candidate (Figure 24 on P. 63) and confirmed it was a DA WD. The second, ID:21883, had a much closer proper-motion to the TGAS star with smaller PPMXL proper-motion errors. If this was an actual common proper-motion pair, it had a minimum binary separation of 14,249AU and had a good fit with only the DA Holberg and Bergeron (2006) models. Therefore, this was possibly another WD+WD+MS triple system.

3.4.1 WD spectra from La Palma

Spectra was obtained for 2 companions of the final WD-MS binary candidates using the William Herschel Telescope (WHT) at La Palma.

Looking firstly at the companion in the candidate system with the ID:15357, this system was in the 'Good DA or DB' group. This meant that the companion could have been either a DA or DB WD based on its photometry.

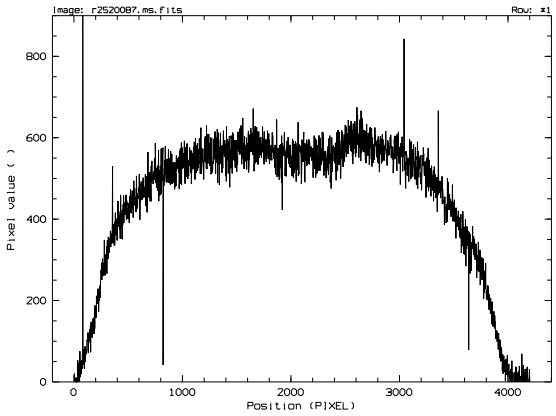

Figure 23: The uncalibrated spectrum of ID:15357 is featureless, suggesting this is a cool DC WD.

Its spectrum (as seen in Figure 23) had practically no features, suggesting that

it was a cool DC WD.

Spectra was also obtained for the candidate system with the ID:21882. This system was again in the 'Good DA or DB' group, which meant that the companion could be either a DA or DB WD.

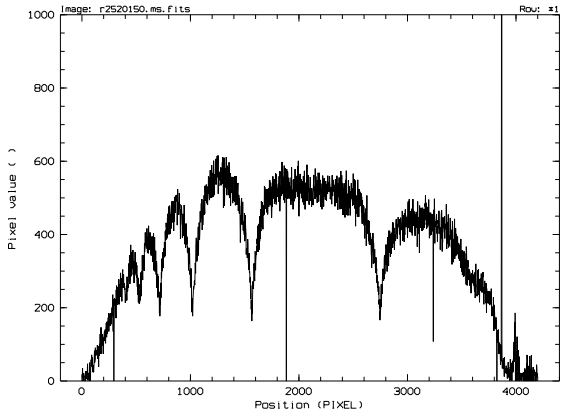

Figure 24: The uncalibrated spectrum of ID:21882 suggests this is a DA WD.

The WHT spectrum confirmed that this was a newly discovered DA WD (as seen in Figure 24).

4 Discussion

The parameters of the WD-MS binary candidates and what they mean are discussed in this section. The potential uses for the binary candidates containing cool WDs and their impact on multiple aspects of astronomy is also highlighted.

4.1 The parameters of the WD-MS binary candidates and what they mean

WD MS progenitor mass compared to the MS companion mass

Wide WD-MS binaries are systems that originally contained 2 MS stars with separations wide enough that they did not undergo any mass transfer. Therefore the stars evolved as if they were single stars and eventually the more massive star of the binary evolved into a WD (Rebassa-Mansergas et al., 2016b). Therefore, for a genuine WD-MS binary the WD MS progenitor mass must be greater than MS companion mass.

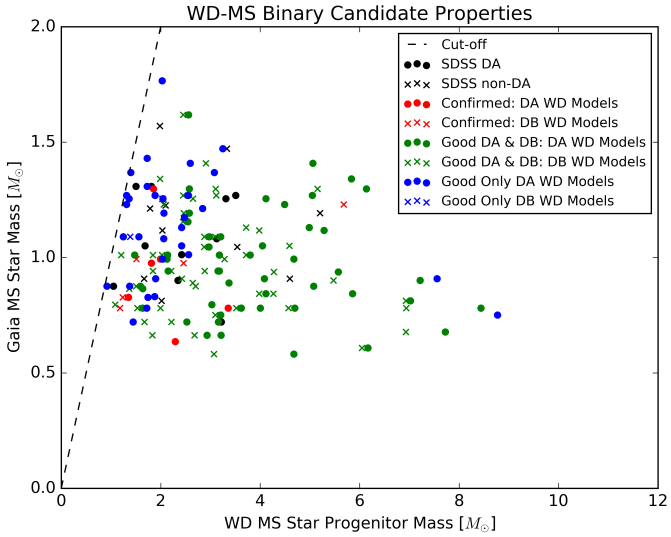

Figure 25: WD MS progenitor mass vs. MS companion mass. The black line is the cut-off where the WD MS progenitor's mass is equal to the TGAS MS star's mass. Candidate definitions in Sect. 3.3.1 on P. 55.

There has been debate among astronomers regarding higher mass stars ($\geq 10 M_\odot$) favouring equal-mass binaries (Pinsonneault and Stanek, 2006; Sana et al., 2012),

i.e. a mass ratio close to 1. Figures 25 and 26 suggest that among stars of $< 10M_{\odot}$, there is no statistical correlation between the initial mass of the 2 MS stars in the binary. Otherwise more of the candidates would lie near the black dotted line in Figure 25, representing the WD MS progenitor mass being equal to the MS companion mass.

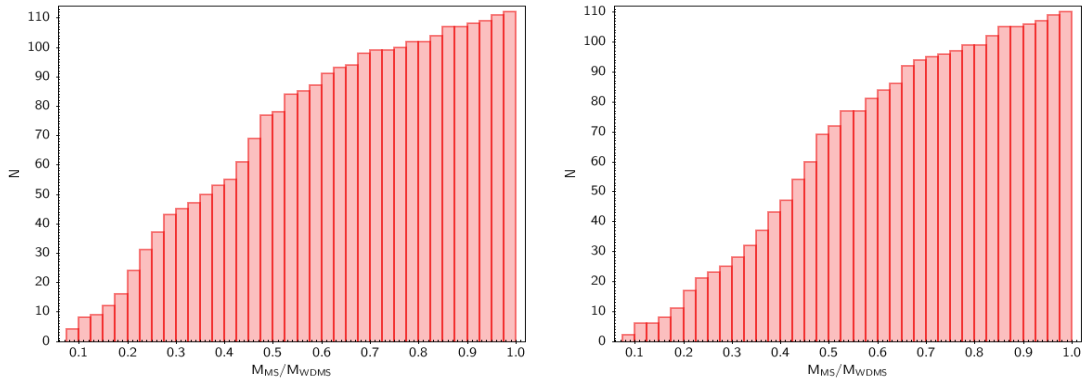

(a) (b)

Figure 26: Cumulative frequency histograms of mass ratio (TGAS MS mass / WD MS progenitor mass). Shown in (a): Catalogues 1 and 2-DA, shown in (b): Catalogues 1 and 2-DB (catalogue definitions on P. 56).

Binary distance compared to the minimum binary separation

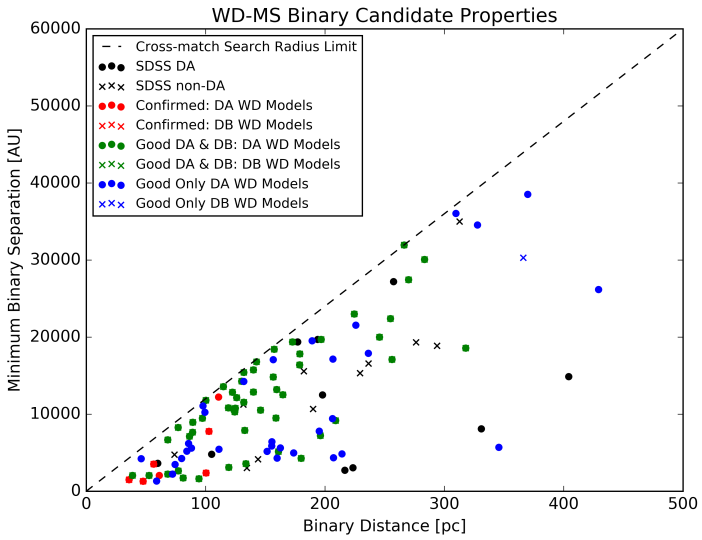

Figure 27: Binary distance vs. minimum binary separation. The black line is the limit of the 2 arc-minute search radius with PPMXL for wide companions. Candidate definitions in Sect. 3.3.1 on P. 55.

Looking at binary distance and binary separation can indicate whether the 2 arc-minute radius cross-match with PPMXL was an appropriate choice. The search radius was based on the median distance of the TGAS stars in the clean TGAS subset. Figure 27 shows that a large amount of the parameter space below the 2 arc-minute search radius line was covered. This appears to have been a self-imposed limitation on the amount of binaries that could have been found as many lie along the line. Additionally, the distribution is not levelling off at a particular distance indicating that this limitation applies at all distances. Even considering this information we now have, increasing the search radius would provide too many binary candidates to visually inspect. Carrying out a search for companions within a wider radius will only be feasible once more accurate proper-motions are available.

It is interesting to consider if there is a maximum binary separation a binary can have, so looking at binary distance vs. binary separation could help indicate if this is the case. The trend present in Figure 27 supports the natural assumption that with a search radius of 2 arc-minutes, larger binary separations are present at larger distances. Also, at a binary distance $\gtrapprox$200pc the number of systems seem

to drop off. This could be a consequence of WDs at these distances becoming too faint to have good PPMXL measurements or a PPMXL measurement at all. With a deeper proper-motion survey research could be conducted on whether there is a particular binary separation limit, regardless of binary distance. Any binary with a separation larger than this limit could be dissolved through processes such as Galactic tides or close encounters with other stars (Jiang and Tremaine, 2010).

4.2 The implications of our WD-MS binary candidates containing cool WDs

As mentioned previously, wide WD-MS binaries can be viewed as the smallest and simplest forms of stellar clusters (Koester, 2013; Kouwenhoven et al., 2010). Open clusters only exist up to ≈1Gyr before being dissolved by Galactic tides and stellar encounters (Jiang and Tremaine, 2010; Vande Putte et al., 2010). However, wide WD-MS binaries with old cool WDs can be older than open clusters. Therefore, these binaries provide important insight into stellar evolution (Koester, 2013).

We can define a WD with a cooling age of ≥0.5-1Gyr as a cool WD. Using the initial-final mass relation equations and the MS lifetime for a 1Gyr cooling age (Sect. 2.2.3), this corresponds to a WD with a T_{eff} of ≈8000K and a mass of ≈0.6$M_{\odot}$.

Comparison with the catalogue from Holberg et al. (2013)

It is important to compare our catalogue with one of the largest wide WD-MS binary catalogues to date by Holberg et al. (2013). Their catalogue contains 98 binaries. Using 8000K as a cutoff for cool WDs, their catalogue contains 11 (≈11%) binaries containing a WD with a $T_{eff} \leq 8000$K (as seen in Figure 28).

We have 3 separate final catalogues as explained in Sect. 3.3.2, and can combine them in 2 different ways. The first way is combining Catalogues 1 and 2-DA. Therefore, the DA Holberg and Bergeron (2006) WD model parameters for the 'Good DA or DB' and 'Confirmed WDs' are included. With these catalogues there are 65 (≈58%) candidate systems containing a WD with a $T_{eff} \leq 8000$K (as seen in Figure 29).

The other way to combine our separate final catalogues is combining Catalogues 1 and 2-DB. Therefore, the DB Holberg and Bergeron (2006) WD model parameters for the 'Good DA or DB' and 'Confirmed WDs' are included. With

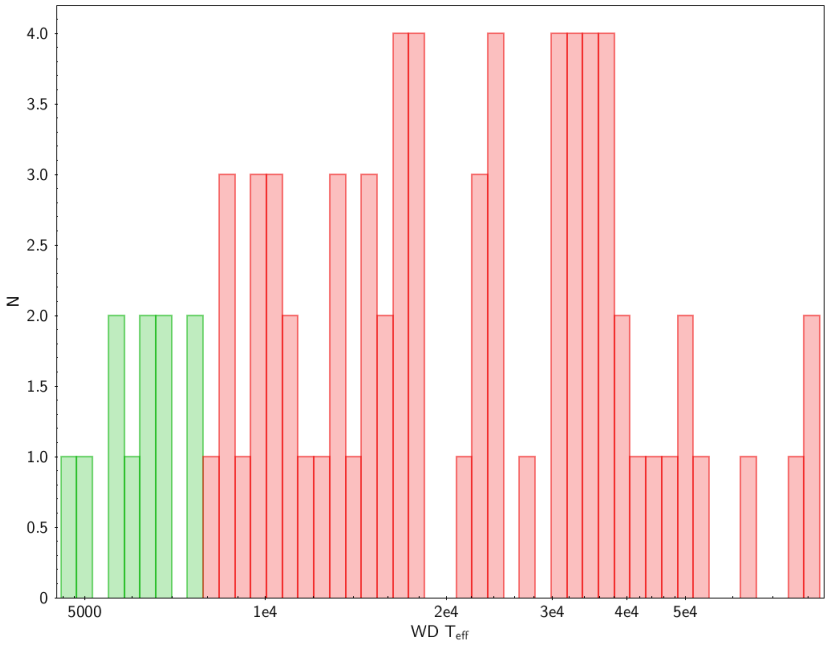

Figure 28: Histogram of WD T_{eff} from the Holberg et al. (2013) catalogue. In green are the 11 binaries with WDs $T_{eff} \leq 8000$K, in red are $T_{eff} > 8000$K.

these catalogues there are 66 (60%) candidate systems containing a WD with a $T_{eff} \leq 8000$K (as seen in Figure 30).

For our 65 and 66 cool WD-MS binary candidate systems, there are 56 and 57 'Good candidates', respectively. This means there is no SDSS spectroscopy available for these WD candidates, but their location in colour-colour and reduced proper-motion - colour diagrams indicate a WD nature. Therefore, these candidate systems are prime candidates to obtain spectra for.

If these candidates are in fact wide WD-MS binaries, this is a substantial increase in the number of WD-MS binaries containing cool WDs. These binaries will be useful in order to further improve our understanding of stellar evolution.

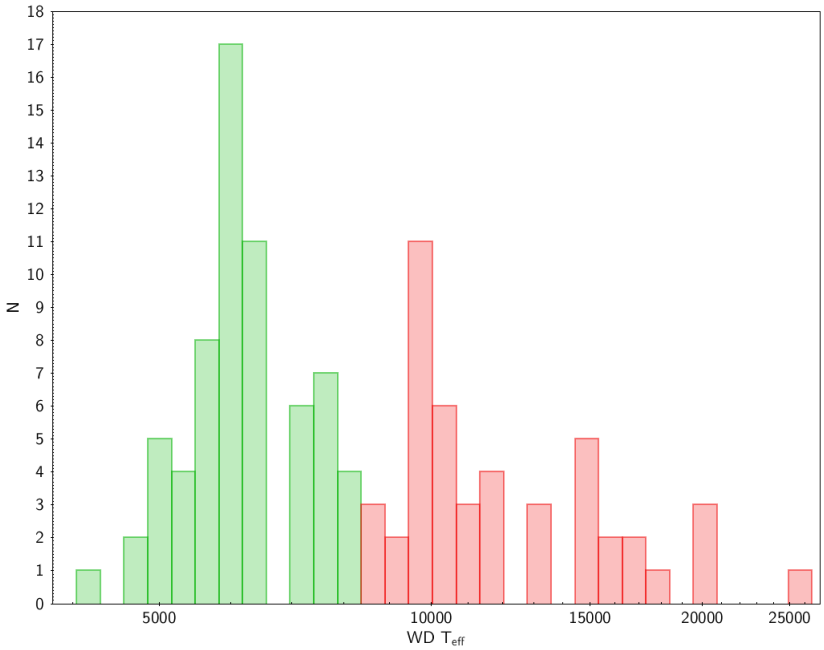

Figure 29: Histogram of WD T_{eff} from our Catalogues 1 and 2-DA (Sect. 3.3.2). In green are the 65 binaries with WDs $T_{eff} \leq 8000$K, in red are $T_{eff} > 8000$K. Ignoring 1 candidate with T_{eff}=140,000K.

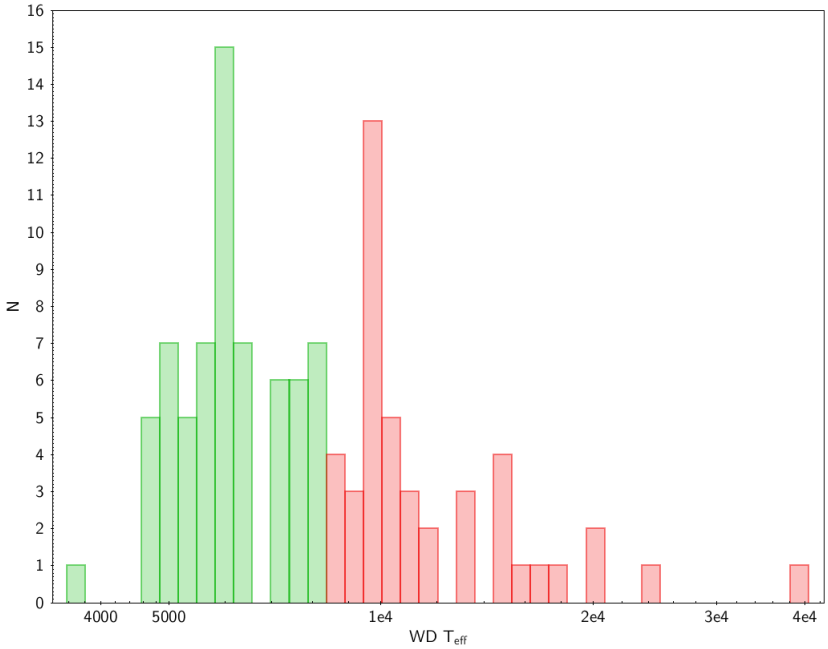

Figure 30: Histogram of WD T_{eff} from our Catalogues 1 and 2-DB (Sect. 3.3.2). In green are the 66 binaries with WDs $T_{eff} \leq 8000$K, in red are $T_{eff} > 8000$K.

The age-metallicity relation

Rebassa-Mansergas et al. (2016a) use 23 WD-MS binaries as observational inputs to constrain the properties of the AMR robustly. However, Rebassa-Mansergas et al. (2016a) use no WD-MS binaries with cool WDs. Even though they have physically wide WD-MS binaries with ≈100AU separation, they are within only a few 100pc so are still unresolved. Our cool WD-MS binaries are not only ≥1Gyr old, but also spatially resolved so spectroscopy for each constituent can be independently obtained, simplifying the analysis. Our binary candidates could help with understanding how the Galactic disc formed and evolved chemically in time, and help refine the AMR in the future.

The rotation-age relationship

Our candidates contain both smaller WDs and more massive MS stars, ranging from young to ≥1Gyr for the binary candidates containing cool WDs. These binary candidates are in a sense a collection of many small clusters, containing not only different types of stars with different masses, but also many systems with a distribution of ages. Our candidates will provide a better distribution for the rotation-age relationship than an open cluster containing stars all with the same age (Prialnik, 2000). This is because many open clusters would be required to understand the full picture. Additionally, open clusters dissolve with time so it is very hard to study the rotation-age relationship for stars older than ≈1Gyr (Vande Putte et al., 2010). This is in contrast to our binary candidates containing cool WDs.

5 Conclusion

We present a catalogue of 112 candidate wide WD-MS binaries of TGAS stars and PPMXL WDs within the SDSS footprint. Our catalogue is comprised of 84 high confidence WD-MS binary candidates, 21 candidates with SDSS spectroscopy for the WD companion and 7 binary candidates containing WDs confirmed from SIMBAD. We have also recovered 8 binaries from Tremblay et al. (2017), including 1 binary from Farihi et al. (2005a). This is after restricting our search to the SDSS footprint which is ≈1/3 of the sky only. Our catalogue contains ≈65 wide WD-MS binary candidates containing cool WDs which significantly increases the number of these systems currently known. We expect these binary candidates will be used for a range of astrophysical studies in the future to help gain a better understanding of these objects, the processes within them and stellar evolution.

6 Appendix

6.1 A1: Master Plots for the systems discussed in Sect. 3.4.

These plots were used to reduce the 271 common proper-motion pair candidates to the most likely binary systems containing a WD (P. 34). They contain:

i) An SDSS image of the MS star
ii) An SDSS image of the WD companion
iii) A POSS-2 red image of the WD-MS binary with arrows indicating the individual proper-motions
iv) A POSS-2 red image of the WD-MS binary illustrating the proper-motions of all objects within a 2 arc-minute radius
v) A colour-colour diagram of the WD
vi) A reduced proper-motion - colour diagram of the WD
vii) The spectrum of the WD (if available)

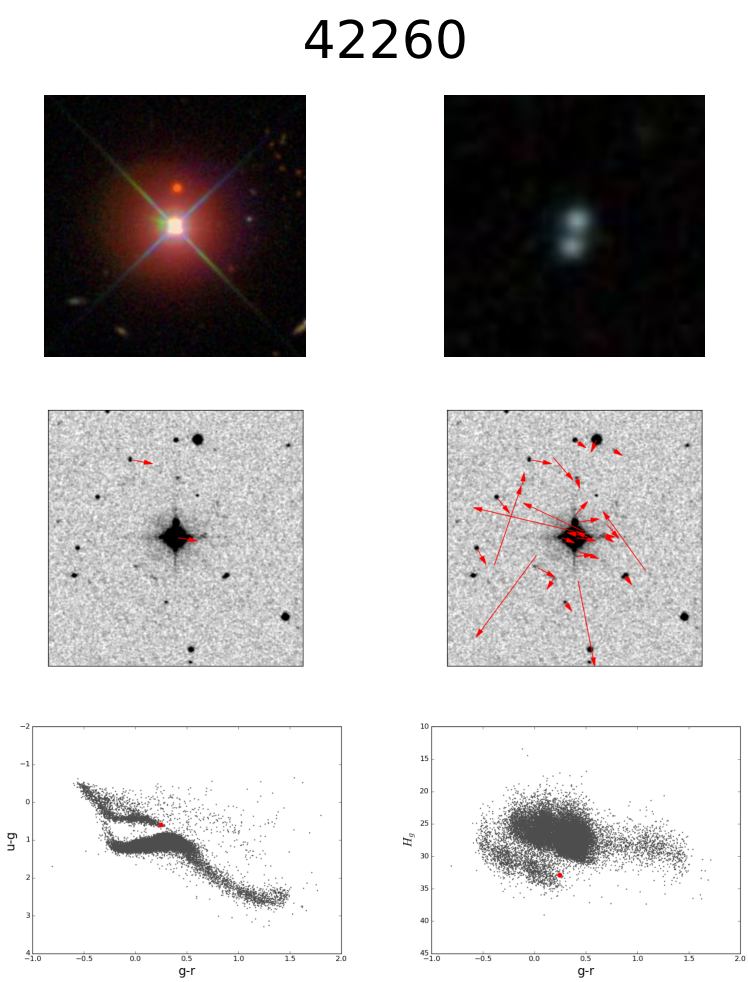

MS RA=13:58:17.4 MS DEC=+04:48:52.2
WD RA=13:58:20.9 WD DEC=+04:50:23.0

MS PMRA=-44.5±1.4 MS PMDEC=-7.0±0.6
WD PMRA=-45.2±4.6 WD PMRA=-8.2±4.6

Model SpT=G.0 TYC2/HIP ID=312-254-1
Distance=122pc±4 Min Binary Sep=12846au

Figure 31: ID:42260, a triple system candidate. Proper-motions in milli-arc-seconds yr^{-1}.

19392

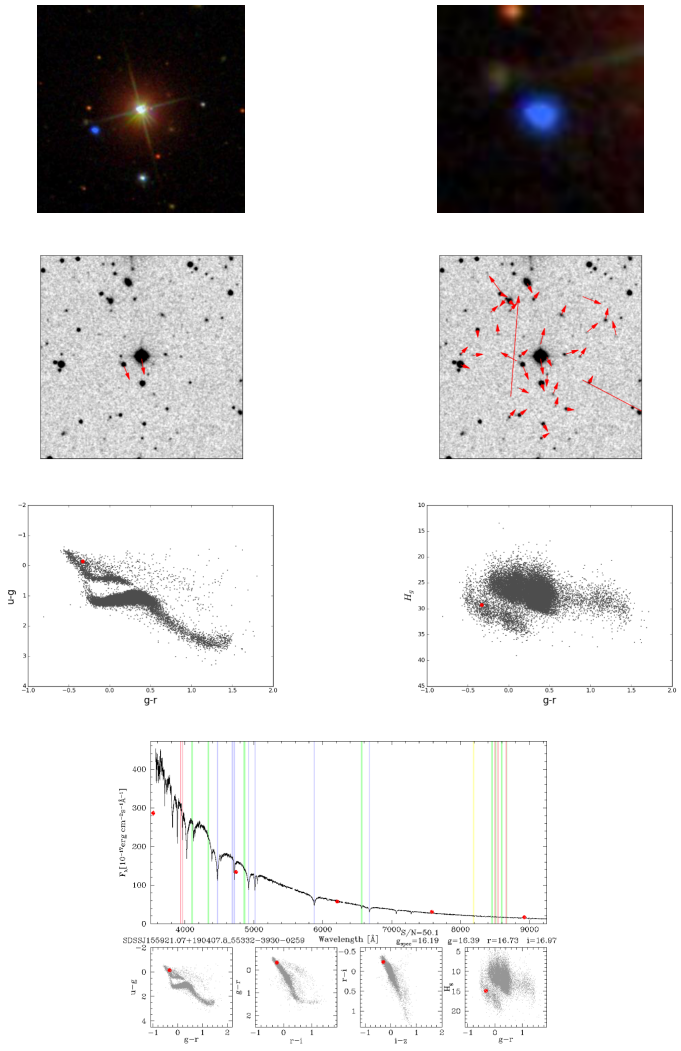

MS RA=15:59:19.2 MS DEC=+19:04:20.1
WD RA=15:59:21.1 WD DEC=+19:04:08.5

MS PMRA=-7.1±1.7 MS PMDEC=-45.1±0.7
WD PMRA=-14.4±5.2 WD PMRA=-34.5±5.2

Model SpT=K.0 TYC2/HIP ID=1499-1002-1
Distance=144pc±6 Min Binary Sep=4150au

Figure 32: ID:19392, a WD-MS binary system candidate containing a spectroscopically confirmed DB WD. Proper-motions in milli-arc-seconds yr^{-1}.

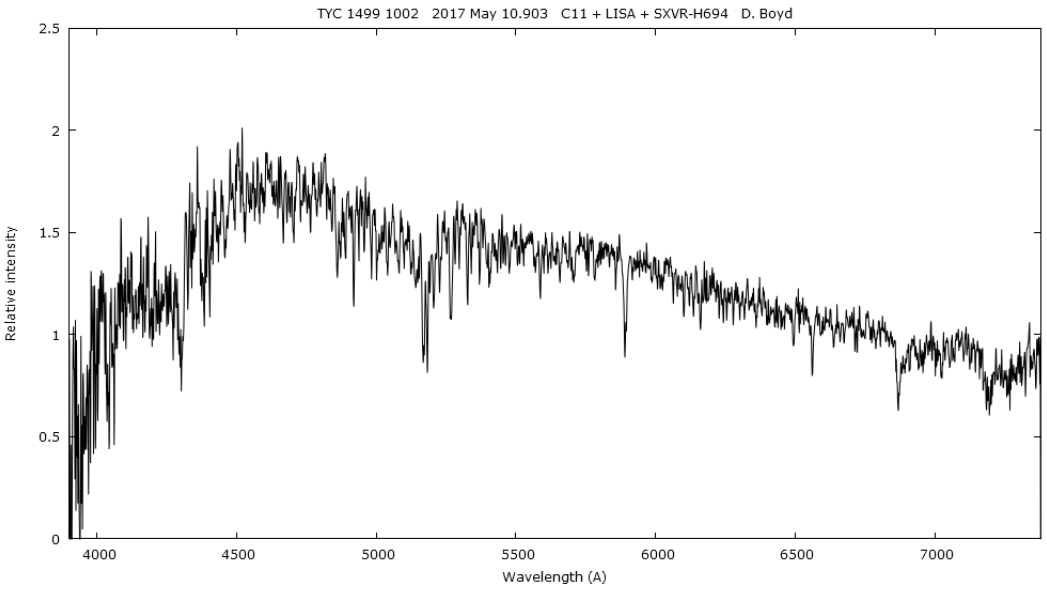

Figure 33: MS spectrum for TYC 1499-1002-1 (Figure 32) obtained by David Boyd, confirming an early K-star spectral type. ID:19392.

21483

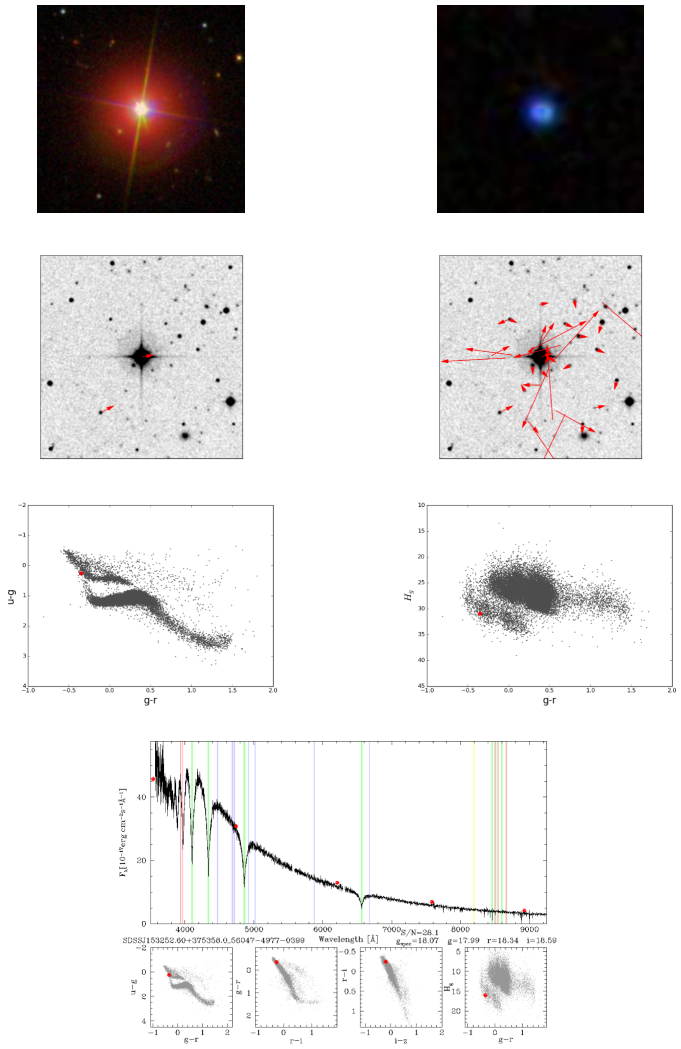

MS RA=15:32:47.4 MS DEC=+37:55:18.8
WD RA=15:32:52.6 WD DEC=+37:53:58.0

MS PMRA=-26.2±0.5 MS PMDEC=2.8±0.9
WD PMRA=-36.2±4.9 WD PMRA=14.3±4.9

Model SpT=F.5 TYC2/HIP ID=3052-1941-1
Distance=194pc±8 Min Binary Sep=19701au

Figure 34: ID:21483, a WD-MS binary system candidate containing a spectroscopically confirmed DA WD. Proper-motions in milli-arc-seconds yr^{-1}.

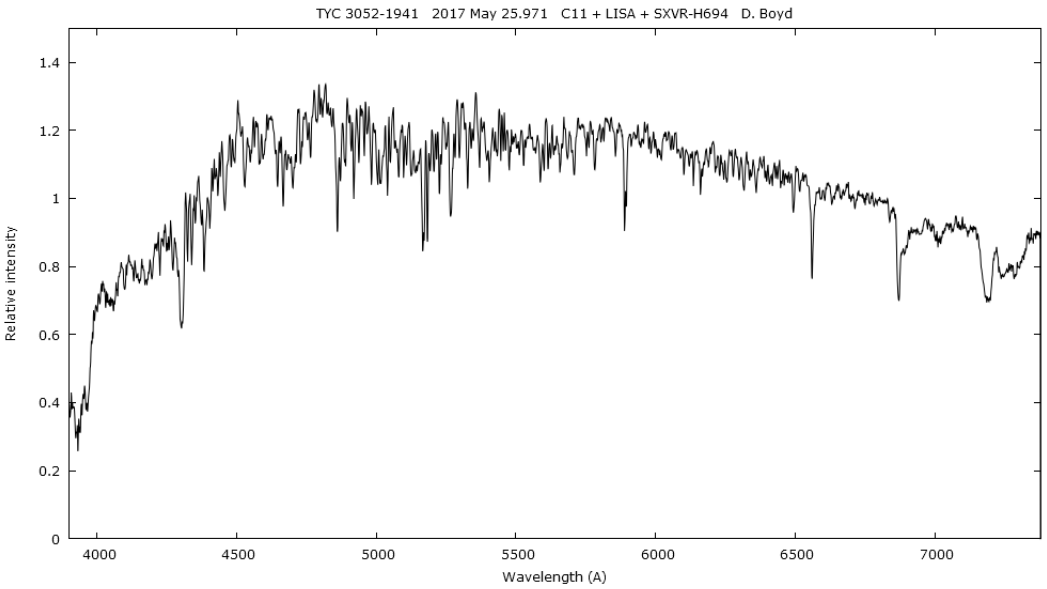

Figure 35: MS spectrum for TYC 3052-1491-1 (Figure 34) obtained by David Boyd, confirming a G-star spectral type. ID:21483

16996

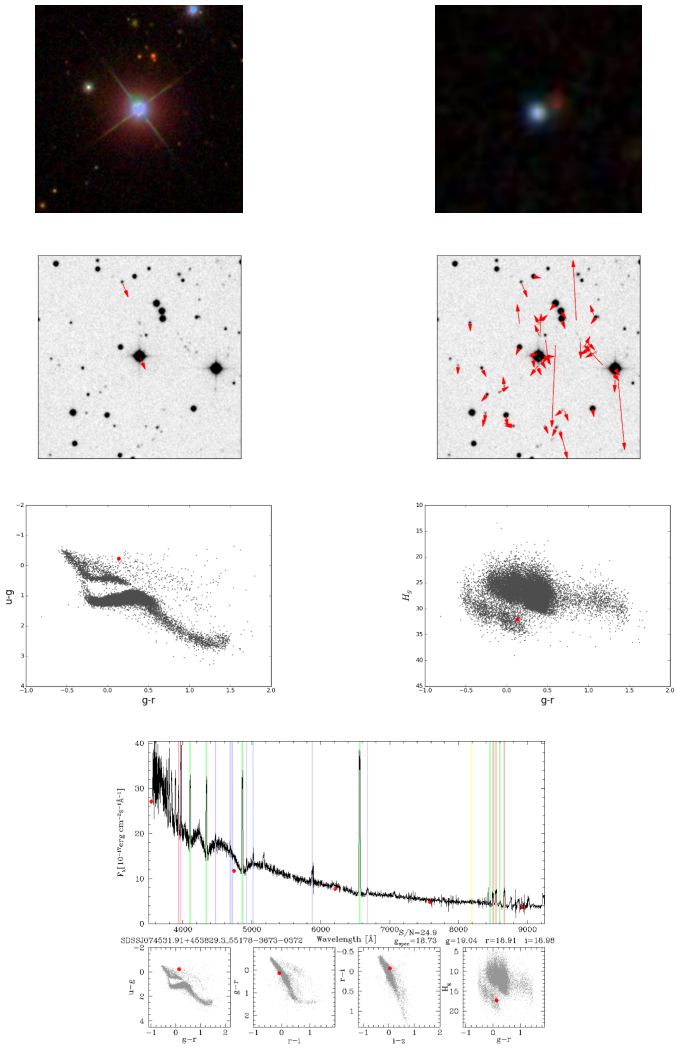

MS RA=07:45:29.0 MS DEC=+45:36:42.3
WD RA=07:45:31.9 WD DEC=+45:38:30.0

MS PMRA=-19.2±0.9 MS PMDEC=-26.9±1.3
WD PMRA=-21.8±4.9 WD PMRA=-33.9±4.9

Model SpT=F.5 TYC2/HIP ID=3407-1377-1
Distance=313pc±25 Min Binary Sep=35001au

Figure 36: ID:16996, a CV-MS binary system candidate containing a spectroscopically confirmed CV. Proper-motions in milli-arc-seconds yr^{-1}.

21882

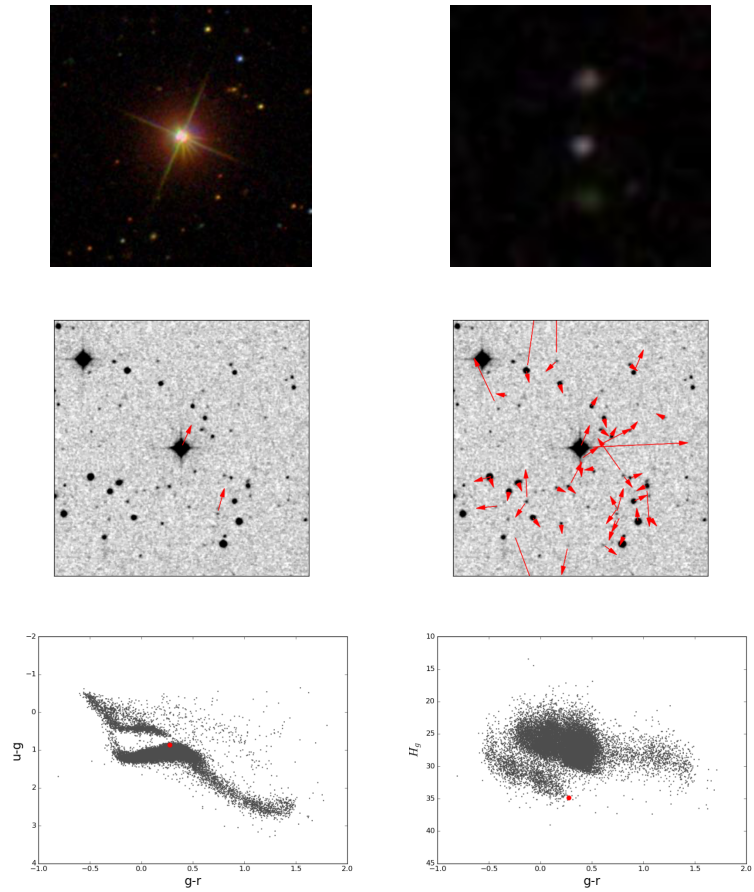

MS RA=16:39:20.3 MS DEC=+47:47:06.4
WD RA=16:39:15.9 WD DEC=+47:45:50.7

MS PMRA=-30.8±1.2 MS PMDEC=49.3±1.4
WD PMRA=-20.6±7.8 WD PMRA=55.3±7.8

Model SpT=K.0 TYC2/HIP ID=3502-104-1
Distance=132pc±7 Min Binary Sep=11559au

Figure 37: ID:21882, a triple system candidate containing the MS star TYC 3502-104-1 which is also in the binary candidate ID: 21883 in Figure 38. Proper-motions in milli-arc-seconds yr^{-1}.

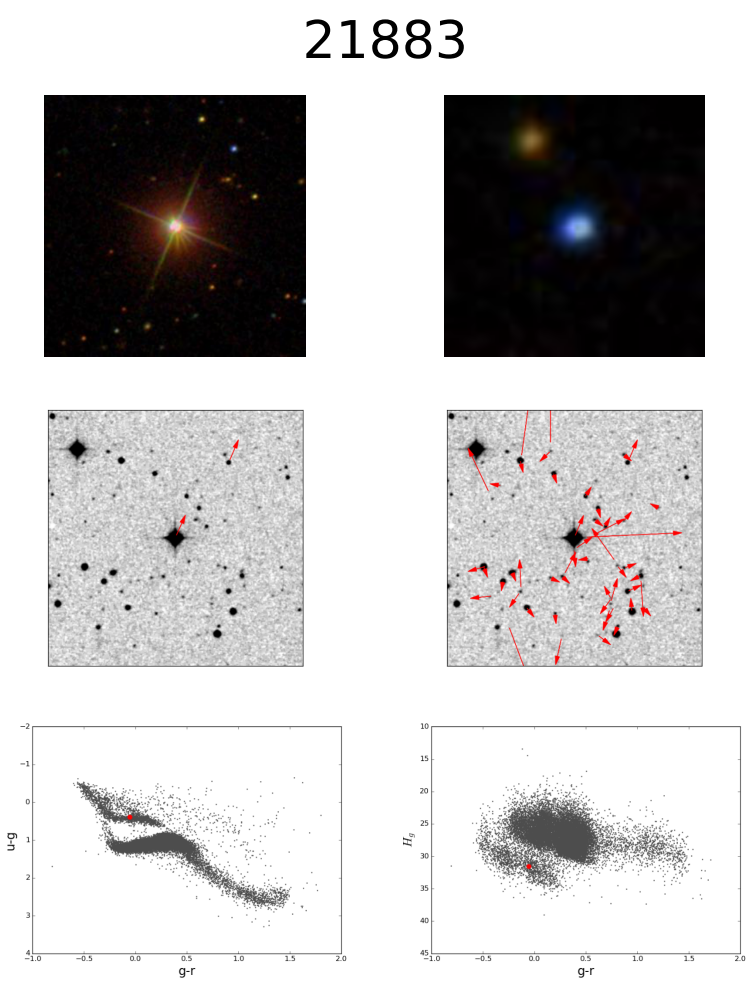

Figure 38: ID:21883, a triple system candidate containing the MS star TYC 3502-104-1 which is also in the binary candidate ID: 21882 in Figure 37. Proper-motions in milli-arc-seconds yr^{-1}.

6.2 A2: Further justification of the adopted cuts

The cuts imposed in Section 2.2.2 on P. 26 were discussed in this appendix.

A difficult aspect of the methodology was the 2 arc-minute cross-match with PPMXL to look for possible WD companions (PPMXL_{WD}). Specifically, it was deciding what value of σ to use regarding the proper-motion significances and for the 2σ proper-motion ranges. It was difficult to find the balance between finding genuine binaries but not having too many to visually inspect. The results of 3 tests to help decide which values of σ to use were displayed in this appendix.

These tests were conducted starting with the clean TGAS subset up until before visually inspecting the Master Plots (P. 34). The things that varied were:

i) the value of n for the significance cut ($\mu/\delta\mu \geq n$) on the PPMXL_{WD} proper-motions.

ii) the value of n for the nσ proper-motion ranges for TGAS and PPMXL_{WD}.

The binaries from Tremblay et al. (2017) were used as test cases to see how many were retained before visually inspecting the Master Plots (P. 34). There should have been as many Tremblay et al. (2017) binaries left as possible with as few multiple companion matches as possible (as seen in Table 11).

Binaries Left (Total Matches)	i) $\mu/\delta\mu \geq n$	ii) nσ proper-motion ranges
11 (12)	5	1
11 (12)	6	1
11 (12)	7	1
22 (26)	5	2
22 (25)	6	2
22 (25)	7	2
22 (23)	8	2
23 (29)	5	3
23 (27)	6	3
23 (26)	7	3

Table 11: Test case binaries from Tremblay et al. (2017). Tests of different values of σ for: i) the PPMXL_{WD} proper-motions and ii) proper-motion ranges for TGAS and PPMXL_{WD}. The row in grey is the method we used in the methodology.

100 random TGAS stars were used as test cases to see how many were left before visually inspecting the Master Plots (P. 34). There should not have been any candidates remaining from such a small random sample (as seen in Table 12).

'TGAS Stars + PM Companion's Left	i) $\mu/\delta\mu \geq n$	ii) nσ proper-motion ranges
1	5	1
0	6	1
0	7	1
8	5	2
2	6	2
0	7	2
0	8	2
22	5	3
8	6	3
2	7	3

Table 12: 100 random TGAS stars test. Tests of different values of σ for: i) the PPMXL_{WD} proper-motions and ii) proper-motion ranges for TGAS and PPMXL_{WD}. The row in grey is the method we used in the methodology. (PM=proper-motion.)

Finally, a group of 5000 TGAS Stars were used as a test case. There should only have been some candidates remaining as a result from this large amount of TGAS test cases. However, not too many (as seen in Table 13).

'TGAS Stars + PM Companion's Left	i) $\mu/\delta\mu \geq n$	ii) nσ proper-motion ranges
416	5	2
196	6	2
104	7	2
61	8	2
1060	5	3
521	6	3
269	7	3

Table 13: 5000 random TGAS stars test. Tests of different values of σ for: i) the PPMXL_{WD} proper-motions and ii) proper-motion ranges for TGAS and PPMXL_{WD}. The row in grey is the method we used in the methodology. (PM=proper-motion.)

As seen in Tables 11, 12 and 13, a 7σ significance cut on the PPMXL_{WD} proper-motions and 2σ proper-motion ranges were used in the final methodology. We concluded this was the best balance of retaining the most binaries from Tremblay et al. (2017) but also not having too many candidates to visually inspect later.

7 Further Acknowledgments

This research has made use of TOPCAT and STILTS:
http://www.starlink.ac.uk/topcat/ and http://www.starlink.ac.uk/stilts/

This research has made use of the Python programming language and various Python packages.

This research has made use of the VizieR catalogue access tool, CDS, Strasbourg, France. The original description of the VizieR service was published in A&AS 143, 23.

This research has made use of the SIMBAD database, operated at CDS, Strasbourg, France
2000,A&AS,143,9 , "The SIMBAD astronomical database", Wenger et al.
This publication makes use of vosa, developed under the spanish virtual observatory project supported from the spanish micinn through grant aya2011-24052.

POSS-2: Caltech - http://stdatu.stsci.edu/dss/acknowledging.html
http://stdatu.stsci.edu/data_use.html
The National Geographic Society - Palomar Observatory Sky Atlas (POSS-I) was made by the California Institute of Technology with grants from the National Geographic Society.

The Second Palomar Observatory Sky Survey (POSS-II) was made by the California Institute of Technology with funds from the National Science Foundation, the National Geographic Society, the Sloan Foundation, the Samuel Oschin Foundation, and the Eastman Kodak Corporation.

The SDSS is managed by the Astrophysical Research Consortium (ARC) for the Participating Institutions. The Participating Institutions are The University of Chicago, Fermilab, the Institute for Advanced Study, the Japan Participation Group, The Johns Hopkins University, Los Alamos National Laboratory, the Max-Planck-Institute for Astronomy (MPIA), the Max-Planck-Institute for Astrophysics (MPA), New Mexico State University, University of Pittsburgh, Princeton University, the United States Naval Observatory, and the University of Washington.

SDSS Skyserver: http://skyserver.sdss.org/dr13/en/tools/chart/navi.aspx
Funding for the Sloan Digital Sky Survey (SDSS) has been provided by the Alfred P. Sloan Foundation, the Participating Institutions, the National Aeronautics and

Space Administration, the National Science Foundation, the U.S. Department of Energy, the Japanese Monbukagakusho, and the Max Planck Society. The SDSS Web site is http://www.sdss.org/.

References

Alam S. et al., 2015. *ApJS*, 219,12.

Attridge J.M. and Herbst W., 1992. *ApJL*, 398,L61–L64.

Bahcall J.N., Hut P., and Tremaine S., 1985. *ApJ*, 290,15–20.

Bayo A. et al., 2008. *A&A*, 492,277–287.

Bergeron P., Leggett S.K., and Ruiz M.T., 2001. *ApJS*, 133,413–449.

Bergeron P., Saffer R.A., and Liebert J., 1992. *ApJ*, 394,228–247.

Carraro G., Ng Y.K., and Portinari L., 1998. *MNRAS*, 296,1045–1056.

Casamiquela L. et al., 2016. *MNRAS*, 458,3150–3167.

Catalán S. et al., 2008a. *A&A*, 477,213–221.

Catalán S. et al., 2008b. *MNRAS*, 387,1693–1706.

Chanamé J. and Gould A., 2004. *ApJ*, 601,289–310.

Chandrasekhar S., 1931. *ApJ*, 74,81.

Cummings J.D. et al., 2016. *ApJ*, 818,84.

Day-Jones A.C. et al., 2011. *MNRAS*, 410,705–716.

Dhital S. et al., 2010. *Aj*, 139,2566–2586.

Eisenstein D.J. et al., 2006. *ApJS*, 167,40–58.

Epstein C.R. and Pinsonneault M.H., 2014. *ApJ*, 780,159.

European Space Agency E., 2016. Gaia dr1 information. Available at `https://www.cosmos.esa.int/web/gaia/dr1` (26/07/2017).

Falcon R.E. et al., 2012. *ApJ*, 757,116.

Farihi J., Becklin E.E., and Zuckerman B., 2005a. *ApJS*, 161,394–428.

Farihi J., Becklin E.E., and Zuckerman B., 2005b. *ApJS*, 161,394–428.

Ferrario L. et al., 2005. *MNRAS*, 361,1131–1135.

Fontaine G., Brassard P., and Bergeron P., 2001. *PASP*, 113,409–435.

Fowler R.H., 1926. *MNRAS*, 87,114–122.

Friel E.D., 1995. *ARAA*, 33,381–414.

Gaia Collaboration et al., 2016. *A&A*, 595,A2.

Gentile Fusillo N.P., Gänsicke B.T., and Greiss S., 2015. *MNRAS*, 448,2260–2274.

Hartkopf W.I., Harmanec P., and Guinan E.F., editors, 2007. *Binary Stars as Critical Tools and Tests in Contemporary Astrophysics (IAU S240)*, volume 240 of *IAU Symposium*.

Hernandez X. and Lee W.H., 2008. *MNRAS*, 387,1727–1734.

Holberg J.B. and Bergeron P., 2006. *Aj*, 132,1221–1233.

Holberg J.B. et al., 2013. *MNRAS*, 435,2077–2091.

Husser T.O. et al., 2013. *A&A*, 553,A6.

Jiang Y.F. and Tremaine S., 2010. *MNRAS*, 401,977–994.

Kleinman S.J. et al., 2013. *The Astrophysical Journal Supplement Series*, 204(1),5.

Koester D., 1987. *ApJ*, 322,852–855.

Koester D., 2013. *White Dwarf Stars*, 559. Springer.

Koester D., Schulz H., and Weidemann V., 1979. *A&A*, 76,262–275.

Kondo M., Noguchi T., and Maehara H., 1984. *Annals of the Tokyo Astronomical Observatory*, 20,130–189.

Köppen J. and Hensler G., 2005. *A&A*, 434,531–541.

Kouwenhoven M.B.N. et al., 2010. *MNRAS*, 404,1835–1848.

Lépine S. and Bongiorno B., 2007. *Aj*, 133,889–905.

Makarov V.V., Zacharias N., and Hennessy G.S., 2008. *ApJ*, 687,566-578.

Massey P. and Meyer M.R., 2001. *Encyclopedia of Astronomy and Astrophysics*. IOPP and Macmillan Publishers Ltd.

Mestel L., 1952. *MNRAS*, 112,583.

Minchev I. et al., 2011. *A&A*, 527,A147.

Monet D.G. et al., 2003. *Aj*, 125,984–993.

Mukadam A.S. et al., 2013. *Aj*, 146,54.

Munari U. et al., 2005. *A&A*, 442,1127–1134.

Pancino E. et al., 2010. *A&A*, 511,A56.

Pauli W., 1925. *Zeitschrift für Physik*, 31(1),765–783. ISSN 0044-3328.

Perlmutter S. et al., 1999. *ApJ*, 517,565–586.

Pickles A.J., 1998. *PASP*, 110,863–878.

Pilyugin L.S. and Edmunds M.G., 1996. *A&A*, 313,783–791.

Pinsonneault M.H. and Stanek K.Z., 2006. *ApJL*, 639,L67–L70.

Prialnik D., 2000. *An introduction to the theory of stellar structure and evolution*. Cambridge University Press.

Quinn D.P. et al., 2009. *MNRAS*, 396,L11–L15.

Rebassa-Mansergas A. et al., 2016a. *MNRAS*, 463,1137–1143.

Rebassa-Mansergas A. et al., 2016b. *MNRAS*, 458,3808–3819.

Renedo I. et al., 2010. *ApJ*, 717,183–195.

Riess A.G. et al., 1998. *Aj*, 116,1009–1038.

Roeser S., Demleitner M., and Schilbach E., 2010. *Aj*, 139,2440–2447.

Roškar R. et al., 2008. *ApJL*, 684,L79.

Sana H. et al., 2012. *Science*, 337,444.

Sellwood J.A. and Binney J.J., 2002. *MNRAS*, 336,785–796.

Shipman H.L., 1979. *ApJ*, 228,240–256.

Skrutskie M.F. et al., 2006. *Aj*, 131,1163–1183.

Skumanich A., 1972. *ApJ*, 171,565.

Stauffer J.R., Hartmann L.W., and Jones B.F., 1989. *ApJ*, 346,160–167.

Tremblay P.E. et al., 2017. *MNRAS*, 465,2849–2861.

Vande Putte D. et al., 2010. *MNRAS*, 407,2109–2121.

Wasserman I. and Weinberg M.D., 1991. *ApJ*, 382,149–167.

Wegner G. and Swanson S.R., 1990. *Aj*, 99,330–338.

Zhao J.K. et al., 2011. *Aj*, 141,107.

Zhao J.K. et al., 2012. *ApJ*, 746,144.